NIKHEF 05-006
DCPT/05/28, IPPP/05/14
DESY 05-063, SFB/CPP-05-13
April 2005

hep-ph/0504242

The third-order QCD corrections to deep-inelastic scattering by photon exchange

J.A.M. Vermaseren[a], A. Vogt[b] and S. Moch[c]

[a]*NIKHEF Theory Group*
Kruislaan 409, 1098 SJ Amsterdam, The Netherlands

[b]*IPPP, Department of Physics, University of Durham*
South Road, Durham DH1 3LE, United Kingdom

[c]*Deutsches Elektronensynchrotron DESY*
Platanenallee 6, D–15738 Zeuthen, Germany

Abstract

We compute the full three-loop coefficient functions for the structure functions F_2 and F_L in massless perturbative QCD. The results for F_L complete the next-to-next-to-leading order description of unpolarized electromagnetic deep-inelastic scattering. The third-order coefficient functions for F_2 form, at not too small values of the Bjorken variable x, the dominant part of the next-to-next-to-next-to-leading order corrections, thus facilitating improved determinations of the strong coupling α_s from scaling violations. The three-loop corrections to F_L are larger than those for F_2. Especially for the latter quantity the expansion in powers of α_s is very stable, for photon virtualities $Q^2 \gg 1\ \mathrm{GeV}^2$, over the full x-range accessible to fixed-target and collider measurements.

1 Introduction

Structure functions in deep-inelastic scattering (DIS) and their scale evolution are closely related to the origins of Quantum Chromodynamics (QCD) and its very formulation as the gauge theory of the strong interaction [1–5]. In fact, ever since the pioneering measurements at SLAC [6–8], DIS structure functions have been the subject of detailed theoretical and experimental investigations, see, e.g., the Review of Particle Properties [9] and references therein. Today, with high-precision data from the electron–proton collider HERA and in view of the outstanding importance of hard scattering processes at proton–(anti-)proton colliders like the TEVATRON and the forthcoming LHC, a quantitative understanding of deep-inelastic processes is indispensable.

For quantitatively reliable predictions of DIS and hard hadronic scattering processes, perturbative QCD corrections beyond the next-to-leading order (NLO) need to be taken into account. We have therefore calculated the three-loop splitting functions for the evolution of unpolarized parton distributions of hadrons [10, 11]. Together with the second-order coefficient functions [12–16], these recent results form the complete next-to-next-to-leading order (NNLO, N^{2}LO) approximation of massless perturbative QCD for the structure functions F_1, F_2 and F_3 in DIS.

In the present article, we extend the calculation of electromagnetic (photon-exchange) DIS in perturbative QCD to the three-loop coefficient functions for both F_2 and $F_L = F_2 - 2xF_1$. This represents the first calculation of third-order perturbative corrections to hard scattering observables depending on a dimensionless variable (Bjorken-x in the case at hand) in the Standard Model. For the longitudinal structure function F_L the third-order corrections are actually required to complete the NNLO predictions, since the leading contribution to the coefficient functions is of first order in the strong coupling constant α_s. In a recent letter [17] we have already presented the corresponding results in a compact numerical form, and briefly discussed their phenomenological implications.

For the structure functions F_1 and F_2, on the other hand, the three-loop coefficient functions are part of the next-to-next-to-next-to-leading order (N^{3}LO) description of DIS in perturbative QCD. In fact, due to the fast convergence of the splitting function series [10, 11], these coefficient functions dominate the N^{3}LO corrections for not too small values of the Bjorken variable, $x \gtrsim 10^{-2}$. Thus the extraction of α_s from the scaling violations of structure functions can be effectively promoted to N^{3}LO accuracy, reducing the (formerly dominant) uncertainty due to the truncation of the perturbation series to less than 1%, see, e.g., Refs. [18–22]. The three-loop coefficient functions are also of considerable theoretical interest, for example facilitating the derivation of higher-order results for the resummation of threshold logarithms [23–28] and the quark form factor [29,30]. We will address these issues in a forthcoming publication [31].

As discussed in Refs. [10, 11], see also Refs. [32–35], the NNLO splitting functions have been determined via a Mellin-N space calculation of physical matrix elements of electromagnetic DIS at three loops in dimensional regularization with $D = 4 - 2\varepsilon$. While the splitting functions are extracted from the $1/\varepsilon$ poles, the coefficient functions are obtained from the finite terms of the physical matrix elements corresponding to the structure functions F_2 and F_L. This is possible since we have taken care to control all necessary three-loop integrals up to (and including) the finite contributions. In this respect our approach closely follows the third-order calculations of sum rules in DIS [36, 37] and of low integer moments of structure functions [38–42], however with the obvious distinction that we now derive the analytic dependence on N and, consequently, on x.

The outline of this article is as follows. In Section 2 we briefly recall the formalism, based on the operator product expansion, for calculating inclusive DIS in Mellin-N space and discuss the extraction of the anomalous dimensions (splitting functions) and coefficient functions. Section 3 explains selected details of the method to calculate the analytic N-dependence of the diagrams and addresses issues which did not occur in the calculation of the splitting functions. In Section 4 we present our results for F_2 in a compact parametrized form and discuss the end-point behaviour of the coefficient functions for F_2 and F_L. The lengthy full expressions for both coefficient functions are deferred to Appendix A (N-space) and Appendix B (x-space). The numerical implications of these results are illustrated in Section 5 before we summarize our findings in Section 6.

2 General formalism

The subject of our calculation is unpolarized inclusive deep-inelastic lepton-nucleon scattering,

$$l(k) + \mathrm{nucl}(p) \;\rightarrow\; l(k') + X \tag{2.1}$$

where X stands for all hadronic states allowed by quantum number conservation. Specifically, we here consider the lowest-order (one-photon exchange) QED contribution to this process. The hadronic part of the corresponding amplitude is given by the (spin-averaged) tensor

$$\begin{aligned} W_{\mu\nu}(p,q) &= \frac{1}{4\pi}\int d^4z\, \mathrm{e}^{\mathrm{i}q\cdot z}\, \langle \mathrm{nucl,p}|J_\mu(z)J_\nu(0)|\mathrm{nucl,p}\rangle \\ &= \left(\frac{q_\mu q_\nu}{q^2} - g_{\mu\nu}\right) F_1(x,Q^2) - (q_\mu + 2xp_\mu)(q_\nu + 2xp_\nu)\,\frac{1}{2xq^2}\, F_2(x,Q^2)\;. \end{aligned} \tag{2.2}$$

Here $|\mathrm{nucl},p\rangle$ denotes the nucleon state with momentum p, and J_μ represents the electromagnetic current. $q = k - k'$ is the momentum transferred by the lepton, $Q^2 = -q^2$, and $x = Q^2/(2p\cdot q)$ is the Bjorken variable with $0 < x \leq 1$. The longitudinal structure function F_L is related to the structure function F_1 in Eq. (2.2) by $F_L = F_2 - 2xF_1$.

The hadronic tensor $W_{\mu\nu}$ is connected by the optical theorem to the imaginary part of the forward amplitude $T_{\mu\nu}$ for the scattering of a virtual photon off the nucleon,

$$T_{\mu\nu}(p,q) = i\int d^4z\, e^{iqz}\, \langle \mathrm{nucl},p|\, T(J_\mu(z)J_\nu(0))\, |\mathrm{nucl},p\rangle\;. \tag{2.3}$$

This quantity represents a convenient starting point for practical calculations, due to the presence of the time-ordered product of currents to which standard perturbation theory applies.

Approaching the Bjorken limit, $Q^2 \to \infty$ for fixed x, the integrations in Eq. (2.2) and (2.3) are dominated by the region near the light-cone, $z^2 \approx 0$, as only there the phase of the exponential factor becomes stationary. In this situation, the operator-product expansion (OPE) can be applied to the product of currents in Eq. (2.3) together with a dispersion relation [43]. This procedure is identical to that in previous lower-order and fixed-N third-order calculations. Thus we will recall it only briefly, referring the reader to Refs. [16,40] and the reviews [44,45] for more details.

Disregarding contributions suppressed by powers of $1/Q^2$, the OPE involves the standard set of the spin-N twist-two irreducible flavour non-singlet quark, singlet quark and gluon operators,

$$\begin{aligned} O_{\rm ns}^{\{\mu_1,\ldots,\mu_N\}} &= \overline{\psi}\lambda^{\alpha}\gamma^{\{\mu_1}D^{\mu_2}\ldots D^{\mu_N\}}\psi\,, \qquad \alpha = 3,8,\ldots,(n_f^2-1)\,,\\ O_{\rm q}^{\{\mu_1,\ldots,\mu_N\}} &= \overline{\psi}\gamma^{\{\mu_1}D^{\mu_2}\ldots D^{\mu_N\}}\psi\,,\\ O_{\rm g}^{\{\mu_1,\ldots,\mu_N\}} &= F^{\nu\{\mu_1}D^{\mu_2}\ldots D^{\mu_{N-1}}F^{\mu_N\}\nu}\,, \end{aligned} \tag{2.4}$$

and their respective coefficient functions $C_{a,i}(N)$ for $a = 2, L$. Here ψ represents the quark field, $F^{\mu\nu}$ the gluon field strength tensor, and D^{μ} the covariant derivative. The diagonal generators of the flavour group $SU(n_f)$ are denoted by λ^{α}. The spin-averaged matrix elements of the (renormalized) operators in Eq. (2.4) are given by

$$\langle {\rm nucl},p|\, O_i^{\{\mu_1,\ldots,\mu_N\}}\, |{\rm nucl},p\rangle \;=\; p^{\{\mu_1}\ldots p^{\mu_N\}}A_{i,\rm nucl}(N,\mu^2)\,, \qquad i = {\rm ns, q, g}\,, \tag{2.5}$$

where μ stands for the renormalization scale. It is understood in Eqs. (2.4) and (2.5) that the symmetric and traceless part is taken with respect to the indices in curved brackets.

The application of the operator-product expansion to the forward Compton amplitude (2.3), neglecting $1/Q^2$ power corrections, leads to the expansion

$$\begin{aligned} T_{\mu\nu}(p,q) \;=\; \sum_{N,i}\left(\frac{2p\cdot q}{Q^2}\right)^N A_{i,\rm nucl}(N,\mu^2)\Bigg[&\left(g_{\mu\nu}+\frac{q_\mu q_\nu}{Q^2}\right)C_{L,i}\left(N,\frac{Q^2}{\mu^2},\alpha_s\right)\\ &-\left(g_{\mu\nu}-p_\mu p_\nu\frac{4x^2}{Q^2}-(p_\mu q_\nu+p_\nu q_\mu)\frac{2x}{Q^2}\right)C_{2,i}\left(N,\frac{Q^2}{\mu^2},\alpha_s\right)\Bigg]\,. \end{aligned} \tag{2.6}$$

The continuation of this result to the physical region $0 < x \le 1$ by a dispersion relation in the complex-x plane finally yields the even-integer Mellin-N moments of the structure functions $\frac{1}{x}F_2$ and $\frac{1}{x}F_L$ in Eq. (2.2),

$$F_a(N,Q^2) \;=\; \int_0^1 dx\, x^{N-1}\,\frac{1}{x}\,F_a(x,Q^2)\,, \tag{2.7}$$

in terms of the matrix elements (2.5) and the corresponding coefficient functions,

$$\frac{1+(-1)^N}{2}\,F_a(N,Q^2) = \sum_{i={\rm ns,q,g}} C_{a,i}\left(N,\frac{Q^2}{\mu^2},\alpha_{\rm s}\right)A_{i,\rm nucl}(N,\mu^2)\,, \qquad a = 2,L\,. \tag{2.8}$$

Note that all (complex) moments N, and thus, by the inverse of the Mellin transformation (2.7), the complete x-dependence, are uniquely fixed by analytic continuation of these even-N results.

The operators $O_{\rm q}$ and $O_{\rm g}$ in Eq. (2.4) mix under renormalization. Expressing the renormalized operators in terms of their bare counterparts, this mixing can be written as

$$O_i \;=\; Z_{ik}\, O_k^{\rm bare} \; . \tag{2.9}$$

The anomalous dimensions γ_{ik} governing the scale dependence of the operators O_i,

$$\frac{d}{d\ln\mu^2}\, O_i \;=\; -\gamma_{ik}\, O_k \;\equiv\; P_{ik}\, O_k \; , \tag{2.10}$$

are connected to the mixing matrix Z_{ik} in Eq. (2.9) by

$$\gamma_{ik} \;=\; -\left(\frac{d}{d\ln\mu^2}\, Z_{ij}\right) (Z^{-1})_{jk} \; . \tag{2.11}$$

The summation convention is understood in Eqs. (2.9) – (2.11), and the dependence on N has been suppressed for brevity. In Eq. (2.10) we have taken the opportunity to recall the conventional relation between the anomalous dimensions and the moments of the splitting functions $P_{ik}(x)$. Corresponding scalar relations, independent of the generator λ^α in Eq. (2.4), hold for the non-singlet operators collectively denoted by $O_{\rm ns}$.

In order to make practical use of Eq. (2.11) a regularization procedure and a renormalization scheme need to be selected. We choose dimensional regularization [46–49] and the modified [50] minimal subtraction [51] scheme, $\overline{\rm MS}$, the standard choice for modern higher-order calculations in QCD. For this choice the running coupling in $D = 4-2\varepsilon$ dimensions evolves according to

$$\frac{d}{d\ln\mu^2}\,\frac{\alpha_{\rm s}}{4\pi} \;\equiv\; \frac{d\,a_{\rm s}}{d\ln\mu^2} \;=\; -\varepsilon\, a_{\rm s} - \beta_0\, a_{\rm s}^2 - \beta_1\, a_{\rm s}^3 - \beta_2\, a_{\rm s}^4 - \dots \; , \tag{2.12}$$

where $\beta_{\rm n}$ denote the usual four-dimensional expansion coefficients of the beta function in QCD [52–57], $\beta_0 = 11 - 2/3\, n_f$ etc, with n_f representing the number of active quark flavours.

In this framework, the renormalization factors Z_{ik} in Eq. (2.9) and $Z_{\rm ns}$ are a series of poles in $1/\varepsilon$, expressed in terms of $\beta_{\rm n}$ and the expansion coefficients $\gamma^{(l)}$ of the anomalous dimensions in terms of $a_{\rm s}$,

$$\gamma(N) \;=\; \sum_{l=0}^{\infty} a_{\rm s}^{l+1}\, \gamma^{(l)}(N) \; . \tag{2.13}$$

For example, the expansion of $Z_{\rm ns}$ up to the third order in the coupling constant reads

$$\begin{aligned} Z_{\rm ns} \;=\;\; & 1 + a_{\rm s}\,\frac{1}{\varepsilon}\gamma_{\rm ns}^{(0)} + a_{\rm s}^2\left[\frac{1}{2\varepsilon^2}\left\{\left(\gamma_{\rm ns}^{(0)}-\beta_0\right)\gamma_{\rm ns}^{(0)}\right\} + \frac{1}{2\varepsilon}\gamma_{\rm ns}^{(1)}\right] \\ & + a_{\rm s}^3\left[\frac{1}{6\varepsilon^3}\left\{\left(\gamma_{\rm ns}^{(0)}-2\beta_0\right)\left(\gamma_{\rm ns}^{(0)}-\beta_0\right)\gamma_{\rm ns}^{(0)}\right\}\right. \\ & \left. + \frac{1}{6\varepsilon^2}\left\{3\,\gamma_{\rm ns}^{(0)}\gamma_{\rm ns}^{(1)} - 2\beta_0\,\gamma_{\rm ns}^{(1)} - 2\beta_1\,\gamma_{\rm ns}^{(0)}\right\} + \frac{1}{3\varepsilon}\gamma_{\rm ns}^{(2)}\right] \; . \end{aligned} \tag{2.14}$$

The anomalous dimensions $\gamma^{(l)}$ can thus be read off from the ε^{-1} terms of the renormalization factors at order a_s^{l+1}, while the higher poles in $1/\varepsilon$ can serve as checks for the calculation. The coefficient functions in Eq. (2.6), on the other hand, have an expansion in positive powers of ε, viz

$$C_{a,i} = \delta_{a2}\,(1-\delta_{\rm ig}) + \sum_{l=1}^{\infty} a_s^l \left(c_{a,i}^{(l)} + \varepsilon a_{a,i}^{(l)} + \varepsilon^2 b_{a,i}^{(l)} + \ldots \right) \qquad (2.15)$$

where $a = 2, L$ and i = ns, q, g, and we have again suppressed the dependence on N (and Q^2/μ^2).

Due to the non-perturbative character of the nucleon state $|\mathrm{nucl},p\rangle$, Eqs. (2.3) and (2.8) are not accessible to a perturbative computation. However, as the OPE represents an operator relation, the anomalous dimensions (2.13) and the coefficient functions (2.15) do not depend on this state. Hence the calculation can be performed using quark and gluon states $|k,p\rangle$. Instead of Eq. (2.3) we thus consider

$$T_{\mu\nu}^{k}(p,q) = i\int d^4z\, e^{iqz}\, \langle k,p|\, T\left(J_\mu(z)J_\nu(0)\right)|k,p\rangle\ , \quad k = \mathrm{ns,\ q,\ g}\ . \qquad (2.16)$$

At leading-twist accuracy the decomposition of $T_{\mu\nu}^{k}$ into $T_{2,k}$ and $T_{L,k}$ analogous to Eq. (2.2) is provided by

$$\begin{aligned} T_{L,k}(p,q) &= -\frac{q^2}{(p\cdot q)^2}\, p^\mu p^\nu\, T_{\mu\nu}^{k}(p,q) \\ T_{2,k}(p,q) &= -\left(\frac{3-2\varepsilon}{2-2\varepsilon}\,\frac{q^2}{(p\cdot q)^2}\, p^\mu p^\nu + \frac{1}{2-2\varepsilon}\, g^{\mu\nu}\right) T_{\mu\nu}^{k}(p,q) \end{aligned} \qquad (2.17)$$

with spin-averaging again being understood. The $N^{\rm th}$ moments are obtained from Eqs. (2.17) by applying the projection operator [58, 59]

$$T_{a,k}\left(N,\frac{Q^2}{\mu^2},\alpha_s,\varepsilon\right) = \left[\frac{q^{\{\mu_1}\cdots q^{\mu_N\}}}{2^N N!}\,\frac{\partial^N}{\partial p^{\mu_1}\ldots\partial p^{\mu_N}}\right] T_{a,k}(p,q,\alpha_s,\varepsilon)\bigg|_{p=0}\ , \qquad (2.18)$$

where $q^{\{\mu_1}\cdots q^{\mu_N\}}$ is the harmonic, i.e., the symmetric and traceless part of the tensor $q^{\mu_1}\cdots q^{\mu_N}$.

This operator does not act on the coefficient functions $C_{a,k}$ and the renormalization constants Z_{ik} in Eq. (2.9), which are functions only of N, a_s, and ε. It does act, however, on the bare matrix elements $A_{i,k}$ (defined analogously to Eq. (2.5)) and eliminates all diagrams containing loops, as the nullification of p transform these diagrams to massless tadpole diagrams which are zero in dimensional regularization. Hence only the matrix elements $A_{k,k}^{\rm tree}(N,\varepsilon)$ remain, leading to

$$T_{a,k}\left(N,\frac{Q^2}{\mu^2},\alpha_s,\varepsilon\right) = C_{a,i}\left(N,\frac{Q^2}{\mu^2},\alpha_s,\varepsilon\right) Z_{ik}\left(N,\alpha_s,\frac{1}{\varepsilon}\right) A_{k,k}^{\rm tree}(N,\varepsilon) \qquad (2.19)$$

for $a = 2, L$ and k = ns, q, g. Here summation over i = q, g is understood for the singlet cases k = q, g, while $C_{a,i}$ and Z_{ik} have to be replaced by $C_{a,\rm ns}$ and $Z_{\rm ns}$ of Eq. (2.14), respectively, for the non-singlet case k = ns. Expansion of (2.19) in powers of α_s and ε provides a system of equations which can be solved for the anomalous dimensions (2.13) and coefficient functions (2.15).

For brevity suppressing the function arguments for the rest of this section, the expansion of the 'master formula' (2.19) to the third order in the strong coupling α_s can by written as

$$T_{a,k} \,=\, \sum_{l=0}^{3} a_s^l \, S_\varepsilon^l \Big(\frac{\mu^2}{Q^2}\Big)^{l\varepsilon} \delta_k \, T_{a,k}^{(l)} A_{k,k}^{\rm tree} \; . \tag{2.20}$$

The factor $S_\varepsilon = \exp(\varepsilon\{\ln(4\pi) - \gamma_e\})$, where γ_e denotes the Euler-Mascheroni constant, is an artefact of dimensional regularization [46–49] kept out of the coefficient functions and anomalous dimensions in the $\overline{\rm MS}$ scheme [50]. δ_k collects the quark charge factors,

$$\delta_{\rm ns} \,=\, 1, \qquad \delta_{\rm q} \,=\, \delta_{\rm g} \,=\, \frac{1}{n_f} \sum_{i=1}^{n_f} e_{q_i}^2 \,\equiv\, \langle e^2 \rangle \; . \tag{2.21}$$

The $\alpha_s = 0$ parts $T_{2,\rm ns}^{(0)}$ and $T_{2,\rm q}^{(0)}$ can be rendered equal by a suitable normalization of non-singlet matrix elements $A_{\rm ns,ns}^{\rm tree}$. The amplitudes $T_{a,\rm ns}$ and $T_{a,\rm q}$ are then identical also at the first order in α_s. Consequently, the same holds for the anomalous dimensions and coefficient functions (recall the different counting of the superscripts in Eqs. (2.13) and (2.15)),

$$\gamma_{\rm ns}^{(0)} \,=\, \gamma_{\rm qq}^{(0)} \; , \qquad \tilde{c}_{\rm ns}^{(1)} \,=\, \tilde{c}_{\rm q}^{(1)} \; , \quad \tilde{c} = c,\, a,\, b \, \ldots \; . \tag{2.22}$$

In the expansions shown below, we will use these right-hand sides also in the results for $T_{a,\rm ns}^{(n>1)}$.

The zeroth-order contributions, with $T_{2,\rm q}^{(0)}$ being normalized by virtue of Eq. (2.21), read

$$T_{2,\rm q}^{(0)} \,=\, c_{2,\rm q}^{(0)} = 1 \; , \qquad T_{2,\rm g}^{(0)} \,=\, T_{L,\rm q}^{(0)} \,=\, T_{L,\rm g}^{(0)} \,=\, 0 \; . \tag{2.23}$$

As will become clear below, the amplitudes at the first order in α_s need to be calculated up to order ε^2 for our purposes, yielding

$$T_{2,\rm p}^{(1)} \,=\, \frac{1}{\varepsilon}\gamma_{\rm qp}^{(0)} + c_{2,\rm p}^{(1)} + \varepsilon a_{2,\rm p}^{(1)} + \varepsilon^2 b_{2,\rm p}^{(1)} \tag{2.24}$$

and

$$T_{L,\rm p}^{(1)} \,=\, c_{L,\rm p}^{(1)} + \varepsilon a_{L,\rm p}^{(1)} + \varepsilon^2 b_{L,\rm p}^{(1)} \; , \tag{2.25}$$

with p = q, g. Correspondingly the α_s^2 contributions, where the non-singlet and singlet quark amplitudes differ for the first time, are required up to order ε. These quantities are given by

$$\begin{aligned} T_{2,\rm ns}^{(2)} \,&=\, \frac{1}{2\varepsilon^2}\Big\{ \Big(\gamma_{\rm qq}^{(0)} - \beta_0\Big)\gamma_{\rm qq}^{(0)} \Big\} + \frac{1}{2\varepsilon}\Big\{ \gamma_{\rm ns}^{(1)} + 2\,c_{2,\rm q}^{(1)}\gamma_{\rm qq}^{(0)} \Big\} \\ &\quad + c_{2,\rm ns}^{(2)} + a_{2,\rm q}^{(1)}\gamma_{\rm qq}^{(0)} + \varepsilon\Big\{ a_{2,\rm ns}^{(2)} + b_{2,\rm q}^{(1)}\gamma_{\rm qq}^{(0)} \Big\} \; , \end{aligned} \tag{2.26}$$

$$\begin{aligned} T_{2,\rm p}^{(2)} \,&=\, \frac{1}{2\varepsilon^2}\Big\{ \Big(\gamma_{\rm qi}^{(0)} - \beta_0\delta_{\rm qi}\Big)\gamma_{\rm ip}^{(0)} \Big\} + \frac{1}{2\varepsilon}\Big\{ \gamma_{\rm qp}^{(1)} + 2\,c_{2,\rm i}^{(1)}\gamma_{\rm ip}^{(0)} \Big\} \\ &\quad + c_{2,\rm p}^{(2)} + a_{2,\rm i}^{(1)}\gamma_{\rm ip}^{(0)} + \varepsilon\Big\{ a_{2,\rm p}^{(2)} + b_{2,\rm i}^{(1)}\gamma_{\rm ip}^{(0)} \Big\} \; , \end{aligned} \tag{2.27}$$

where δ_{ik} is the Kronecker symbol, and

$$T^{(2)}_{L,\mathrm{ns}} = \frac{1}{\varepsilon}\left\{c^{(1)}_{L,\mathrm{q}}\gamma^{(0)}_{\mathrm{qq}}\right\} + c^{(2)}_{L,\mathrm{ns}} + a^{(1)}_{L,\mathrm{q}}\gamma^{(0)}_{\mathrm{qq}} + \varepsilon\left\{a^{(2)}_{L,\mathrm{p}} + b^{(1)}_{L,\mathrm{q}}\gamma^{(0)}_{\mathrm{qq}}\right\}\,, \tag{2.28}$$

$$T^{(2)}_{L,\mathrm{p}} = \frac{1}{\varepsilon}\left\{c^{(1)}_{L,\mathrm{i}}\gamma^{(0)}_{\mathrm{ip}}\right\} + c^{(2)}_{L,\mathrm{p}} + a^{(1)}_{L,\mathrm{i}}\gamma^{(0)}_{\mathrm{ip}} + \varepsilon\left\{a^{(2)}_{L,\mathrm{p}} + b^{(1)}_{L,\mathrm{i}}\gamma^{(0)}_{\mathrm{ip}}\right\}\,. \tag{2.29}$$

We are now finally ready to write down the third-order coefficients $T^{(3)}_{a,k}$ in Eq. (2.20), reading

$$\begin{aligned}
T^{(3)}_{2,\mathrm{ns}} = \; & \frac{1}{6\varepsilon^3}\left\{\left(\gamma^{(0)}_{\mathrm{qq}} - 2\beta_0\right)\left(\gamma^{(0)}_{\mathrm{qq}} - \beta_0\right)\gamma^{(0)}_{\mathrm{qq}}\right\} \\
& + \frac{1}{6\varepsilon^2}\left\{3\gamma^{(1)}_{\mathrm{ns}}\gamma^{(0)}_{\mathrm{qq}} - 2\beta_0\gamma^{(1)}_{\mathrm{ns}} - 2\beta_1\gamma^{(0)}_{\mathrm{qq}} + 3c^{(1)}_{2,\mathrm{q}}\left(\gamma^{(0)}_{\mathrm{qq}} - \beta_0\right)\gamma^{(0)}_{\mathrm{qq}}\right\} \\
& + \frac{1}{6\varepsilon}\left\{2\gamma^{(2)}_{\mathrm{ns}} + 3c^{(1)}_{2,\mathrm{q}}\gamma^{(1)}_{\mathrm{ns}} + 6c^{(2)}_{2,\mathrm{ns}}\gamma^{(0)}_{\mathrm{qq}} + 3a^{(1)}_{2,\mathrm{q}}\left(\gamma^{(0)}_{\mathrm{qq}} - \beta_0\right)\gamma^{(0)}_{\mathrm{qq}}\right\} \\
& + c^{(3)}_{2,\mathrm{ns}} + \frac{1}{2}a^{(1)}_{2,\mathrm{q}}\gamma^{(1)}_{\mathrm{ns}} + a^{(2)}_{2,\mathrm{ns}}\gamma^{(0)}_{\mathrm{qq}} + \frac{1}{2}b^{(1)}_{2,\mathrm{q}}\left(\gamma^{(0)}_{\mathrm{qq}} - \beta_0\right)\gamma^{(0)}_{\mathrm{qq}}\,,
\end{aligned} \tag{2.30}$$

$$\begin{aligned}
T^{(3)}_{2,\mathrm{p}} = \; & \frac{1}{6\varepsilon^3}\left\{\gamma^{(0)}_{\mathrm{qi}}\gamma^{(0)}_{\mathrm{ik}}\gamma^{(0)}_{\mathrm{kp}} - 3\beta_0\gamma^{(0)}_{\mathrm{qi}}\gamma^{(0)}_{\mathrm{ip}} + 2\beta_0^2\gamma^{(0)}_{\mathrm{qp}}\right\} \\
& + \frac{1}{6\varepsilon^2}\left\{\gamma^{(0)}_{\mathrm{qi}}\gamma^{(1)}_{\mathrm{ip}} + 2\gamma^{(1)}_{\mathrm{qi}}\gamma^{(0)}_{\mathrm{ip}} - 2\beta_0\gamma^{(1)}_{\mathrm{qp}} - 2\beta_1\gamma^{(0)}_{\mathrm{qp}} + 3c^{(1)}_{2,\mathrm{i}}\left(\gamma^{(0)}_{\mathrm{ik}} - \beta_0\delta_{\mathrm{ik}}\right)\gamma^{(0)}_{\mathrm{kp}}\right\} \\
& + \frac{1}{6\varepsilon}\left\{2\gamma^{(2)}_{\mathrm{qp}} + 3c^{(1)}_{2,\mathrm{i}}\gamma^{(1)}_{\mathrm{ip}} + 6c^{(2)}_{2,\mathrm{i}}\gamma^{(0)}_{\mathrm{ip}} + 3a^{(1)}_{2,\mathrm{i}}\left(\gamma^{(0)}_{\mathrm{ik}} - \beta_0\delta_{\mathrm{ik}}\right)\gamma^{(0)}_{\mathrm{kp}}\right\} \\
& + c^{(3)}_{2,\mathrm{p}} + \frac{1}{2}a^{(1)}_{2,\mathrm{i}}\gamma^{(1)}_{\mathrm{ip}} + a^{(2)}_{2,\mathrm{i}}\gamma^{(0)}_{\mathrm{ip}} + \frac{1}{2}b^{(1)}_{2,\mathrm{i}}\left(\gamma^{(0)}_{\mathrm{ik}} - \beta_0\delta_{\mathrm{ik}}\right)\gamma^{(0)}_{\mathrm{kp}}
\end{aligned} \tag{2.31}$$

and

$$\begin{aligned}
T^{(3)}_{L,\mathrm{ns}} = \; & \frac{1}{2\varepsilon^2}\left\{c^{(1)}_{L,\mathrm{q}}\left(\gamma^{(0)}_{\mathrm{qq}} - \beta_0\right)\gamma^{(0)}_{\mathrm{qq}}\right\} \\
& + \frac{1}{2\varepsilon}\left\{c^{(1)}_{L,\mathrm{q}}\gamma^{(1)}_{\mathrm{ns}} + 2c^{(2)}_{L,\mathrm{ns}}\gamma^{(0)}_{\mathrm{qq}} + a^{(1)}_{L,\mathrm{q}}\left(\gamma^{(0)}_{\mathrm{qq}} - \beta_0\right)\gamma^{(0)}_{\mathrm{qq}}\right\} \\
& + c^{(3)}_{L,\mathrm{n}} + \frac{1}{2}a^{(1)}_{L,\mathrm{q}}\gamma^{(1)}_{\mathrm{ns}} + a^{(2)}_{L,\mathrm{ns}}\gamma^{(0)}_{\mathrm{qq}} + \frac{1}{2}b^{(1)}_{L,\mathrm{q}}\left(\gamma^{(0)}_{\mathrm{qq}} - \beta_0\right)\gamma^{(0)}_{\mathrm{qq}}\,,
\end{aligned} \tag{2.32}$$

$$\begin{aligned}
T^{(3)}_{L,\mathrm{p}} = \; & \frac{1}{2\varepsilon^2}\left\{c^{(1)}_{L,\mathrm{i}}\left(\gamma^{(0)}_{\mathrm{ik}} - \beta_0\delta_{\mathrm{ik}}\right)\gamma^{(0)}_{\mathrm{kp}}\right\} \\
& + \frac{1}{2\varepsilon}\left\{c^{(1)}_{L,\mathrm{i}}\gamma^{(1)}_{\mathrm{ip}} + 2c^{(2)}_{L,\mathrm{i}}\gamma^{(0)}_{\mathrm{ip}} + a^{(1)}_{L,\mathrm{i}}\left(\gamma^{(0)}_{\mathrm{ik}} - \beta_0\delta_{\mathrm{ik}}\right)\gamma^{(0)}_{\mathrm{kp}}\right\} \\
& + c^{(3)}_{L,\mathrm{p}} + \frac{1}{2}a^{(1)}_{L,\mathrm{i}}\gamma^{(1)}_{\mathrm{ip}} + a^{(2)}_{L,\mathrm{i}}\gamma^{(0)}_{\mathrm{ip}} + \frac{1}{2}b^{(1)}_{L,\mathrm{i}}\left(\gamma^{(0)}_{\mathrm{ik}} - \beta_0\delta_{\mathrm{ik}}\right)\gamma^{(0)}_{\mathrm{kp}}\,.
\end{aligned} \tag{2.33}$$

Summation over $\mathrm{i,k = q,g}$ is understood in the singlet relations (2.27), (2.29), (2.31) and (2.33).

The object of the present calculation, the coefficient functions $c^{(3)}_{a,\mathrm{ns}}$ and $c^{(3)}_{a,\mathrm{p}}$ with $a = 2, L$ and $\mathrm{p = q, g}$, can therefore be extracted from the projected three-loop contributions (2.30) – (2.33) to the partonic forward-Compton amplitudes (2.16), once the respective ε^2 terms $b_{a,k}$ at one loop and ε^1 pieces $a_{a,k}$ up to two loops have been determined using Eqs. (2.24) – (2.29).

The relations (2.30) and (2.31) are also part of the system of equations from which we have determined the three-loop anomalous dimensions [10, 11]. The ε^{-1} term of Eq. (2.30) fixes one of the three non-singlet combinations, denoted by $\gamma_{\rm ns}^{(2)+}$ in Ref. [10]. To obtain the other two combinations, quark–antiquark differences inaccessible in electromagnetic DIS, we have also computed the W-exchange neutrino–nucleon structure function $F_3^{\nu N+\bar{\nu}N}$. The results for the corresponding coefficient function will be presented elsewhere. In the flavour-singlet sector, Eq. (2.31) includes $\gamma_{\rm qq}^{(2)}$ and $\gamma_{\rm qg}^{(2)}$, but, since the gluon does not directly couple to the photon, not the lower row of the anomalous dimension matrix, $\gamma_{\rm gq}^{(2)}$ and $\gamma_{\rm gg}^{(2)}$. These quantities have been computed in Ref. [11] via DIS by exchange of a (not entirely) fictitious scalar ϕ directly coupling only to gluons.

The forward Compton diagrams contributing to the present calculation of the electromagnetic three-loop coefficient functions, generated automatically with the diagram generator QGRAF [60], are enumerated in Table 1. Among the partons k in Eq. (2.16) we also include an external ghost h. This is a standard procedure, allowing us to take the sum over external gluon spins by contracting with $-g_{\mu\nu}$ instead of the full physical expression which would, due to the presence of extra powers of the gluon momentum p, lead to a considerable complication of our task. For the same reason our all-N computations have been performed in the Feynman gauge. We have however checked the gauge independence for a few low values of N using the MINCER program [61, 62]. The latest version version of FORM [63, 64] has been employed for all symbolic manipulations.

process	tree	1-loop	2-loop	3-loop
$q\gamma \to q\gamma$	1	3	25	359
$g\gamma \to g\gamma$		2	17	345
$h\gamma \to h\gamma$			2	56
sum	2	10	88	1520

Table 1: The number of diagrams for the amplitudes employed for the calculation of the three-loop coefficient functions. The sums includes a factor of two from Lorentz projections to F_2 and F_L.

We close this section by briefly noting that a new flavour structure enters at the third order in $\alpha_{\rm s}$. In this flavour structure, denoted by fl_{11} below, the in- and outgoing photons couple to different quark lines, see Fig. 1. The corresponding flavour factors are listed in Table 2. Note that these diagrams do not upset the λ^{α} independence of the non-singlet quantities, as discussed in Ref. [39].

flavour factor	fl_2	fl_{02}	fl_{11}	fl_2^g	fl_{11}^g
non-singlet	1	0	$3\langle e\rangle$	–	–
singlet	1	1	$\frac{\langle e\rangle^2}{\langle e^2\rangle}$	1	$\frac{\langle e\rangle^2}{\langle e^2\rangle}$

Table 2: The charge factors for the flavour topologies entering up to three loops, see also Ref. [40].

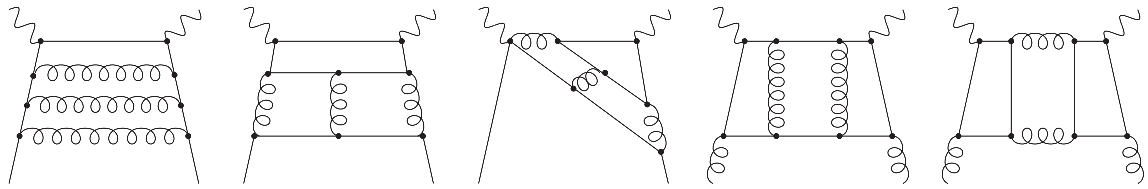

Figure 1: Representative three-loop diagrams of the flavour classes (from left to right) fl_2, fl_{02} and fl_{11} for photon–quark scattering and fl_2^g and fl_{11}^g for photon–gluon scattering.

3 Method of the calculation

In this section we discuss selected aspects relevant to our N-space calculation of the three-loop coefficient functions in DIS. Recalling Eq. (2.6) we need to extract, analytically, the coefficients of $(2p\cdot q)^N/Q^{2N}$ of the partonic forward-Compton amplitudes (2.16) up to the third order. While one of the two-loop topologies with a self-energy insertion is also not too simple, we will focus on genuine three-loop integrals, which are required to order $O(1)$ in the Laurent series in ε. Various aspects of our approach have been discussed already in Refs. [10, 11, 16, 32–35]. In particular, the key idea to systematically determine reduction identities based on sets of derivative equations for the N-th Mellin moment of a given loop integral, the solution of which leads to harmonic sums, has been explained before in these articles.

Let us start with a brief overview of the loop topologies. We need to calculate massless four-point integrals with external momenta p, $p^2 = 0$, and q, $q^2 \neq 0$. Classifying the topologies of these integrals is a two-stage process. It begins with two-point functions of the external momentum q. Here we follow the notations of Refs. [61, 62] recalled in Fig. 2 for the top-level topologies, the ladder (LA), benz (BE) and non-planar (NO) topologies. Other three-loop topologies are special cases of LA, BE or NO, with one or more of the lines $1,\ldots,8$ missing. A complete list is provided in Table 3 below. The most important examples denoted FA and BU are shown in Fig. 3.

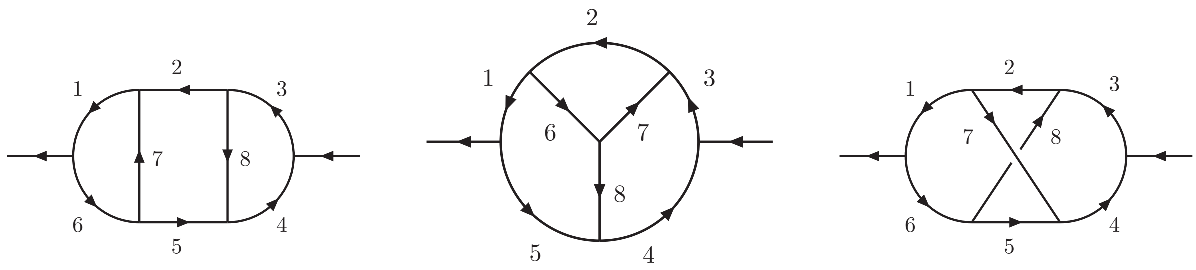

Figure 2: The top-level two-point topologies LA (left), BE (center) and NO (right) at three loops. The arrows indicate the assigned momentum flow. The external momentum is q with $q^2 \neq 0$.

Subsequently all four-point functions can be constructed from these two-point functions by attaching two p-dependent external legs in all topologically independent ways to the various lines. When the four-point functions have been constructed in this way, we are referring to subtopologies.

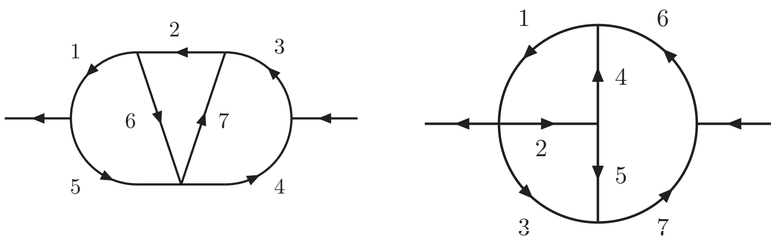

Figure 3: As Fig. 2, but for the second-level topologies FA (left) and BU (right).

For instance, NO_{25} is a subtopology of type NO in which the momentum p enters in line 2 and leaves in line 5, employing the numbering of the NO topology as in Fig. 2. Then we define basic building blocks (BBBs) as integrals in which both the incoming and the outgoing p-momentum are attached to the same line as, for instance, in LA_{11}. Composite building blocks (CBBs), on the other hand, have incoming and outgoing p-momentum attached to different lines, as in the case of NO_{25} mentioned above. At the top level, there are 10 BBBs (3 LA, 5 BE and 2 NO) and 32 CBBs (10 LA, 16 BE and 6 NO), the smaller number of non-planar topologies being due to symmetries.

Solving all four-point integrals in Mellin N-space in terms of harmonic sums [65–69] and the values ζ_3, ζ_4 and ζ_5 of the Riemann ζ-function requires an elaborate reduction scheme. This scheme is derived from algebraic relations based on integration by parts [46, 70–72], scaling equations, form-factor analysis [73] and some equations [10] that fall in a special category because they involve higher twist and a careful study of the parton-momentum limit $p \cdot p \to 0$.

Within this scheme, as a first step, we systematically reduce all CBB integrals to such of BBB type. This is necessary because a direct application of the projection operator (2.18) on the CBBs is not recommendable. The resulting brute-force expansions would generate sums which are not in the class of single-parameter nested sums, and could therefore not be solved with the algorithms used to express the result in harmonic sums [65–69]. The second step of the reduction scheme consists of successively simplifying the topologies. For example, if one line is removed from the top-level diagrams of Fig. 2, its topology is reduced according to

$$\mathrm{NO} \longrightarrow \mathrm{BU, FA}\ , \qquad \mathrm{BE} \longrightarrow \mathrm{BU, FA}, \ldots\ , \qquad \mathrm{LA} \longrightarrow \mathrm{FA}, \ldots\ , \tag{3.1}$$

where topologies below the level of Fig. 3 have not been written out.

The main problem we are faced with, as compared to the corresponding two-loop calculation [16], is that the reduction equations become much more complicated. This requires extensive automatization and the standard approach proceeds as follows. One writes down all equations based on the relations between integrals mentioned above and combines them to construct equations that can systematically bring the powers of the denominators in a given integral down, either reducing them to zero or leaving them at a fixed unique value. When a line is eliminated a simpler topology or subtopology is reached. Then we can refer to the reduction equations for that topology and so on. Eventually, this procedure will lead to an integral simple enough to be evaluated.

Different methods have emerged over the last years for practical implementations. One approach, commonly referred to as the Laporta algorithm [74–77], consists of systematically solving the system of linear equations of a given topology for a set of integrals with fixed numerical combinations of powers of numerators and denominators. The result for each integral of the set is one algebraic relation in terms of a unique (small) set of so-called master integrals. This approach works well for a large variety of processes and has been successfully automated [78, 79].

Another approach follows the original MINCER paper [61, 62] and also attempts to solve the system of linear equations for a given topology, but using symbolic lowering (and raising) operators for all numerators and denominators occurring in a given topology. This leads to a chain of algebraic relations for any given integral which maps it, for fixed numerical values of the numerator and denominator powers, to the same unique set of master integrals.

We have adopted the MINCER approach (although not in a fully systematic manner for some very difficult subtopologies) for two reasons. Firstly, we have encountered such a huge number of different integrals that we have made no attempt at a fully complete tabulation. Secondly, and more importantly, because we need to calculate the Mellin moments (coefficient of $(2p\cdot q)^N/Q^{2N}$) of the integrals for symbolic N, it is necessary to look for operator relations. For a given integral $I(N)$ these operator relations give rise to difference equations, which can generally be written as

$$a_0(N)\,I(N)+a_1(N)\,I(N-1)+\ldots+a_m(N)\,I(N-m) \;=\; G(N)\;, \tag{3.2}$$

where the inhomogeneous term $G(N)$ collects the simpler integrals resulting, e.g., from removing one or more lines. Such recursion relations in N (or, in the above terminology, m-th order difference equations) were introduced to loop calculations in Ref. [80]. The solution of Eq. (3.2) requires m boundary conditions $I(0),\ldots,I(m-1)$, which can be computed with the standard MINCER techniques [61, 62].

Single-step difference equations can be summed analytically in a closed form. The solution of Eq. (3.2) for $m=1$ reads

$$I(N) \;=\; \frac{\prod_{j=1}^{N} a_1(j)}{\prod_{j=1}^{N} a_0(j)}\, I(0) \;+\; \sum_{i=1}^{N} \frac{\prod_{j=i+1}^{N} a_1(j)}{\prod_{j=i}^{N} a_0(j)}\, G(i)\;. \tag{3.3}$$

In case that the functions $a_i(N)$ can be factorized in linear polynomials in N of the type $N+m+n\varepsilon$ with integer m,n, the products can be written as combinations of Γ-functions. In the presence of parametric dependence on ε the Γ-functions should be expanded around $\varepsilon=0$. This will lead to factorials and harmonic sums. If the function $G(N)$ is expressed as a Laurent series in ε with the coefficients being combinations of harmonic sums in $N+m$ and powers of $N+m$, with m a fixed integer, the sum in Eq. (3.3) can be performed, and $I(N)$ is expressed as a combination of harmonic sums in $N+k$ and powers of $N+k$, where k is a fixed integer. A condition for a solution in terms of harmonic sums, to which we will refer later below Eq. (3.14), is that the highest powers in N in the polynomials a_0 and a_1 have prefactors with the same modulus.

Higher-order difference equations require a completely different approach. Under conditions which are fulfilled by all cases we have encountered in the present calculation, their solution can be expressed in terms of harmonic sums, and hence a corresponding ansatz can by used. Suppose we have for some integral $I(N)$ a relation like Eq. (3.2) with $m \geq 2$. The inhomogeneous function $G(N)$ is again assumed to be a Laurent series in ε with the coefficients being combinations of harmonic sums in $N+k$ with a fixed integer k. The functions $a_i(N)$ in Eq. (3.2) are polynomials in N and ε subject to certain conditions. In order to solve for $I(N)$ under these assumptions, we write down an ansatz in powers of ε, harmonic sums $S_{\vec{m}}$ of given weight, possibly in combination with values of the ζ-function and factors $(-1)^N$. The harmonic sums have arguments $N+l$, where the integer l samples the various offsets. One may have to introduce positive powers of N^k multiplying the harmonic sums as well (see also the discussion below). Thus $I(N)$ is written as

$$
\begin{aligned}
I(N) \quad = \quad & \sum c_+(j,k,l,\vec{m})\,\varepsilon^j\,(N-l)^k\,S_{\vec{m}}(N-l) + \\
& \sum c_-(j,k,l,\vec{m})\,\varepsilon^j\,(-1)^N\,(N-l)^k\,S_{\vec{m}}(N-l) + \\
& \sum c_+(j,k,l,\vec{m},n)\,\varepsilon^j\,(N-l)^k\,\zeta_n\,S_{\vec{m}}(N-l) + \\
& \sum c_-(j,k,l,\vec{m},n)\,\varepsilon^j\,(-1)^N\,(N-l)^k\,\zeta_n\,S_{\vec{m}}(N-l)\;. \qquad (3.4)
\end{aligned}
$$

The sum runs over a suitable set of the parameter space spanned by the powers ε^j, the weight $\vec{m}$ of the harmonic sums, positive powers N^k, and the offset l in the argument of the harmonic sums. For efficiency, it is important to take into account the correlation between the loop order and the weight of harmonic sums in the ansatz, i.e. in the choice of the parameter set $j,k,l,\vec{m},n$. In the case of DIS structure functions, one- (two-, three-) loop integrals can be expressed, at order ε^0, in terms of harmonic sums up to weight two (four, six). Accordingly, the single (double, triple) pole terms in ε are expressed through harmonic sums with maximal weights decreased by one (two, three).

The solution for the integral $I(N)$ is obtained by determining the coefficients c_- and c_+. To that end, we insert the ansatz (3.4) into Eq. (3.2) and normalize the left hand side by pulling all expressions back to the unique basis in harmonic sums. This synchronization can be performed with the algorithms of the SUMMER package [67] in FORM. The coefficients of all individual terms such as $\varepsilon^j\,(-1)^N\,(N-l)^k\,S_{\vec{m}}(N-l)\,\zeta_n$ then determine a set of linear equations for the unknown c_- and c_+ in our ansatz (3.4), which can be solved by standard means if the chosen parameter set $j,k,l,\vec{m},n$ was large enough. In practice, an iterative procedure for the determination of the coefficients c_- and c_+ is advantageous, since an improved ansatz reduces the size of the system of equations. We will give an explicit example for a two-step difference equation below.

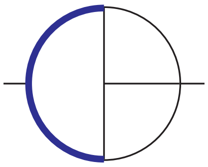

$$= \frac{(2p\cdot q)^N}{(Q^2)^{N+\alpha}}\,\mathrm{BE}_{15}(N)\;,$$

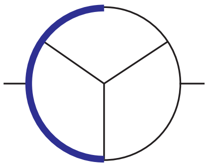

$$= \frac{(2p\cdot q)^N}{(Q^2)^{N+\alpha}}\,\mathrm{BE}_{25}(N)$$

Figure 4: Generic BE_{15} (BU-type) and BE_{25} subtopologies. The momenta q and p (fat lines) flow from right to left and from top to bottom through the diagram, respectively.

A crucial issue in the derivation of reduction relations is the implementation of symmetries of the Feynman integrals under consideration, because the discrete symmetries are reflected in the

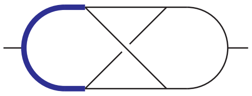 $= \frac{(2p\cdot q)^N}{(Q^2)^{N+\alpha}} \mathrm{NO}_{16}(N)$, 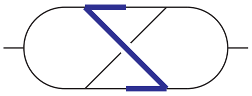 $= \frac{(2p\cdot q)^N}{(Q^2)^{N+\alpha}} \mathrm{NO}_{25}(N)$

Figure 5: As Fig. 4, but for the generic NO_{16} and NO_{25} topologies.

recursion relations. In the presence of an even-N symmetry, the odd coefficients $a_1, a_3, \ldots$ vanish in Eq. (3.2). Particular examples which we like to mention here are the even-N symmetry of the BE_{15} (BU-type), BE_{25}, NO_{16} and NO_{25} topologies shown in Figs. 4 and 5. Here and below, the fat lines indicate the flow of the parton momentum p through the diagram. The equations in Figs. 4 and 5 indicate that we calculate the N-th Mellin moment of the respective diagram, given precisely by the dimensionless functions of N written on the right-hand sides.

The discrete symmetry in N of the examples displayed in Figs. 4 and 5 is realized as follows. BE_{15} which is actually a certain BU-type since the line 3 is missing, can be turned upside down under interchange of the pairs of lines (1,5), (2,4) and (6,8) (see the labeling in Fig. 2) and $p \to -p$, which introduces a factor of $(-1)^N$. BE_{25} can be flipped around the vertical axis, interchanging the pairs of lines (1,3), (4,5) and (6,7) and $q \to -q$, which again leads to a factor of $(-1)^N$. In addition, the p-momentum flow has to be rerouted internally. The situation is similar for NO_{16}, which can be turned upside down, and for NO_{25}. In the latter case two symmetry operations are possible, either turning it upside down or flipping around the vertical axis, both choices requiring also the p-momentum flow to be rerouted internally.

To illustrate the discussion of recursion relations and symmetries, let us present as an example the basic integral of the NO_{25} topology. The general scalar NO_{25} integral is defined by

$$\begin{aligned} \mathrm{NO}_{25}(N;n_1,\ldots,n_6,n_8,m_2,m_5,m_7) &= (Q^2)^{n_1+\ldots+n_6+n_8+m_2+m_5+m_7-6+3\varepsilon} \cdot \\ \cdot P_N \int \prod_{n=1}^{3} d^D l_n \Big[&(l_1)^{2n_1} (l_2)^{2n_2} (l_2+p)^{2m_2} (l_3)^{2n_3} (l_3-q)^{2n_4} (l_1-l_2+l_3-q)^{2n_5} \cdot \\ &\cdot (l_1-l_2+l_3-q-p)^{2m_5} (l_1-q)^{2n_6} (l_2-l_1+p)^{2m_7} (l_2-l_3)^{2n_8} \Big]^{-1} , \end{aligned} \tag{3.5}$$

where P_N represents the Mellin-N projection (2.18), and $l_{1,2,3}$ denote the loop momenta in the notation of Fig. 2. The integral we now consider was among the most complicated ones of the whole calculation,

$$\mathrm{NO}_{25}(N;1,1,1,1,1,1,1,1,1,1) \equiv \mathrm{NO}_{25}(N;\mathbf{1}_{10}) , \tag{3.6}$$

where we have introduced a short-hand notation for m identical arguments i,

$$\mathbf{i}_m = \underbrace{i,\ldots,i}_{m} . \tag{3.7}$$

We obtain a two-step recursion relation, $m=2$ in Eq. (3.2), for $\mathrm{NO}_{25}(N;\mathbf{1}_{10})$ with the coefficients

$$\begin{aligned} a_0(N) &= -(N+4+4\varepsilon)(N+2)(N+1-2\varepsilon) , \\ a_1(N) &= 0 , \\ a_2(N) &= (N+4+6\varepsilon)(N+3+3\varepsilon)(N+2+3\varepsilon) . \end{aligned} \tag{3.8}$$

Using the short-hand notation (3.7) the corresponding function $G_{\rm NO}(N)$, expressed in terms of simpler (sub-) topologies, reads

$$
\begin{aligned}
G_{\rm NO}(N) \; = & \\
& (N+4+4\varepsilon)(N+2-2\varepsilon)(N+1-2\varepsilon)\{\mathrm{NO}_{25}(N+1;1,0,\mathbf{1}_8)-\mathrm{NO}_{25}(N+1;\mathbf{1}_4,0,\mathbf{1}_5) \\
& -\mathrm{NO}_{25}(N+1;\mathbf{1}_7,0,\mathbf{1}_2)+\mathrm{NO}_{25}(N+1;\mathbf{1}_8,0,1)\} \\
& +(N+4+4\varepsilon)(N+1-2\varepsilon)\{\mathrm{NO}_{25}(N;2,\mathbf{1}_8,0)-\mathrm{NO}_{25}(N;1,0,2,\mathbf{1}_7)-\mathrm{NO}_{25}(N;\mathbf{1}_3,2,\mathbf{1}_5,0) \\
& -2\mathrm{NO}_{25}(N;1,0,\mathbf{1}_5,2,\mathbf{1}_2)-\mathrm{NO}_{25}(N;\mathbf{1}_5,2,0,\mathbf{1}_3)+\mathrm{NO}_{25}(N;\mathbf{1}_3,2,\mathbf{1}_4,0,1) \\
& +\mathrm{NO}_{25}(N;\mathbf{1}_2,2,\mathbf{1}_3,0,\mathbf{1}_3)+\mathrm{NO}_{25}(N;\mathbf{1}_4,0,2,\mathbf{1}_4)\} \\
& +(N+4+4\varepsilon)(N+3+3\varepsilon)(N+1-2\varepsilon)\{\mathrm{NO}_{25}(N;\mathbf{1}_2,0,\mathbf{1}_7)-\mathrm{NO}_{25}(N;\mathbf{1}_5,0,\mathbf{1}_4) \\
& -\mathrm{NO}_{25}(N;\mathbf{1}_3,0,\mathbf{1}_6)+\mathrm{NO}_{25}(N;0,\mathbf{1}_9)\}+2(N+2+\varepsilon)(N+1-2\varepsilon)\{\mathrm{NO}_{25}(N;2,\mathbf{1}_3,0,\mathbf{1}_5) \\
& -\mathrm{NO}_{25}(N;2,\mathbf{1}_7,0,1)\}+(N+3+3\varepsilon)(N+1-2\varepsilon)(N-2\varepsilon)\{\mathrm{NO}_{25}(N;\mathbf{1}_4,0,\mathbf{1}_5) \\
& -\mathrm{NO}_{25}(N;\mathbf{1}_8,0,1)+\mathrm{NO}_{25}(N;\mathbf{1}_7,0,\mathbf{1}_2)-\mathrm{NO}_{25}(N;1,0,\mathbf{1}_8)\} \\
& -(N+1-2\varepsilon)(N-2\varepsilon)\mathrm{NO}_{25}(N;2,\mathbf{1}_6,0,\mathbf{1}_2)-2(2+3\varepsilon)(N+1-2\varepsilon)\mathrm{NO}_{25}(N;2,0,\mathbf{1}_8) \\
& +2(N+2+\varepsilon)\{\mathrm{NO}_{25}(N-1;2,\mathbf{1}_4,2,0,\mathbf{1}_3)-\mathrm{NO}_{25}(N-1;2,0,2,\mathbf{1}_7) \\
& -\mathrm{NO}_{25}(N-1;2,\mathbf{1}_3,0,2,\mathbf{1}_4)+\mathrm{NO}_{25}(N-1;2,1,2,\mathbf{1}_3,0,\mathbf{1}_3)\} \\
& +2(2+3\varepsilon)\{\mathrm{NO}_{25}(N-1;2,\mathbf{1}_2,2,\mathbf{1}_4,0,1)-\mathrm{NO}_{25}(N-1;2,\mathbf{1}_2,2,\mathbf{1}_5,0) \\
& +2\mathrm{NO}_{25}(N-1;3,\mathbf{1}_6,0,\mathbf{1}_2)-2\mathrm{NO}_{25}(N-1;3,\mathbf{1}_8,0)\} \\
& +(N+3+3\varepsilon)(N-2\varepsilon)\{2\mathrm{NO}_{25}(N-1;\mathbf{1}_8,0,2)-2\mathrm{NO}_{25}(N-1;2,\mathbf{1}_5,0,\mathbf{1}_3) \\
& +\mathrm{NO}_{25}(N-1;1,0,2,\mathbf{1}_7)-\mathrm{NO}_{25}(N-1;\mathbf{1}_5,2,0,\mathbf{1}_3)+\mathrm{NO}_{25}(N-1;\mathbf{1}_3,2,\mathbf{1}_5,0) \\
& +\mathrm{NO}_{25}(N-1;\mathbf{1}_4,0,2,\mathbf{1}_4)-2\mathrm{NO}_{25}(N-1;\mathbf{1}_3,0,\mathbf{1}_5,2)-\mathrm{NO}_{25}(N-1;\mathbf{1}_3,2,\mathbf{1}_4,0,1) \\
& -\mathrm{NO}_{25}(N-1;\mathbf{1}_2,2,\mathbf{1}_3,0,\mathbf{1}_3)+\mathrm{NO}_{25}(N-1;2,\mathbf{1}_6,0,\mathbf{1}_2)+2\mathrm{NO}_{25}(N-1;2,\mathbf{1}_7,0,1) \\
& -\mathrm{NO}_{25}(N-1;2,\mathbf{1}_8,0)\}+2(2+3\varepsilon)(N+3+3\varepsilon)\{\mathrm{NO}_{25}(N-1;2,\mathbf{1}_2,0,\mathbf{1}_6) \\
& -\mathrm{NO}_{25}(N-1;2,1,0,\mathbf{1}_7)-\mathrm{NO}_{25}(N-1;2,\mathbf{1}_4,0,\mathbf{1}_4)\} \\
& +2(N+3+3\varepsilon)\{\mathrm{NO}_{25}(N-2;2,\mathbf{1}_3,0,2,\mathbf{1}_4)-\mathrm{NO}_{25}(N-2;2,\mathbf{1}_4,2,0,\mathbf{1}_3) \\
& -\mathrm{NO}_{25}(N-2;2,1,2,\mathbf{1}_3,0,\mathbf{1}_3)+\mathrm{NO}_{25}(N-2;2,0,2,\mathbf{1}_7)\} \\
& +(N+3+3\varepsilon)(N+2+3\varepsilon)(N-2\varepsilon)\{\mathrm{NO}_{25}(N-1;\mathbf{1}_5,0,\mathbf{1}_4)-\mathrm{NO}_{25}(N-1;0,\mathbf{1}_9) \\
& -\mathrm{NO}_{25}(N-1;\mathbf{1}_2,0,\mathbf{1}_7)+\mathrm{NO}_{25}(N-1;\mathbf{1}_3,0,\mathbf{1}_6)\} \\
& +2(N+3+3\varepsilon)(N+2+3\varepsilon)\{\mathrm{NO}_{25}(N-2;1,0,\mathbf{1}_5,2,\mathbf{1}_2)-\mathrm{NO}_{25}(N-2;\mathbf{1}_4,0,2,\mathbf{1}_4) \\
& +\mathrm{NO}_{25}(N-2;\mathbf{1}_3,0,\mathbf{1}_5,2)-\mathrm{NO}_{25}(N-2;\mathbf{1}_8,0,2)+\mathrm{NO}_{25}(N-2;\mathbf{1}_5,2,0,\mathbf{1}_3) \\
& -\mathrm{NO}_{25}(N-2;2,\mathbf{1}_3,0,\mathbf{1}_5)+\mathrm{NO}_{25}(N-2;2,\mathbf{1}_5,0,\mathbf{1}_3)\}\,.
\end{aligned} \tag{3.9}
$$

Each term of $G_{\rm NO}(N)$ has to be determined in terms of harmonic sums by finding and solving the appropriate reduction equations (which in turn involve simpler integrals which have to be solved by more reduction equations, etc). Once all that has been done, $G_{\rm NO}(N)$ can finally be used to solve the difference equation (3.2) with the coefficients (3.8) for $\mathrm{NO}_{25}(N;\mathbf{1}_{10})$, using an ansatz (3.4).

Since the complete results for both $G_{\rm NO}(N)$ and $\mathrm{NO}_{25}(N;\mathbf{1}_{10})$ contain of the order of 1000 terms, they are too long to be presented here. However we write down the two leading poles in ε for illustration. We choose a compact representation for the harmonic sums, employing the abbreviation $S_{\vec{m}} \equiv S_{\vec{m}}(N)$, together with the notation

$$\mathbf{N}_{\pm} S_{\vec{m}} = S_{\vec{m}}(N \pm 1) , \qquad \mathbf{N}_{\pm\mathbf{i}} S_{\vec{m}} = S_{\vec{m}}(N \pm i) , \tag{3.10}$$

for arguments shifted by ± 1 or a larger integer i. In the G-scheme [61,81], in which l-loop integrals are divided by the l-th power of the basic massless one-loop integral, $G_{\rm NO}(N)$ then reads

$$\begin{aligned}
G_{\rm NO}(N) \;=\; & \frac{16}{3\varepsilon^3}(1+(-1)^N)\Big(6-(8+6N+N^2)\Big[3S_{-3}-2S_{-2,1}+S_3\Big]-(13+4N)\Big[S_{-2} \\
& +S_2\Big]-7S_1-3\mathbf{N}_{+\mathbf{2}}S_1+(3-3\mathbf{N}_{+}-\mathbf{N}_{+\mathbf{2}}+\mathbf{N}_{+\mathbf{3}})\Big[S_{1,-2}+S_{1,1}+S_{1,2}+2S_{2,1}-S_2-2S_3\Big] \\
& +11S_{1,1}-11S_2-\mathbf{N}_{+}\Big[13S_{1,1}-17S_2\Big]+2\mathbf{N}_{+\mathbf{2}}\Big[S_{1,1}-3S_2\Big]\Big)+\frac{16}{3\varepsilon^2}(1+(-1)^N)(-24 \\
& +(8+6N+N^2)\Big[\frac{79}{4}S_{-4}+\frac{37}{4}S_{-3}-\frac{85}{4}S_{-3,1}-S_{-2,-2}-\frac{11}{2}S_{-2,1}+10S_{-2,1,1}-\frac{13}{2}S_{-2,2} \\
& +\frac{11}{2}S_{1,-2,1}-\frac{37}{4}S_{1,-3}-\frac{7}{2}S_{1,3}+2S_{2,-2}+S_{2,2}+\frac{7}{2}S_3-\frac{1}{2}S_{3,1}+\frac{17}{4}S_4\Big]-N\Big[\frac{93}{8}S_{-3} \\
& -\frac{17}{2}S_{-2}-\frac{7}{4}S_{-2,1}+9S_{1,-2}+\frac{21}{2}S_{1,2}-\frac{41}{4}S_2+\frac{11}{2}S_{2,1}+\frac{11}{4}S_3\Big]-\frac{87}{2}S_{-3}+\frac{39}{4}S_{-2} \\
& +16S_{-2,1}+9S_1-\frac{111}{4}S_{1,-2}-\frac{101}{2}S_{1,1}+55S_{1,1,1}-\frac{437}{8}S_{1,2}+\frac{329}{8}S_2-\frac{393}{4}S_{2,1}+\frac{345}{8}S_3 \\
& +(3-3\mathbf{N}_{+}-\mathbf{N}_{+\mathbf{2}}+\mathbf{N}_{+\mathbf{3}})\Big[\frac{7}{4}S_{1,-3}+\frac{7}{4}S_{1,-2}-2S_{1,-2,1}-S_{1,1}+5S_{1,1,1}+\frac{3}{2}S_{1,1,-2} \\
& +\frac{9}{4}S_{1,1,2}-\frac{1}{4}S_{1,2}+\frac{7}{4}S_{1,2,1}-\frac{11}{4}S_{1,3}+S_2+10S_{2,1,1}-\frac{31}{4}S_{2,2}-3S_{2,-2}-\frac{7}{2}S_{2,1}+\frac{1}{2}S_3 \\
& -\frac{83}{4}S_{3,1}+\frac{31}{2}S_4\Big]+\mathbf{N}_{+}\Big[14S_1+\frac{1}{4}S_{1,-2}+\frac{163}{8}S_{1,1}-65S_{1,1,1}+\frac{227}{8}S_{1,2}-\frac{113}{8}S_2 \\
& +\frac{381}{4}S_{2,1}-\frac{443}{8}S_3\Big]+\mathbf{N}_{+\mathbf{2}}\Big[16S_1+\frac{1}{2}S_{1,-2}-\frac{159}{8}S_{1,1}+10S_{1,1,1}-\frac{27}{4}S_{1,2}+\frac{57}{8}S_2 \\
& -16S_{2,1}+\frac{41}{4}S_3\Big]\Big) \;+\; O\Big(\frac{1}{\varepsilon}\Big) \;.
\end{aligned} \tag{3.11}$$

Note the positive powers of N multiplying some harmonic sums in Eq. (3.11). We will return to this issue below. The boundary conditions for the $\mathrm{NO}_{25}(N;\mathbf{1}_{10})$ integral of Eq. (3.6) are shorter,

$$\begin{aligned}
\mathrm{NO}_{25}(0;\mathbf{1}_{10}) &= -\frac{10}{3}\frac{1}{\varepsilon^3}+\frac{1}{3}\frac{1}{\varepsilon^2}+O\Big(\frac{1}{\varepsilon}\Big) , \\
\mathrm{NO}_{25}(1;\mathbf{1}_{10}) &= 0 .
\end{aligned} \tag{3.12}$$

Finally the following expression for $\mathrm{NO}_{25}(N;\mathbf{1}_{10})$ in the G-scheme is obtained:

$$\begin{aligned}
\mathrm{NO}_{25}(N;\mathbf{1}_{10}) \;=\; & \frac{16}{3}(1+(-1)^N)\frac{1}{\varepsilon^3}\Big(-\frac{3}{2}S_{-3}+S_{-2,1}+(\mathbf{N}_{+\mathbf{2}}-2\mathbf{N}_{+\mathbf{3}}+\mathbf{N}_{+\mathbf{4}})\Big[S_1+S_{1,1}-S_2\Big] \\
& +\frac{1}{2}(\mathbf{N}_{+\mathbf{2}}-\mathbf{N}_{+\mathbf{4}})\Big[S_{1,-2}+S_{1,2}\Big]+(1-2\mathbf{N}_{+}+2\mathbf{N}_{+\mathbf{2}})\Big[S_{2,1}-\frac{3}{2}S_3\Big]-\mathbf{N}_{+\mathbf{3}}S_{2,1}+\mathbf{N}_{+\mathbf{4}}S_3\Big)
\end{aligned}$$

$$
\begin{aligned}
&+\frac{16}{3}(1+(-1)^N)\frac{1}{\varepsilon^2}\Big(\frac{79}{8}S_{-4}+\frac{15}{2}S_{-3}-\frac{85}{8}S_{-3,1}-\frac{1}{2}S_{-2,-2}-5S_{-2,1}+5S_{-2,1,1}-\frac{13}{4}S_{-2,2}\\
&+(\mathbf{N_{+2}}-2\mathbf{N_{+3}}+\mathbf{N_{+4}})\Big[\frac{27}{16}S_{1,-3}-\frac{3}{2}S_{1,-2}-\frac{9}{4}S_{1,-2,1}-11S_1-4S_{1,1}-\frac{3}{2}S_{1,1,-2}+5S_{1,1,1}\\
&-\frac{3}{2}S_{1,1,2}-\frac{3}{2}S_{1,2}-\frac{1}{2}S_{1,2,1}-\frac{1}{2}S_{1,3}-9S_{2,1}+\frac{7}{2}S_{2,2}+5S_3\Big]-(1-2\mathbf{N_+}+2\mathbf{N_{+2}})\Big[\frac{1}{2}S_{2,-2}\\
&+5S_{2,1}-5S_{2,1,1}+\frac{13}{4}S_{2,2}-\frac{15}{2}S_3+\frac{85}{8}S_{3,1}-\frac{79}{8}S_4\Big]+(\mathbf{N_{+2}}-\mathbf{N_{+3}})\Big[\frac{9}{4}S_{1,1,-2}+\frac{21}{8}S_{1,1,2}\\
&-4S_{1,2}+\frac{11}{8}S_{1,2,1}+7S_2+6S_{2,1}\Big]-\mathbf{N_{+2}}\Big[\frac{87}{16}S_{1,-3}+2S_{1,-2}-4S_{1,-2,1}+\frac{21}{8}S_{1,3}+\frac{29}{8}S_{2,2}\\
&+5S_3\Big]+\mathbf{N_{+3}}\Big[\frac{7}{8}S_{1,3}-2S_{2,-2}+5S_{2,1}-5S_{2,1,1}+\frac{59}{8}S_{2,2}+\frac{51}{8}S_{3,1}-\frac{7}{4}S_4\Big]+\mathbf{N_{+4}}\Big[\frac{13}{16}S_{1,-3}\\
&+2S_{1,-2}-\frac{5}{4}S_{1,-2,1}+\frac{7}{2}S_{2,-2}+4S_{3,1}-6S_4\Big]\Big)\;+\;O\Big(\frac{1}{\varepsilon}\Big)\;. \qquad (3.13)
\end{aligned}
$$

In the remainder of this section we briefly address three issues which are, to a varying extent, special to the calculation of the coefficient functions. The first is the control of the expansion in powers of the dimensional offset ε. This is more critical here than for the computation of the anomalous dimensions [10, 11], as we now rely on the last coefficients in ε kept in Eqs. (2.24) – (2.33). In other words, if some three-loop integrals entering the diagram calculation were actually not accurate to order ε^0 (something, in fact, our extensive fixed-N checks using the MINCER program [61,62] would have indicated), then that would not have affected the results for the anomalous dimensions, but spoiled the present calculation of the coefficient functions.

The one- (two-, three-) loop integrals are required to order ε^2 (ε^1, ε^0) for the calculation of the respective diagrams entering Eqs. (2.24) – (2.33). However, all but the top-level topologies are also required in the reduction schemes for higher-level topologies. Guided by the rule of the triangle [70–72], a factor $1/\varepsilon$ is expected for each line (completely) removed, which then has to be compensated by controlling the lower-level topologies to one more power in ε. If this pattern holds, the various topologies are maximally required to the accuracies shown in Table 3. For instance, the LA topology in Fig. 2 is reduced to FA case in Fig. 3 by removing line 2 or line 5.

number of loops	topologies	expansion depth
1	L1	ε^5
2	T2, T3	ε^4
2	T1	ε^3
3	Y1, ..., Y5	ε^3
3	O1, ..., O4	ε^2
3	FA, BU	ε^1
3	LA, BE, NO	ε^0

Table 3: The two-point topologies up to three loops, using the notation of Refs. [61, 62], with the maximal power of ε kept for the determination of the third-order coefficient functions.

If a reduction equation introduces a factor ε^{-2} while removing a line, or a factor ε^{-1} in a simplification not removing a line, the equation is said to contain a spurious pole. The lower-level topologies are worked out to a finite accuracy as well, either for efficiency or since the underlying integrals, for instance providing the boundary conditions for Eq. (3.2), are known only to a certain accuracy in ε. Therefore spurious poles endanger the integrity of the reduction procedure. Indeed, one of the greatest difficulties in constructing reduction schemes is to avoid such poles.

Actually, for some cases we have not found expressions free of spurious poles. Consequently these integrals have not been calculated to the design order in ε. For instance, most $\mathrm{O1}_{15}$ integrals, generated by removing line 2 from the FA_{17} subtopology, have only been computed to order ε instead of including the ε^2 terms as indicated in Table 3. This was only permissible since in fact many more reductions are actually more benign than the triangle reduction, removing lines without introducing any ε^{-1} pole, see, e.g., Eq. (3.9). Carefully utilizing this fact, we were able to reach the required ε^0 accuracy for all three-loop integrals entering the diagram calculations.

The second issue specific for the calculation of the coefficient functions is the appearance of one integral (finite for $\varepsilon \to 0$) which can not be expressed in terms of harmonic sums. This integral, denoted by $\mathrm{LA}_{27}\mathrm{box}$ and graphically illustrated in Fig. 6, is given by

$$\begin{aligned}
\mathrm{LA}_{27}\mathrm{box}(N) \;=\; & (Q^2)^{2+3\varepsilon}\, P_N \int \prod_{n=1}^{3} d^D l_n \,\cdot \qquad (3.14)\\
& \cdot \Big[(l_1)^2\,(l_2+p)^2\,(l_3)^2\,(l_3-q)^2\,(l_2-q)^2\,(l_1-q)^2\,(l_1-l_2-p)^2\,(l_3-l_2)^2\Big]^{-1} \,,
\end{aligned}$$

where P_N again stands for the Mellin-N projection. $\mathrm{LA}_{27}\mathrm{box}$ is subject to a first-order difference equation of the form

$$\mathrm{LA}_{27}\mathrm{box}(N) - \frac{1}{2}\mathrm{LA}_{27}\mathrm{box}(N-1) \;=\; G_{\mathrm{LA}}(N)\,. \qquad (3.15)$$

This equation does not fulfill, due to the factor $1/2$, the condition for a solution in terms of harmonic sums specified at the end of the paragraph below Eq. (3.3).

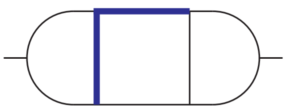
$$= \frac{(2p\cdot q)^N}{(Q^2)^{N-2-3\varepsilon}}\,\mathrm{LA}_{27}\mathrm{box}(N)$$

Figure 6: The integral $\mathrm{LA}_{27}\mathrm{box}$. All propagators have unit power. The momenta q and p (fat lines) flow from right to left and top to bottom through the diagram, respectively.

The solution of Eq. (3.15) can be written in terms of generalized harmonic sums [69] given by

$$\begin{aligned}
S(n) &= \begin{cases} 1, & n>0\,,\\ 0, & n\le 0\,,\end{cases}\\
S(n;m_1,\ldots,m_k;x_1,\ldots,x_k) &= \sum_{i=1}^{n} \frac{x_1^i}{i^{m_1}}\, S(i;m_2,\ldots,m_k;x_2,\ldots,x_k)\,. \qquad (3.16)
\end{aligned}$$

Using the short-hand notation of Eq. (3.7) the result reads

$$
\begin{aligned}
\mathrm{LA}_{27}\mathrm{box}(N) &= (-1)^N 2^{-N-1}\Big(20S(N+1;1;2)\zeta_5 + 4S(N+1;\mathbf{1}_3;2,\mathbf{1}_2)\zeta_3 \\
&\quad + 6S(N+1;\mathbf{1}_4,2;2,\mathbf{1}_3,-1) + 3S(N+1;\mathbf{1}_4,2;2,\mathbf{1}_4) - S(N+1;\mathbf{1}_3,2,1;2,\mathbf{1}_4) \\
&\quad - 9S(N+1;\mathbf{1}_3,3;2,\mathbf{1}_2,-1) - 3S(N+1;\mathbf{1}_3,3;2,\mathbf{1}_3) - 2S(N+1;\mathbf{1}_2,2,\mathbf{1}_2;2,\mathbf{1}_4) \\
&\quad - 6S(N+1;\mathbf{1}_2,\mathbf{2}_2;2,\mathbf{1}_2,-1) + 6S(N+1;\mathbf{1}_2,3,1;2,\mathbf{1}_3) + 6S(N+1;\mathbf{1}_2,4;2,1,-1) \\
&\quad - 6S(N+1;\mathbf{1}_2,4;2,\mathbf{1}_2) + 12S(N+1;1,2;2,-1)\zeta_3 - 6S(N+1;1,2,1,2;2,\mathbf{1}_2,-1) \\
&\quad - 3S(N+1;1,2,1,2;2,\mathbf{1}_3) - 12S(N+1;1,\mathbf{2}_2,1;2,-1,-1,1) - 3S(N+1;1,\mathbf{2}_2,1;2,\mathbf{1}_3) \\
&\quad + 18S(N+1;1,2,3;2,-1,-1) + 9S(N+1;1,2,3;2,1,-1) + 9S(N+1;1,2,3;2,\mathbf{1}_2) \\
&\quad + 6S(N+1;1,3,\mathbf{1}_2;2,\mathbf{1}_3) + 6S(N+1;1,3,2;2,1,-1) - 6S(N+1;1,3,2;2,\mathbf{1}_2) \\
&\quad - 4S(N+1;2,1;2,1)\zeta_3 - 6S(N+1;2,\mathbf{1}_2,2;2,\mathbf{1}_2,-1) - 3S(N+1;2,\mathbf{1}_2,2;2,\mathbf{1}_3) \\
&\quad + S(N+1;2,1,2,1;2,\mathbf{1}_3) + 9S(N+1;2,1,3;2,1,-1) + 3S(N+1;2,1,3;2,\mathbf{1}_2) \\
&\quad + 2S(N+1;\mathbf{2}_2,\mathbf{1}_2;2,\mathbf{1}_3) + 6S(N+1;\mathbf{2}_3;2,1,-1) - 6S(N+1;2,3,1;2,\mathbf{1}_2) \\
&\quad - 6S(N+1;2,4;2,-1) + 6S(N+1;2,4;2,1) - 12S(N+1;3;-2)\zeta_3 - 9S(N+1;\mathbf{3}_2;2,1) \\
&\quad + 6S(N+1;3,1,2;2,1,-1) + 3S(N+1;3,1,2;2,\mathbf{1}_2) + 12S(N+1;3,2,1;-2,-1,1) \\
&\quad + 3S(N+1;3,2,1;2,\mathbf{1}_2) - 18S(N+1;\mathbf{3}_2;-2,-1) - 9S(N+1;\mathbf{3}_2;2,-1) \\
&\quad - 6S(N+1;4,\mathbf{1}_2;2,\mathbf{1}_2) - 6S(N+1;4,2;2,-1) + 6S(N+1;4,2;2,1)\Big)\ , \qquad (3.17)
\end{aligned}
$$

including terms with $x_j = \pm 2$ in the sums (3.16). Note also the overall factor of 2^{-N}, which keeps also sums over $\mathrm{LA}_{27}\mathrm{box}$ within the class of generalized S-sums.

We did not need sums over $\mathrm{LA}_{27}\mathrm{box}$, for which all algorithms are however known from Ref. [69], in our reduction procedures for higher-level subtopologies, e.g., LA_{78}. Thus we actually kept this integral as an ‘unknown’ function in all intermediate expressions, only using Eq. (3.15) to shift the argument N. Finally, while terms $N^k\,\mathrm{LA}_{27}\mathrm{box}(N)$ occurred in the results of individual diagrams, all dependence on $\mathrm{LA}_{27}\mathrm{box}$ cancelled in the final results for the coefficient functions.

The final issue we need to mention is that certain combinations of harmonic sums multiplied with positive powers of N occur in the three-loop coefficient functions. Such structures are encountered in very many integrals also at the level of the $1/\varepsilon$ poles, see Eq. (3.11) above, but they cancel in the final results for the anomalous dimensions. On the other hand, the following combinations are present in the final result for the coefficient functions:

$$
\begin{aligned}
g_1(N) &= N f(N)\ , && (3.18)\\
g_2(N) &= N^2 f(N)\ , && (3.19)\\
g_3(N) &= N^3 f(N) - 2N(\zeta_3 - S_{-3} - S_{-2} + 2S_{-2,1})\ , && (3.20)
\end{aligned}
$$

with the function $f(N)$ given by

$$
f(N) = 5\zeta_5 - 2S_{-5} + 4S_{-2}\zeta_3 - 4S_{-2,-3} + 8S_{-2,-2,1} + 4S_{3,-2} - 4S_{4,1} + 2S_5\ . \qquad (3.21)
$$

This function vanishes sufficiently fast for $N \to \infty$ for Eqs. (3.18) – (3.20) to behave at most as constants in this limit. Thus the standard asymptotic behaviour $\ln^k(N)$, $k = 1, \ldots, 6$ of the three-loop quark coefficient functions $c^{(3)}_{2,\mathrm{ns}}$ and $c^{(3)}_{2,q}$ is unaffected by these new structures.

Positive powers as in Eqs. (3.18) – (3.20), unlike negative powers of N, cannot be written entirely in terms of harmonic sums. Consequently a larger class of functions is required also in x-space, as a one-to-one relation exists between the set of harmonic sums of weight w and the harmonic polylogarithms [83–85] $H_{\vec{m}}(x)/(1\pm x)$ where $\vec{m}$ has weight $w-1$. The Mellin inverse of $g_1(N)$ in Eq. (3.18) can be derived by partial integration from that of $f(N)$ in Eq. (3.21),

$$
\begin{aligned}
g_1(N) \;&=\; Nf(N) \;=\; N\int_0^1 dx\, x^{N-1} f(x) \;=\; f(1) - \int_0^1 dx\, x^{N-1}\, x f'(x) \\
&=\; \int_0^1 dx\, x^{N-1} \Big\{ \delta(1-x) f(1) - x f'(x) \Big\} \;, \qquad (3.22)
\end{aligned}
$$

where $g_1(x)$ is given by the expression in curved brackets in the second line. This procedure is then repeated for the functions g_2 and g_3, leading to the x-space expressions

$$
\begin{aligned}
g_1(x) \;=\;& \frac{1}{(1-x)^2}\Big(-\frac{4}{5}\zeta_2^{\,2} + 8\mathrm{H}_{-2}\zeta_2 - 4\mathrm{H}_{-2,0,0} - 8\mathrm{H}_{-2,2} - 6\mathrm{H}_0\zeta_3 - 6\mathrm{H}_{0,0}\zeta_2 + 2\mathrm{H}_{0,0,0,0} \\
&+ 4\mathrm{H}_4\Big) + \frac{1}{1-x}\Big(\frac{4}{5}\zeta_2^{\,2} - 6\zeta_3 - 8\mathrm{H}_{-2}\zeta_2 + 4\mathrm{H}_{-2,0,0} + 8\mathrm{H}_{-2,2} + 8\mathrm{H}_{-1}\zeta_2 - 4\mathrm{H}_{-1,0,0} \\
&- 8\mathrm{H}_{-1,2} - 6\mathrm{H}_0\zeta_2 + 6\mathrm{H}_0\zeta_3 + 6\mathrm{H}_{0,0}\zeta_2 + 2\mathrm{H}_{0,0,0} - 2\mathrm{H}_{0,0,0,0} + 4\mathrm{H}_3 - 4\mathrm{H}_4\Big) \\
&+ \frac{1}{(1+x)^2}\Big(\frac{21}{5}\zeta_2^{\,2} + 4\mathrm{H}_{-3,0} + 4\mathrm{H}_0\zeta_3 + 2\mathrm{H}_{0,0}\zeta_2 - 2\mathrm{H}_{0,0,0,0}\Big) + \frac{1}{1+x}\Big(-\frac{21}{5}\zeta_2^{\,2} + 4\zeta_3 \\
&- 4\mathrm{H}_{-3,0} + 4\mathrm{H}_{-2,0} + 2\mathrm{H}_0\zeta_2 - 4\mathrm{H}_0\zeta_3 - 2\mathrm{H}_{0,0}\zeta_2 - 2\mathrm{H}_{0,0,0} + 2\mathrm{H}_{0,0,0,0}\Big) + 2\zeta_3 - 4\mathrm{H}_{-2,0} \\
&- 8\mathrm{H}_{-1}\zeta_2 + 4\mathrm{H}_{-1,0,0} + 8\mathrm{H}_{-1,2} + 4\mathrm{H}_0\zeta_2 - 4\mathrm{H}_3 \;, \qquad (3.23)
\end{aligned}
$$

$$
\begin{aligned}
g_2(x) \;=\;& \frac{1}{(1-x)^3}\Big(\frac{8}{5}\zeta_2^{\,2} - 16\mathrm{H}_{-2}\zeta_2 + 8\mathrm{H}_{-2,0,0} + 16\mathrm{H}_{-2,2} + 12\mathrm{H}_0\zeta_3 + 12\mathrm{H}_{0,0}\zeta_2 - 4\mathrm{H}_{0,0,0,0} \\
&- 8\mathrm{H}_4\Big) + \frac{1}{(1-x)^2}\Big(-\frac{12}{5}\zeta_2^{\,2} + 12\zeta_3 + 24\mathrm{H}_{-2}\zeta_2 - 12\mathrm{H}_{-2,0,0} - 24\mathrm{H}_{-2,2} - 16\mathrm{H}_{-1}\zeta_2 \\
&+ 8\mathrm{H}_{-1,0,0} + 16\mathrm{H}_{-1,2} + 12\mathrm{H}_0\zeta_2 - 18\mathrm{H}_0\zeta_3 - 18\mathrm{H}_{0,0}\zeta_2 - 4\mathrm{H}_{0,0,0} + 6\mathrm{H}_{0,0,0,0} - 8\mathrm{H}_3 \\
&+ 12\mathrm{H}_4\Big) + \frac{1}{1-x}\Big(2\zeta_2 + \frac{4}{5}\zeta_2^{\,2} - 12\zeta_3 - 8\mathrm{H}_{-2}\zeta_2 + 4\mathrm{H}_{-2,0,0} + 8\mathrm{H}_{-2,2} + 16\mathrm{H}_{-1}\zeta_2 \\
&- 8\mathrm{H}_{-1,0,0} - 16\mathrm{H}_{-1,2} - 12\mathrm{H}_0\zeta_2 + 6\mathrm{H}_0\zeta_3 + 6\mathrm{H}_{0,0}\zeta_2 + 4\mathrm{H}_{0,0,0} - 2\mathrm{H}_{0,0,0,0} + 8\mathrm{H}_3 - 4\mathrm{H}_4\Big) \\
&+ \frac{1}{(1+x)^3}\Big(-\frac{42}{5}\zeta_2^{\,2} - 8\mathrm{H}_{-3,0} - 8\mathrm{H}_0\zeta_3 - 4\mathrm{H}_{0,0}\zeta_2 + 4\mathrm{H}_{0,0,0,0}\Big) + \frac{1}{(1+x)^2}\Big(\frac{63}{5}\zeta_2^{\,2} - 8\zeta_3 \\
&+ 12\mathrm{H}_{-3,0} - 8\mathrm{H}_{-2,0} - 4\mathrm{H}_0\zeta_2 + 12\mathrm{H}_0\zeta_3 + 6\mathrm{H}_{0,0}\zeta_2 + 4\mathrm{H}_{0,0,0} - 6\mathrm{H}_{0,0,0,0}\Big) + \frac{1}{1+x}\Big(-6\zeta_2 \\
&- \frac{21}{5}\zeta_2^{\,2} + 8\zeta_3 - 4\mathrm{H}_{-3,0} + 8\mathrm{H}_{-2,0} - 4\mathrm{H}_{-1,0} + 4\mathrm{H}_0\zeta_2 - 4\mathrm{H}_0\zeta_3 + 4\mathrm{H}_{0,0} - 2\mathrm{H}_{0,0}\zeta_2 \\
&- 4\mathrm{H}_{0,0,0} + 2\mathrm{H}_{0,0,0,0} + 4\mathrm{H}_2\Big) + \delta(1-x)(\zeta_2 + \zeta_3) + 4\zeta_2 + 4\mathrm{H}_{-1,0} - 4\mathrm{H}_{0,0} - 4\mathrm{H}_2 \;, \qquad (3.24)
\end{aligned}
$$

$$
\begin{aligned}
g_3(x) \;=\; & \frac{1}{(1-x)^4}\Big(-\frac{24}{5}\zeta_2{}^2+48\mathrm{H}_{-2}\zeta_2-24\mathrm{H}_{-2,0,0}-48\mathrm{H}_{-2,2}-36\mathrm{H}_0\zeta_3-36\mathrm{H}_{0,0}\zeta_2\\
&+12\mathrm{H}_{0,0,0,0}+24\mathrm{H}_4\Big)+\frac{1}{(1-x)^3}\Big(\frac{48}{5}\zeta_2{}^2-36\zeta_3-96\mathrm{H}_{-2}\zeta_2+48\mathrm{H}_{-2,0,0}+96\mathrm{H}_{-2,2}\\
&+48\mathrm{H}_{-1}\zeta_2-24\mathrm{H}_{-1,0,0}-48\mathrm{H}_{-1,2}-36\mathrm{H}_0\zeta_2+72\mathrm{H}_0\zeta_3+72\mathrm{H}_{0,0}\zeta_2+12\mathrm{H}_{0,0,0}-24\mathrm{H}_{0,0,0,0}\\
&+24\mathrm{H}_3-48\mathrm{H}_4\Big)+\frac{1}{(1-x)^2}\Big(-6\zeta_2-\frac{28}{5}\zeta_2{}^2+54\zeta_3+56\mathrm{H}_{-2}\zeta_2-28\mathrm{H}_{-2,0,0}-56\mathrm{H}_{-2,2}\\
&-72\mathrm{H}_{-1}\zeta_2+36\mathrm{H}_{-1,0,0}+72\mathrm{H}_{-1,2}+54\mathrm{H}_0\zeta_2-42\mathrm{H}_0\zeta_3-42\mathrm{H}_{0,0}\zeta_2-18\mathrm{H}_{0,0,0}+14\mathrm{H}_{0,0,0,0}\\
&-36\mathrm{H}_3+28\mathrm{H}_4\Big)+\frac{1}{1-x}\Big(2\zeta_2+\frac{4}{5}\zeta_2{}^2-18\zeta_3-8\mathrm{H}_{-2}\zeta_2+4\mathrm{H}_{-2,0,0}+8\mathrm{H}_{-2,2}+24\mathrm{H}_{-1}\zeta_2\\
&-12\mathrm{H}_{-1,0,0}-24\mathrm{H}_{-1,2}-18\mathrm{H}_0\zeta_2+6\mathrm{H}_0\zeta_3+2\mathrm{H}_{0,0}+6\mathrm{H}_{0,0}\zeta_2+6\mathrm{H}_{0,0,0}-2\mathrm{H}_{0,0,0,0}+4\mathrm{H}_2\\
&+12\mathrm{H}_3-4\mathrm{H}_4\Big)+\frac{1}{(1+x)^4}\Big(\frac{126}{5}\zeta_2{}^2+24\mathrm{H}_{-3,0}+24\mathrm{H}_0\zeta_3+12\mathrm{H}_{0,0}\zeta_2-12\mathrm{H}_{0,0,0,0}\Big)\\
&+\frac{1}{(1+x)^3}\Big(-\frac{252}{5}\zeta_2{}^2+24\zeta_3-48\mathrm{H}_{-3,0}+24\mathrm{H}_{-2,0}+12\mathrm{H}_0\zeta_2-48\mathrm{H}_0\zeta_3-24\mathrm{H}_{0,0}\zeta_2\\
&-12\mathrm{H}_{0,0,0}+24\mathrm{H}_{0,0,0,0}\Big)+\frac{1}{(1+x)^2}\Big(6\zeta_2+\frac{147}{5}\zeta_2{}^2-36\zeta_3+28\mathrm{H}_{-3,0}-36\mathrm{H}_{-2,0}\\
&+12\mathrm{H}_{-1,0}-6\mathrm{H}_0-18\mathrm{H}_0\zeta_2+28\mathrm{H}_0\zeta_3-6\mathrm{H}_{0,0}+14\mathrm{H}_{0,0}\zeta_2+18\mathrm{H}_{0,0,0}-14\mathrm{H}_{0,0,0,0}\Big)\\
&+\frac{1}{1+x}\Big(-2-2\zeta_2-\frac{21}{5}\zeta_2{}^2+12\zeta_3-4\mathrm{H}_{-3,0}+12\mathrm{H}_{-2,0}-12\mathrm{H}_{-1,0}+8\mathrm{H}_0+6\mathrm{H}_0\zeta_2\\
&-4\mathrm{H}_0\zeta_3+4\mathrm{H}_{0,0}-2\mathrm{H}_{0,0}\zeta_2-6\mathrm{H}_{0,0,0}+2\mathrm{H}_{0,0,0,0}-4\mathrm{H}_2\Big)-\delta(1-x)(\zeta_2+\zeta_3)\\
&+2-2\mathrm{H}_0\,. \qquad (3.25)
\end{aligned}
$$

The above equations are not suitable for a numerical implementation at x-values very close to $x=1$, a region which contributes to all numerical calculations of moments and, more importantly, Mellin convolutions. For application in this region we instead provide the expansions

$$
\begin{aligned}
g_1(x) \;\simeq\; & \zeta_2+\zeta_3-(1-x)(\zeta_2+\zeta_3)+(1-x)^2\Big(\frac{5}{8}-\frac{1}{4}\zeta_2-\frac{1}{2}\zeta_3-\frac{1}{2}\ln(1-x)\Big)\\
&+O((1-x)^3)\,, \qquad (3.26)\\
g_2(x) \;\simeq\; & \delta(1-x)(\zeta_2+\zeta_3)-\zeta_2-\zeta_3+(1-x)\Big(\frac{3}{4}+\frac{1}{2}\zeta_2-\ln(1-x)\Big)\\
&-(1-x)^2\Big(\frac{9}{8}-\frac{1}{4}\zeta_2-\frac{1}{2}\zeta_3-\frac{1}{2}\ln(1-x)\Big)+O((1-x)^3)\,, \qquad (3.27)\\
g_3(x) \;\simeq\; & -\delta(1-x)(\zeta_2+\zeta_3)+\frac{3}{4}+\frac{1}{2}\zeta_2+\ln(1-x)-(1-x)\Big(\frac{1}{2}-\zeta_3\Big)\\
&-(1-x)^2\Big(\frac{7}{24}+\frac{1}{12}\zeta_2-\frac{1}{2}\zeta_3+\frac{1}{2}\ln(1-x)\Big)+O((1-x)^3)\,. \qquad (3.28)
\end{aligned}
$$

These expansions have been derived by expanding the harmonic polylogarithms sufficiently deep in $(1-x)$ via the transformation $t=(1-x)/(1+x)$ and an expansion around $t=0$ as described in Ref. [85] and implemented in FORM [63, 64].

4 Results and discussion

We are now ready to present the third-order contributions $c^{(3)}_{a,i}$ to the coefficient functions $C_{a,i}$ for the structure functions $F_{a=2,L}$ in electromagnetic DIS,

$$x^{-1}F_a \;=\; C_{a,\rm ns}\otimes q_{\rm ns} + \langle e^2\rangle \left(C_{a,\rm q}\otimes q_{\rm s} + C_{a,\rm g}\otimes g\right) \; . \tag{4.1}$$

Recall that q_i and g represent the number distributions of quarks and gluons, respectively, in the fractional hadron momentum, with $q_{\rm s}$ standing for the flavour-singlet quark distribution, $q_{\rm s} = \sum_{i=1}^{n_f}(q_i+\bar{q}_i)$ where n_f denotes the number of effectively massless flavours. The normalization of the corresponding non-singlet combination $q_{\rm ns}$ is defined via Eq. (4.2) below. Again $\langle e^2\rangle$ represents the average squared charge, and $\otimes$ denotes the Mellin convolution which turns into a simple multiplication in N-space. Below the singlet-quark coefficient function is decomposed into the non-singlet and a 'pure singlet' contribution, $c^{(n)}_{a,\rm q} = c^{(n)}_{a,\rm ns} + c^{(n)}_{a,\rm ps}$, and the results are given in the $\overline{\rm MS}$ scheme for the standard choice $\mu_r^2 = \mu_f^2 = Q^2$ of the renormalization and factorization scales. The complete expressions for the dependence on μ_r and μ_f up to the third order in our expansion parameter $a_{\rm s} \equiv \alpha_{\rm s}/(4\pi)$ can be found, for example, in Eqs. (2.16) – (2.18) of Ref. [82].

As discussed above, our calculation via the optical theorem and a dispersion relation directly determines the coefficient functions for all even-integer moments N in terms of harmonic sums [65–69]. From these results the x-space expressions can be reconstructed algebraically [16, 85] in terms of harmonic polylogarithms [83–85]. Unfortunately, but not entirely unexpectedly, the exact results are very lengthy. The complete expressions in both N-space and x-space are therefore deferred to the appendices of this article. Here we confine ourselves to (sufficiently accurate) approximations for $c^{(3)}_{2,i}(x)$, quite analogous to those already presented for $c^{(3)}_{L,i}(x)$ in Ref. [17].

For the convenience of the reader we first recall the known results up to the second order. The coefficient functions at zeroth and first order [50] are given by

$$c^{(0)}_{2,\rm ns}(x) \;=\; \delta(x_1)\; , \quad c^{(0)}_{2,\rm ps}(x) \;=\; c^{(0)}_{2,\rm g}(x) \;=\; c^{(1)}_{2,\rm ps}(x) \;=\; 0 \tag{4.2}$$

and

$$\begin{aligned} c^{(1)}_{2,\rm ns}(x) \;&=\; C_F\{4\,\mathcal{D}_1 - 3\,\mathcal{D}_0 - (9+4\,\zeta_2)\,\delta(x_1) - 2\,(1+x)(L_1-L_0) \\ &\qquad - 4\,x_1^{-1}L_0 + 6 + 4x\}\; , \end{aligned} \tag{4.3}$$

$$c^{(1)}_{2,\rm g}(x) \;=\; n_f\,\{(2-4xx_1)(L_1-L_0) - 2 + 16xx_1\} \tag{4.4}$$

with $C_F = (N_c^2-1)/(2N_c) = 4/3$ in QCD. Here and below we use the abbreviations

$$x_1 \;=\; 1-x\; , \quad L_0 \;=\; \ln x\; , \quad L_1 \;=\; \ln x_1\; , \quad \mathcal{D}_k \;=\; [x_1^{-1}L_1^k]_+ \tag{4.5}$$

where, as usual, the +-distributions are defined via

$$\int_0^1 dx\, a(x)_+ f(x) \;=\; \int_0^1 dx\, a(x)\,\{f(x)-f(1)\} \tag{4.6}$$

for regular functions $f(x)$. Convolutions with the distributions $\mathcal{D}_k$ in Eq. (4.5) can be written as

$$x[\mathcal{D}_k \otimes f](x) = \int_x^1 dy \, \frac{\ln^k(1-x)}{1-x} \left\{ \frac{x}{y} f\left(\frac{x}{y}\right) - x f(x) \right\} + x f(x) \frac{1}{k+1} \ln^{k+1}(1-x) \; . \tag{4.7}$$

With an error of 0.1% or less, the two-loop coefficient functions [12–16] can be represented by

$$\begin{aligned} c^{(2)}_{2,\mathrm{ns}}(x) \;\cong\; & \quad 128/9\,\mathcal{D}_3 - 184/3\,\mathcal{D}_2 - 31.1052\,\mathcal{D}_1 + 188.641\,\mathcal{D}_0 - 338.513\,\delta(x_1) \\ & \quad - 17.74\,L_1^3 + 72.24\,L_1^2 - 628.8\,L_1 - 181.0 - 806.7\,x + 0.719\,xL_0^4 \\ & \quad + L_0L_1(37.75\,L_0 - 147.1\,L_1) - 28.384\,L_0 - 20.70\,L_0^2 - 80/27\,L_0^3 \\ & + \; n_f\,\{\, 16/9\,\mathcal{D}_2 - 232/27\,\mathcal{D}_1 + 6.34888\,\mathcal{D}_0 + 46.8531\,\delta(x_1) - 1.500\,L_1^2 \\ & \quad + 24.87\,L_1 - 7.8109 - 17.82\,x - 12.97\,x^2 - 0.185\,xL_0^3 + 8.113\,L_0L_1 \\ & \quad + 16/3\,L_0 + 20/9\,L_0^2 \,\} \; , \end{aligned} \tag{4.8}$$

$$\begin{aligned} c^{(3)}_{2,\mathrm{ps}}(x) \;\cong\; & n_f\,\{\, (8/3\,L_1^2 - 32/3\,L_1 + 9.8937)\,x_1 + (9.57 - 13.41\,x + 0.08\,L_1^3)\,x_1^2 \\ & \quad + 5.667\,xL_0^3 - L_0^2L_1(20.26 - 33.93\,x) + 43.36\,x_1L_0 - 1.053\,L_0^2 \\ & \quad + 40/9\,L_0^3 + 5.2903\,x^{-1}x_1^2 \,\} \, , \end{aligned} \tag{4.9}$$

$$\begin{aligned} c^{(3)}_{2,\mathrm{g}}(x) \;\cong\; & n_f\,\{\, 58/9\,L_1^3 - 24\,L_1^2 - 34.88\,L_1 + 30.586 - (25.08 + 760.3\,x \\ & \quad + 29.65\,L_1^3)\,x_1 + 1204\,xL_0^2 + L_0L_1(293.8 + 711.2\,x + 1043\,L_0) \\ & \quad + 115.6\,L_0 - 7.109\,L_0^2 + 70/9\,L_0^3 + 11.9033\,x^{-1}x_1 \,\} \; . \end{aligned} \tag{4.10}$$

Eqs. (4.8) – (4.10) are less compact, but more accurate than the previous parametrizations [82, 86].

Now we present our three-loop results. As in Eqs. (4.8)–(4.10) inserting the numerical values of the n_f-independent colour factors, the non-singlet coefficient function can be parametrized as

$$\begin{aligned} c^{(3)}_{2,\mathrm{ns}}(x) \;\cong\; & \quad 512/27\,\mathcal{D}_5 - 5440/27\,\mathcal{D}_4 + 501.099\,\mathcal{D}_3 + 1171.54\,\mathcal{D}_2 - 7328.45\,\mathcal{D}_1 \\ & \quad + 4442.76\,\mathcal{D}_0 - 9170.38\,\delta(x_1) - 512/27\,L_1^5 + 704/3\,L_1^4 - 3368\,L_1^3 \\ & \quad - 2978\,L_1^2 + 18832\,L_1 - 4926 + 7725\,x + 57256\,x^2 + 12898\,x^3 \\ & \quad - 56000\,x_1L_1^2 - L_0L_1(6158 + 1836\,L_0) + 4.719\,xL_0^5 - 775.8\,L_0 \\ & \quad - 899.6\,L_0^2 - 309.1\,L_0^3 - 2932/81\,L_0^4 - 32/27\,L_0^5 \\ & + \; n_f\,\{\, 640/81\,\mathcal{D}_4 - 6592/81\,\mathcal{D}_3 + 220.573\,\mathcal{D}_2 + 294.906\,\mathcal{D}_1 - 729.359\,\mathcal{D}_0 \\ & \quad + 2574.687\,\delta(x_1) - 640/81\,L_1^4 + 153.5\,L_1^3 - 828.7\,L_1^2 - 501.1\,L_1 + 831.6 \\ & \quad - 6752\,x - 2778\,x^2 + 171.0\,x_1L_1^4 + L_0L_1\,(4365 + 716.2\,L_0 - 5983\,L_1) \\ & \quad + 4.102\,xL_0^4 + 275.6\,L_0 + 187.3\,L_0^2 + 12224/243\,L_0^3 + 728/243\,L_0^4 \,\} \\ & + \; n_f^2\,\{\, 64/81\,\mathcal{D}_3 - 464/81\,\mathcal{D}_2 + 7.67505\,\mathcal{D}_1 + 1.00830\,\mathcal{D}_0 - 103.2366\,\delta(x_1) \\ & \quad - 64/81\,L_1^3 + 18.21\,L_1^2 - 19.09\,L_1 + 129.2\,x + 102.5\,x^2 + L_0L_1\,(-96.07 \\ & \quad - 12.46\,L_0 + 85.88\,L_1) - 8.042\,L_0 - 1984/243\,L_0^2 - 368/243\,L_0^3 \,\} \end{aligned}$$

$$
\begin{aligned}
&+ \; fl_{11}^{\rm ns}\, n_f \{(126.42 - 50.29\,x - 50.15\,x^2)x_1 - 11.888\,\delta(x_1) - 26.717 - 9.075\,xx_1L_1 \\
&\quad - xL_0^2(101.8 + 34.79\,L_0 + 3.070\,L_0^2) + 59.59\,L_0 - 320/81\,L_0^2(5 + L_0)\,\}\,x\;.
\end{aligned} \tag{4.11}
$$

Slightly less accurate parametrizations of the (non-fl_{11}) n_f-contributions were already presented in Ref. [32]. The corresponding pure-singlet coefficient function can be approximated by

$$
\begin{aligned}
c^{(3)}_{2,\rm ps}(x) \;\cong\;& n_f \{\,(856/81\,L_1^4 - 6032/81\,L_1^3 + 130.57\,L_1^2 - 542\,L_1 + 8501\; - 4714\,x + 61.5\,x^2) \\
&\quad \cdot x_1 + L_0L_1(8831\,L_0 + 4162\,x_1) - 15.44\,xL_0^5 + 3333\,xL_0^2 + 1615\,L_0 + 1208\,L_0^2 \\
&\quad - 333.73\,L_0^3 + 4244/81\,L_0^4 - 40/9\,L_0^5 - x^{-1}(2731.82\,x_1 + 414.262\,L_0)\} \\
&+ \; n_f^2\,\{\,(-64/81\,L_1^3 + 208/81\,L_1^2 + 23.09\,L_1 - 220.27 + 59.80\,x - 177.6x^2)\,x_1 \\
&\quad - L_0L_1(160.3\,L_0 + 135.4\,x_1) - 24.14\,xL_0^3 - 215.4\,xL_0^2 - 209.8\,L_0 - 90.38L_0^2 \\
&\quad - 3568/243\,L_0^3 - 184/81\,L_0^4 + 40.2426\,x_1x^{-1}\,\} \\
&+ \; fl_{11}^{\rm ps}\, n_f \{(126.42 - 50.29\,x - 50.15\,x^2)x_1 - 11.888\,\delta(x_1) - 26.717 - 9.075\,xx_1L_1 \\
&\quad - xL_0^2(101.8 + 34.79\,L_0 + 3.070\,L_0^2) + 59.59\,L_0 - 320/81\,L_0^2(5 + L_0)\,\}\,x\;.
\end{aligned} \tag{4.12}
$$

Finally the third-order gluon coefficient function can be written as

$$
\begin{aligned}
c^{(3)}_{2,\rm g}(x) \;\cong\;& n_f\,\{\,966/81\,L_1^5 - 1871/18\,L_1^4 + 89.31\,L_1^3 + 979.2\,L_1^2 - 2405\,L_1 + 1372\,x_1L_1^4 \\
&\quad - 15729 - 310510\,x + 331570\,x^2 - 244150\,xL_0^2 - 253.3\,xL_0^5 \\
&\quad + L_0L_1(138230 - 237010\,L_0) - 11860\,L_0 - 700.8\,L_0^2 - 1440\,L_0^3 \\
&\quad + 4961/162\,L_0^4 - 134/9\,L_0^5 - x^{-1}(6362.54 - 932.089\,L_0) + 0.625\,\delta(x_1)\,\} \\
&+ \; n_f^2\,\{\,131/81\,L_1^4 - 14.72\,L_1^3 + 3.607\,L_1^2 - 226.1\,L_1 + 4.762 - 190\,x - 818.4\,x^2 \\
&\quad - 4019\,xL_0^2 - L_0L_1(791.5 + 4646\,L_0) + 739.0\,L_0 + 418.0\,L_0^2 + 104.3\,L_0^3 \\
&\quad + 809/81\,L_0^4 + 12/9\,L_0^5 + 84.423\,x^{-1}\,\} \\
&+ \; fl_{11}^{\rm g}\, n_f^2\,\{3.211\,L_1^2 + 19.04\,xL_1 + 0.623\,x_1L_1^3 - 64.47\,x + 121.6\,x^2 - 45.82\,x^3 \\
&\quad - xL_0L_1(31.68 + 37.24\,L_0) + 11.27\,x^2L_0^3 - 82.40\,xL_0 - 16.08\,xL_0^2 \\
&\quad + 520/81\,xL_0^3 + 20/27\,xL_0^4\,\}\;.
\end{aligned} \tag{4.13}
$$

The new charge factors fl_{11} have been specified in Table 2 above, and $fl_{11}^{\rm ps}$ is given by $fl_{11}^{\rm s} - fl_{11}^{\rm ns}$.

The coefficients of $\mathcal{D}_k$ and of x^{-1} in Eqs. (4.8) – (4.13) are exact up to a truncation of irrational numbers. Also exact are those coefficients of $L_0^k \equiv \ln^k x$ and $L_1^k \equiv \ln^k(1-x)$ given as fractions. Most of the remaining coefficients have been obtained by fits to the exact coefficient functions at $10^{-6} \leq x \leq 1 - 10^{-6}$ which we evaluated using a weight-five extension of the program [87] for the evaluation of the harmonic polylogarithms [85]. Finally the coefficients of $\delta(1-x)$ have been slightly adjusted from their exact values using the lowest integer moments, as discussed in Ref. [11]. Like their second-order counterparts (4.8) – (4.10), the three-loop parametrizations (4.11) – (4.13) deviate from the exact results by less than one part in a thousand.

For use with N-space evolution programs (see, e.g., Refs. [88, 89]) for parton distributions and structure functions, the above approximations can be readily transformed to Mellin space for any complex value of N. For the time being, this is especially important for our new results for which (unlike the two-loop coefficient functions and three-loop splitting functions [90, 91]) the analytic continuations of the exact expressions to $N \neq 2k$, $k = 1, 2, 3\ldots$ are not yet known.

We now address the end-point behaviour of the third-order coefficient functions for F_2. The leading terms at large x are the soft-gluon +-distributions $\mathcal{D}_k$, $k = 0, \ldots, 2n-1$ of $c^{(n)}_{2,\rm ns}(x)$ in Eqs. (4.3), (4.8) and (4.11). For the highest four coefficients at three loops, our exact results

$$c^{(3)}_{2,\rm ns}\Big|_{\mathcal{D}_5} = 8\,C_F^3\,, \tag{4.14}$$

$$c^{(3)}_{2,\rm ns}\Big|_{\mathcal{D}_4} = -\frac{220}{9}C_AC_F^2 - 30\,C_F^3 + \frac{40}{9}C_F^2 n_f\,, \tag{4.15}$$

$$\begin{aligned} c^{(3)}_{2,\rm ns}\Big|_{\mathcal{D}_3} = {} & \frac{484}{27}C_A^2C_F + C_AC_F^2\left[\frac{1732}{9} - 32\,\zeta_2\right] + C_F^3\Big[-36 - 96\,\zeta_2\Big] \\ & - \frac{176}{27}C_FC_An_f - \frac{280}{9}C_F^2n_f + \frac{16}{27}C_Fn_f^2\,, \end{aligned} \tag{4.16}$$

$$\begin{aligned} c^{(3)}_{2,\rm ns}\Big|_{\mathcal{D}_2} = {} & C_A^2C_F\left[-\frac{4649}{27} + \frac{88}{3}\zeta_2\right] + C_AC_F^2\left[-\frac{8425}{18} + \frac{724}{3}\zeta_2 + 240\,\zeta_3\right] \\ & + C_F^3\left[\frac{279}{2} + 288\,\zeta_2 + 16\,\zeta_3\right] + C_AC_Fn_f\left[\frac{1552}{27} - \frac{16}{3}\zeta_2\right] \\ & + C_F^2n_f\left[\frac{683}{9} - \frac{112}{3}\zeta_2\right] - \frac{116}{27}C_Fn_f^2 \end{aligned} \tag{4.17}$$

completely agree with the prediction [92] of the next-to-leading logarithmic threshold resummation [23–26]. The remaining two terms read

$$\begin{aligned} c^{(3)}_{2,\rm ns}\Big|_{\mathcal{D}_1} = {} & C_A^2C_F\left[\frac{50689}{81} - \frac{680}{3}\zeta_2 - 264\,\zeta_3 + \frac{176}{5}\zeta_2^2\right] + C_AC_F^2\left[-\frac{5563}{18}\right. \\ & \left. - 972\,\zeta_2 - \frac{160}{3}\zeta_3 + \frac{764}{5}\zeta_2^2\right] + C_F^3\left[\frac{187}{2} + 240\,\zeta_2 - 360\,\zeta_3 + \frac{376}{5}\zeta_2^2\right] \\ & + C_AC_Fn_f\left[-\frac{15062}{81} + \frac{512}{9}\zeta_2 + 16\,\zeta_3\right] + C_F^2n_f\left[\frac{83}{9} + 168\,\zeta_2 + \frac{112}{3}\zeta_3\right] \\ & + C_Fn_f^2\left[\frac{940}{81} - \frac{32}{9}\zeta_2\right]\,, \end{aligned} \tag{4.18}$$

$$\begin{aligned} c^{(3)}_{2,\rm ns}\Big|_{\mathcal{D}_0} = {} & C_A^2C_F\left[-\frac{599375}{729} + \frac{32126}{81}\zeta_2 + \frac{21032}{27}\zeta_3 - \frac{652}{15}\zeta_2^2 - \frac{176}{3}\zeta_2\zeta_3 - 232\,\zeta_5\right] \\ & + C_AC_F^2\left[\frac{16981}{24} + \frac{26885}{27}\zeta_2 - \frac{3304}{9}\zeta_3 - 209\,\zeta_2^2 - 400\,\zeta_2\zeta_3 - 120\,\zeta_5\right] \\ & + C_F^3\left[-\frac{1001}{8} - 429\,\zeta_2 + 274\,\zeta_3 - 210\,\zeta_2^2 + 32\,\zeta_2\zeta_3 + 432\,\zeta_5\right] \end{aligned}$$

$$+ C_A C_F n_f \left[\frac{160906}{729} - \frac{9920}{81}\zeta_2 - \frac{776}{9}\zeta_3 + \frac{208}{15}\zeta_2^{\,2} \right] + C_F^2 n_f \left[- \frac{2003}{108} - \frac{4226}{27}\zeta_2 - 60\,\zeta_3 + 16\,\zeta_2^2 \right] + C_F n_f^2 \left[- \frac{8714}{729} + \frac{232}{27}\zeta_2 - \frac{32}{27}\zeta_3 \right] . \qquad (4.19)$$

The fermionic (n_f) contributions in Eqs. (4.18) and (4.19) were presented already in Ref. [32]. From this part of Eq. (4.18), the non-fermionic part is actually predicted [32] by the next-to-next-to-leading logarithmic threshold resummation [27] in terms of the leading large-x coefficient A_3 of the three-loop quark-quark splitting function [10], cf. the three-loop prediction for the Drell-Yan coefficient function in Ref. [27]. Our result (4.18) agrees with this prediction, thus constituting the first verification of the next-to-next-to-leading logarithmic soft-gluon resummation by a full calculation at third order. The final coefficient (4.19) of $\mathcal{D}_0$ (of which the leading-n_f part could have been inferred already from Ref. [93]) can in turn be employed for the next order of the soft-gluon resummation which we will present in Ref. [31].

The analytic expression for the $\delta(1-x)$ term of $c^{(3)}_{2,\rm ns}(x)$ can be read off, with a bit of patience, from Eq. (B.8) in the appendix together with Eqs. (3.26) and (3.27). Also this coefficient is relevant for the prediction of higher-order +-distributions by means of the threshold resummation [31].

The subleading class of large-x terms in $c^{(n)}_{2,\rm ns}(x)$ (and the leading one in $c^{(n)}_{2,\rm g}(x)$) is formed by the logarithms L_1^k with $k = 0, \ldots, 2n-1$. For brevity we refrain from writing down the corresponding coefficients. There is, however, a relation between coefficients of the +-distributions and the logarithms in $c^{(n)}_{2,\rm ns}(x)$ which we would like to mention: as predicted in Ref. [94], the coefficient of the highest power L_1^k for a given colour factor equals, up to a sign, that of the leading term $\mathcal{D}_k$. This means that the coefficients of L_1^5 for the C_F^3 term, those of L_1^4 for the $C_A C_F^2$ and $C_F^2 n_f$ terms, and those of L_1^3 for the remaining contributions can be directly read off from Eqs. (4.14) – (4.16).

The small-x limit of the non-singlet coefficient functions $c^{(n)}_{2,\rm ns}(x)$ is dominated by the contributions L_0^k with again $k = 0, \ldots, 2n-1$. The corresponding three-loop coefficients are

$$c^{(3)}_{2,\rm ns}\Big|_{L_0^5} = -\frac{1}{2} C_F^3 \, , \qquad (4.20)$$

$$c^{(3)}_{2,\rm ns}\Big|_{L_0^4} = -\frac{1001}{108} C_A C_F^2 + \frac{67}{12} C_F^3 + \frac{91}{54} C_F^2 n_f \, , \qquad (4.21)$$

$$c^{(3)}_{2,\rm ns}\Big|_{L_0^3} = C_A^2 C_F \left[-\frac{2783}{81} + 20\,\zeta_2 \right] + C_A C_F^2 \left[-\frac{835}{54} - 64\,\zeta_2 \right] + C_F^3 \left[5 + \frac{262}{3}\zeta_2 \right] + \frac{1012}{81} C_F C_A n_f + \frac{5}{27} C_F^2 n_f - \frac{92}{81} C_F n_f^2 \, , \qquad (4.22)$$

$$c^{(3)}_{2,\rm ns}\Big|_{L_0^2} = C_A^2 C_F \left[-\frac{23062}{81} + 84\,\zeta_2 \right] + C_A C_F^2 \left[\frac{17315}{162} - \frac{265}{9}\zeta_2 - 64\,\zeta_3 \right] + C_F^3 \left[-\frac{113}{6} + \frac{299}{3}\zeta_2 + \frac{646}{3}\zeta_3 \right] + C_A C_F n_f \left[\frac{7196}{81} - 8\,\zeta_2 \right]$$

$$+ C_F^2 n_f \left[-\frac{1315}{81} - \frac{266}{9}\zeta_2\right] - \frac{496}{81} C_F n_f^2 \,, \tag{4.23}$$

$$\begin{aligned}
c^{(3)}_{2,\mathrm{ns}}\Big|_{L_0^1} \;=\;& C_A^2 C_F \left[-\frac{78338}{81} + \frac{3058}{9}\zeta_2 + 32\,\zeta_3 - 24\,\zeta_2^2\right] + C_A C_F^2 \left[\frac{106801}{324}\right.\\
&\left. + \frac{599}{9}\zeta_2 + \frac{418}{3}\zeta_3 + \frac{656}{15}\zeta_2^2\right] + C_F^3 \left[\frac{1619}{12} + \frac{764}{3}\zeta_2 + 154\,\zeta_3 - \frac{556}{3}\zeta_2^2\right]\\
& + C_A C_F n_f \left[\frac{7076}{27} - \frac{688}{9}\zeta_2 + \frac{128}{3}\zeta_3\right] + C_F^2 n_f \left[-\frac{2999}{162} - \frac{482}{9}\zeta_2 - 132\,\zeta_3\right]\\
& + C_F n_f^2 \left[-\frac{1204}{81} + \frac{16}{3}\zeta_2\right] \,,
\end{aligned} \tag{4.24}$$

$$\begin{aligned}
c^{(3)}_{2,\mathrm{ns}}\Big|_{L_0^0} \;=\;& C_A^2 C_F \left[-\frac{1779023}{1458} + \frac{14917}{27}\zeta_2 - \frac{1960}{27}\zeta_3 - \frac{148}{3}\zeta_2^2 - \frac{436}{3}\zeta_2\zeta_3 - \frac{152}{3}\zeta_5\right]\\
& + C_A C_F^2 \left[\frac{193961}{648} + \frac{6014}{81}\zeta_2 + \frac{13189}{27}\zeta_3 - \frac{3434}{45}\zeta_2^2 + 520\,\zeta_2\zeta_3 + \frac{1970}{3}\zeta_5\right]\\
& + C_F^3 \left[\frac{5603}{24} + \frac{533}{3}\zeta_2 + \frac{1730}{3}\zeta_3 - \frac{68}{15}\zeta_2^2 - 904\,\zeta_2\zeta_3 - 872\,\zeta_5\right]\\
& + C_A C_F n_f \left[\frac{224219}{729} - \frac{4520}{27}\zeta_2 + \frac{1412}{27}\zeta_3 + \frac{352}{15}\zeta_2^2\right] + C_F^2 n_f \left[-\frac{2881}{324}\right.\\
& \left. + \frac{427}{81}\zeta_2 - \frac{5902}{27}\zeta_3 - \frac{424}{45}\zeta_2^2\right] + C_F n_f^2 \left[-\frac{11170}{729} + \frac{232}{27}\zeta_2 + \frac{32}{27}\zeta_3\right] \,,
\end{aligned} \tag{4.25}$$

or, after inserting $C_A = N_c = 3$ and $C_F = 4/3$ and the numerical values of the ζ-function

$$\begin{aligned}
c^{(3)}_{2,\mathrm{ns}}|_{L_0^5} &\cong -1.18519\\
c^{(3)}_{2,\mathrm{ns}}|_{L_0^4} &\cong -36.1975 + 2.99588\,n_f\\
c^{(3)}_{2,\mathrm{ns}}|_{L_0^3} &\cong -309.079 + 50.3045\,n_f - 1.51440\,n_f^2\\
c^{(3)}_{2,\mathrm{ns}}|_{L_0^2} &\cong -899.553 + 187.429\,n_f - 8.16461\,n_f^2\\
c^{(3)}_{2,\mathrm{ns}}|_{L_0^1} &\cong -787.175 + 278.856\,n_f - 8.12162\,n_f^2\\
c^{(3)}_{2,\mathrm{ns}}|_{L_0^0} &\cong -591.159 + 123.002\,n_f + 0.31540\,n_f^2 \,.
\end{aligned} \tag{4.26}$$

In Fig. 7 the non-singlet coefficient function $c^{(3)}_{2,\mathrm{ns}}(x)$ of Eqs. (B.8) and (4.11) is compared for $n_f = 4$ with the large-x and small-x approximations specified above and with the previous uncertainty band [19] based on the lowest seven even-integer moments $N = 2 \ldots 14$ of Refs. [39–41] and the four large-x coefficients (4.14)–(4.17) predicted by the threshold resummation [92].

The complete soft-gluon contribution including $\mathcal{D}_0 \ldots \mathcal{D}_5$ deviates from the full coefficient function by less than 20% only at $x \geq 0.85$. The corresponding x-range reads $x \leq 0.09$ for the small-x approximation by the terms $\ln x \ldots \ln^5 x$. Note that this range only arises when all small-x

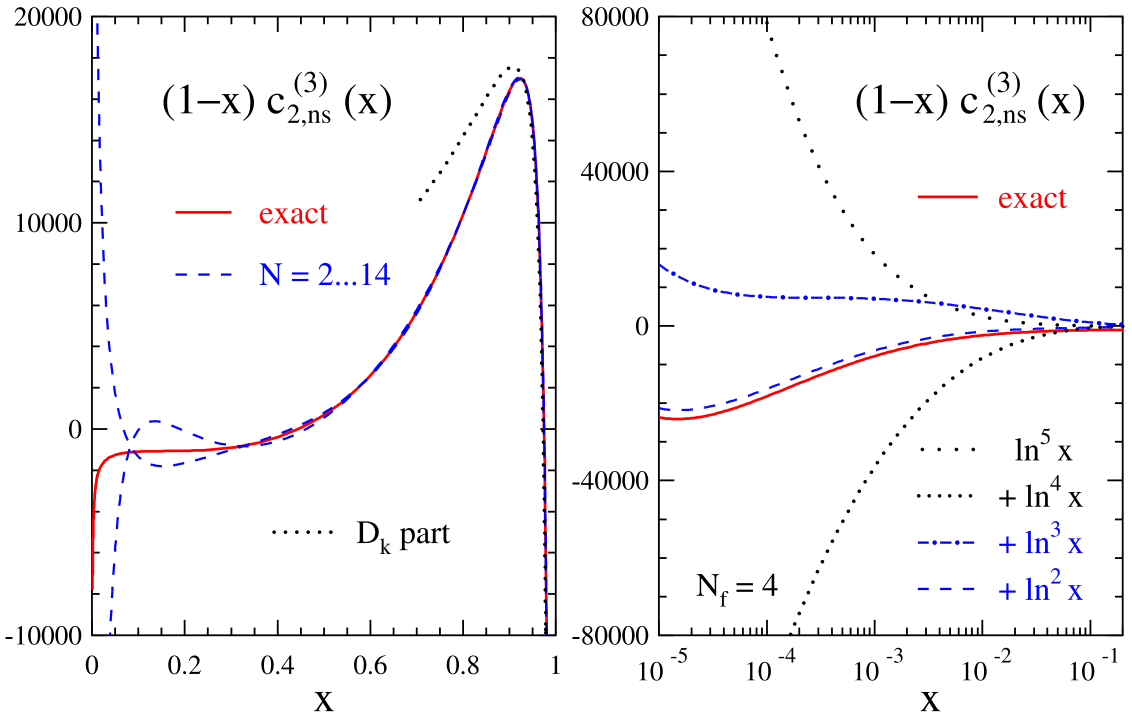

Figure 7: The three-loop non-singlet coefficient function $c^{(3)}_{2,\text{ns}}(x)$ for four flavours, multiplied by $(1-x)$ for display purposes. Also shown (left) are the large-x approximation by all soft-gluon $\mathcal{D}_k$ terms (4.14) – (4.18), the (dashed) uncertainty band of Ref. [19], and (right) the small-x approximations obtained by successively including Eqs. (4.20) – (4.23).

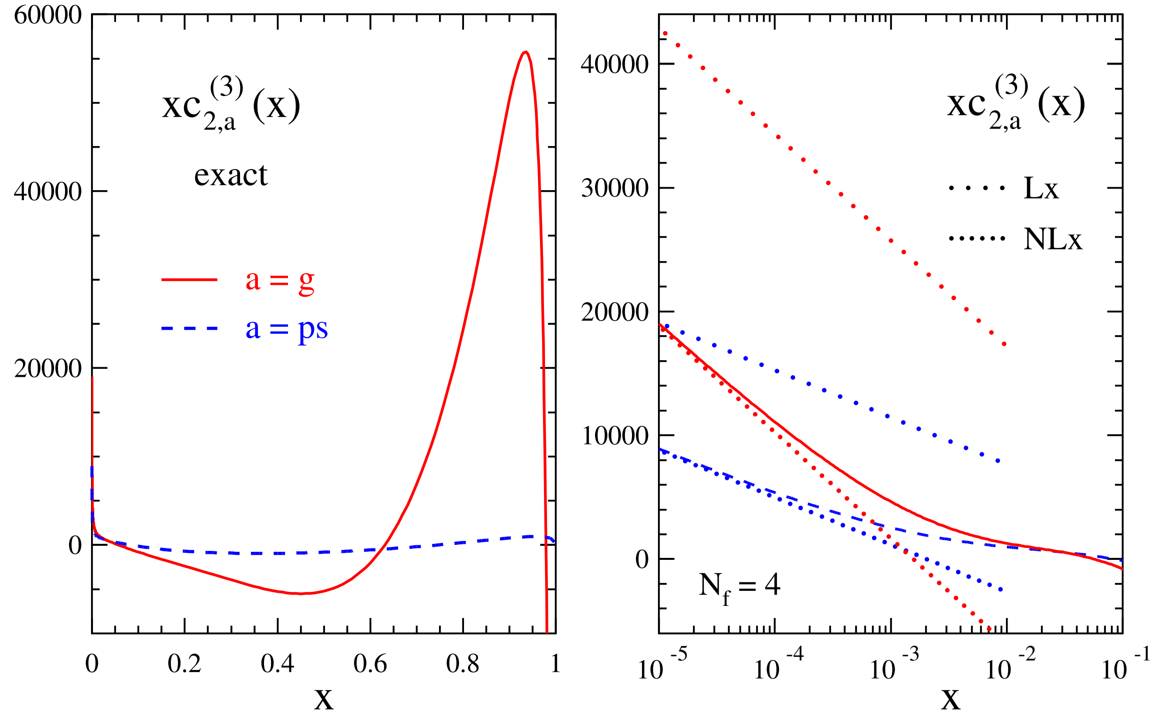

Figure 8: The three-loop pure-singlet and gluon coefficient functions $xc^{(3)}_{2,\text{ps}}(x)$ and $xc^{(3)}_{2,\text{g}}(x)$. Also shown (right) are the leading [95] and next-to-leading (besides Eqs. (4.27) and (4.29) also including Eqs. (4.28) and (4.30)) small-x approximations, respectively denoted by Lx and NLx.

logarithms are taken into account. As obvious from Eq. (4.26), small-x approximations by only the first ($\ln^5 x$), the first two, and even the first three logarithms qualitatively fail in the x-region shown in the figure. In fact, a 20% accuracy is reached with one, two and three small-x logarithms only at $x < 10^{-50}$ (sic), $x < 10^{-14}$ and $x < 10^{-8}$, respectively.

What physically matters, of course, is not Fig. 7 but the contribution to the structure function, given by the convolution with the parton distributions. Using the schematic, but sufficiently typical form $xq_{\rm ns} = x^{0.5}(1-x)^3$ one finds that the effect of the soft-gluon $\mathcal{D}_k$ part approximates the full result to better than 20% only for $x > 0.87$. The approximation by all small-x logarithms actually never reaches this accuracy. The large-x range can be improved to $x > 0.78$ by instead using the large-N version of the threshold expansion, keeping only the $\ln^k N$, $k = 1, \ldots 2n$ terms in $c^{(n=3)}_{2,\rm ns}(N)$. Both versions do however cover a significantly smaller x-range, by about a factor of two, than the corresponding soft-gluon approximations at two loops, which provide good approximations to $c^{(2)}_{2,\rm ns} \otimes q_{\rm ns}$ for $x \geq 0.7$ using the $\mathcal{D}_k$ terms and for $x \geq 0.55$ keeping only the $\ln N$ contributions.

At large x the contributions of the flavour-singlet quantities $C_{2,\rm ps}$ and $C_{2,\rm g}$ are small compared to the non-singlet coefficient functions discussed so far. We therefore do not write out the coefficient of the (leading) large-x terms $(1-x)L_1^k$, $k = 1,\ldots,4$ of $c^{(3)}_{2,\rm ps}(x)$ and $L_1^{k'}$, $k' = 1,\ldots,5$ of $c^{(3)}_{2,\rm g}(x)$ for brevity. The leading small-x contributions to these functions are, at $n \geq 2$ loops, of the form $x^{-1}\ln^k x$, $k = 1,\ldots,n-2$. The numerical QCD values of the three-loop coefficients can be read off from Eqs. (4.12) and Eqs. (4.13) above. The corresponding analytical results read

$$
\begin{aligned}
c^{(3)}_{2,\rm ps}\Big|_{L_0/x} &= C_A C_F n_f \left[-\frac{39488}{243} + \frac{416}{9}\zeta_2 - \frac{128}{9}\zeta_3 \right] , \qquad (4.27) \\
c^{(3)}_{2,\rm ps}\Big|_{1/x} &= C_A C_F n_f \left[-\frac{971284}{729} + \frac{15040}{81}\zeta_2 + \frac{752}{9}\zeta_3 + \frac{3968}{45}\zeta_2^2 \right] \\
&\quad + C_F^2 n_f \left[\frac{1090}{27} - 16\zeta_2 - \frac{800}{9}\zeta_3 + \frac{192}{5}\zeta_2^2 \right] \\
&\quad + C_F n_f^2 \left[\frac{22112}{729} - \frac{32}{9}\zeta_2 + \frac{128}{27}\zeta_3 \right] \qquad (4.28)
\end{aligned}
$$

and

$$
\begin{aligned}
c^{(3)}_{2,\rm g}\Big|_{L_0/x} &= C_A^2 n_f \left[-\frac{39488}{243} + \frac{416}{9}\zeta_2 - \frac{128}{9}\zeta_3 \right] = \frac{C_A}{C_F}\, c^{(3)}_{2,\rm ps}\Big|_{L_0/x} , \qquad (4.29) \\
c^{(3)}_{2,\rm g}\Big|_{1/x} &= C_A^2 n_f \left[-\frac{1002332}{729} + \frac{16096}{81}\zeta_2 + \frac{2192}{9}\zeta_3 + \frac{3968}{45}\zeta_2^2 \right] \\
&\quad + C_A C_F n_f \left[\frac{1090}{27} - 16\zeta_2 - \frac{800}{9}\zeta_3 + \frac{192}{5}\zeta_2^2 \right] + C_A n_f^2 \left[-\frac{572}{729} \right. \\
&\quad \left. + \frac{160}{27}\zeta_2 + \frac{64}{27}\zeta_3 \right] + C_F n_f^2 \left[\frac{45368}{729} - \frac{512}{27}\zeta_2 + \frac{128}{27}\zeta_3 \right] . \qquad (4.30)
\end{aligned}
$$

The leading contributions (4.27) and (4.29) were derived already ten years ago in Ref. [95] in the framework of the small-x resummation. As illustrated in the right part of Fig. 8, these leading terms alone do not provide a useful approximation at x-values relevant to collider measurements. At $x = 10^{-4}$, for example, they overshoot the respective full results for $c^{(3)}_{2,\mathrm{ps}}(x)$ and $c^{(3)}_{2,\mathrm{g}}(x)$ in Eqs. (B.10), (4.12) and (B.9), (4.13) by a factor of about three. This situation is completely analogous to, if somewhat worse than that for the three-loop splitting functions discussed in Ref. [11].

It should be noted that also the singlet coefficient functions receive contributions from non-$1/x$ logarithms up to $\ln^{2k-1} x$ at order α_s^k. In fact, the $1/x$ terms (4.27) – (4.30) contribute more than 80% of $c^{(3)}_{2,\mathrm{ps}}(x)$ and $c^{(3)}_{2,\mathrm{g}}(x)$ only at $x \leq 3 \cdot 10^{-4}$. One may expect this range to shrink further at higher orders due to the double-logarithmic enhancement of the non-$1/x$ terms. However, as the above third-order range is rather similar to that for the second-order coefficient functions, our results do not provide evidence for this effect.

For the rest of this section we turn to the third-order coefficient functions for the longitudinal structure function F_L which we only briefly discussed in Ref. [17]. The behaviour of the coefficient functions $c^{(3)}_{L,\mathrm{i}}(x)$ for $x \to 1$ is given by $\ln^k(1-x) \equiv L_1^k$, $k = 0, \ldots, 4$ for $\mathrm{i} = \mathrm{ns}$, by $(1-x)L_1^k$, $k = 0, \ldots, 4$ for $\mathrm{i} = \mathrm{g}$ and $(1-x)^2 L_1^k$, $k = 0, \ldots, 3$ for $\mathrm{i} = \mathrm{ps}$. The coefficients for the dominant non-singlet contribution read

$$c^{(3)}_{L,\mathrm{ns}}\Big|_{L_1^4} = 8\, C_F^3 \, , \tag{4.31}$$

$$c^{(3)}_{L,\mathrm{ns}}\Big|_{L_1^3} = C_A C_F^2 \left[-\frac{640}{9} + 32\,\zeta_2 \right] + C_F^3 \Big[72 - 64\,\zeta_2 \Big] + \frac{64}{9} C_F n_f^2 \, , \tag{4.32}$$

$$\begin{aligned} c^{(3)}_{L,\mathrm{ns}}\Big|_{L_1^2} = \; & C_A^2 C_F \left[\frac{1276}{9} - 56\,\zeta_2 - 32\,\zeta_3 \right] + C_A C_F^2 \left[-\frac{530}{9} + 80\,\zeta_2 + 80\,\zeta_3 \right] \\ & + C_F^3 \Big[-34 - 32\,\zeta_2 - 32\,\zeta_3 \Big] + C_A C_F n_f \left[-\frac{320}{9} + 16\,\zeta_2 \right] \\ & + C_F^2 n_f \left[\frac{92}{9} - 32\,\zeta_2 \right] + \frac{16}{9} C_F n_f^2 \, , \end{aligned} \tag{4.33}$$

$$\begin{aligned} c^{(3)}_{L,\mathrm{ns}}\Big|_{L_1^1} = \; & C_A^2 C_F \left[-\frac{25756}{27} + \frac{3008}{9}\zeta_2 + \frac{880}{3}\zeta_3 - \frac{128}{5}\zeta_2^2 \right] \\ & + C_A C_F^2 \left[\frac{32732}{27} - \frac{4720}{9}\zeta_2 + \frac{472}{3}\zeta_3 - \frac{1152}{5}\zeta_2^2 \right] + C_F^3 \Big[-264 \\ & + 16\,\zeta_2 - 752\,\zeta_3 - \frac{2816}{5}\zeta_2^2 \Big] + C_A C_F n_f \left[\frac{6640}{27} - \frac{320}{9}\zeta_2 - \frac{256}{3}\zeta_3 \right] \\ & + C_F^2 n_f \left[-\frac{4736}{27} + \frac{352}{9}\zeta_2 + \frac{320}{3}\zeta_3 \right] - \frac{304}{27} C_F n_f^2 \, , \end{aligned} \tag{4.34}$$

$$\begin{aligned} c^{(3)}_{L,\mathrm{ns}}\Big|_{L_1^0} = \; & C_A^2 C_F \left[\frac{67312}{81} + \frac{824}{3}\zeta_2 - \frac{1264}{3}\zeta_3 + 56\,\zeta_2^2 - 80\,\zeta_2\zeta_3 - 160\,\zeta_5 \right] \\ & + C_A C_F^2 \left[-\frac{5255}{6} - \frac{10988}{9}\zeta_2 + \frac{3280}{3}\zeta_3 - 516\,\zeta_2^2 + 416\,\zeta_2\zeta_3 + 1200\,\zeta_5 \right] \end{aligned}$$

$$
\begin{aligned}
&+ C_F^3 \left[\frac{1937}{6} - +508\,\zeta_2 - 88\,\zeta_3 + \frac{3384}{5}\,\zeta_2^2 - 512\,\zeta_2\zeta_3 - 1760\,\zeta_5\right] \\
&+ C_A C_F n_f \left[-\frac{21488}{81} + \frac{32}{9}\,\zeta_2 + \frac{64}{3}\,\zeta_3 - \frac{32}{5}\,\zeta_2^2\right] \\
&+ C_F^2 n_f \left[79 + \frac{1064}{9}\,\zeta_2 - \frac{400}{3}\,\zeta_3 + \frac{256}{5}\zeta_2^2\right] + C_F n_f^2 \left[\frac{1624}{81} - \frac{32}{9}\,\zeta_2\right] \\
&+ 9\, fl_{11}^{\rm ns} n_f \left[-320 - 1120\,\zeta_2 - 1760\,\zeta_3 + 32\,\zeta_2^2 + 320\,\zeta_2\zeta_3 + 3200\,\zeta_5\right] \;. \qquad (4.35)
\end{aligned}
$$

Except for Eq. (4.31) addressed already in Ref. [17], these large-x coefficients do not exhibit any obvious relation to those of $c^{(3)}_{2,\rm ns}$ in Eqs. (4.14) – (4.19). Thus the above coefficients should provide important checks and inputs for an explicit higher-order threshold resummation for F_L along the lines of Refs. [96, 97]. Such a resummation might not be of a large phenomenological relevance in view of the rather narrow region of validity of the large-x approximation, see the left part of Fig. 9, and the experimental status of F_L at large x. It would definitely be useful, however, in conjunction with a possible future four-loop generalization of the fixed-N calculations of Ref. [39].

The leading small-x contributions to $c^{(m)}_{L,\rm ns}(x)$ are given by the terms L_0^k with $k = 0, \ldots, 2m-3$. The corresponding three-loop coefficients read

$$
c^{(3)}_{L,\rm ns}\Big|_{L_0^3} \;=\; -\frac{20}{3} C_F^3 \;, \qquad (4.36)
$$

$$
c^{(3)}_{L,\rm ns}\Big|_{L_0^2} \;=\; -66\, C_A C_F^2 + 32\, C_F^3 + 12\, C_F^2 n_f \;, \qquad (4.37)
$$

$$
\begin{aligned}
c^{(3)}_{L,\rm ns}\Big|_{L_0^1} \;=\;& C_A^2 C_F \left[-\frac{968}{9} + 120\,\zeta_2\right] + C_A C_F^2 \left[-\frac{1832}{9} - 384\,\zeta_2\right] \\
&+ C_F^3 \Big[168 + 416\,\zeta_2\Big] + \frac{352}{9} C_F C_A n_f + \frac{224}{9} C_F^2 n_f - \frac{32}{9} C_F n_f^2 \;, \qquad (4.38)
\end{aligned}
$$

$$
\begin{aligned}
c^{(3)}_{L,\rm ns}\Big|_{L_0^0} \;=\;& C_A^2 C_F \left[-\frac{13060}{27} + 244\,\zeta_2\right] + C_A C_F^2 \left[\frac{5800}{27} - \frac{1696}{3}\,\zeta_2 - 96\,\zeta_3\right] \\
&+ C_F^3 \Big[288 + 608\,\zeta_2\Big] + C_A C_F n_f \left[\frac{4184}{27} - 16\,\zeta_2\right] \\
&+ C_F^2 n_f \left[-\frac{1144}{27} - \frac{32}{3}\,\zeta_2\right] - \frac{304}{27} C_F n_f^2 \;. \qquad (4.39)
\end{aligned}
$$

In the flavour-singlet sector, the dominant n-loop small-x terms for F_L are of the same form as those for F_2 discussed above. The respective $1/x$ contributions to $c^{(3)}_{L,\rm i}$, $\rm i = ps, g$ are given by

$$
c^{(3)}_{L,\rm ps}\Big|_{L_0/x} \;=\; C_A C_F n_f \left[-\frac{2176}{27} + \frac{64}{3}\,\zeta_2\right] \;, \qquad (4.40)
$$

$$
\begin{aligned}
c^{(3)}_{L,\rm ps}\Big|_{1/x} \;=\;& C_A C_F n_f \left[-\frac{14384}{27} + 112\,\zeta_2 + \frac{320}{3}\,\zeta_3\right] \\
&+ C_F^2 n_f \left[\frac{1792}{27} - \frac{32}{3}\,\zeta_2 - \frac{128}{3}\,\zeta_3\right] + C_F n_f^2 \left[\frac{3392}{81} - \frac{64}{9}\,\zeta_2\right] \qquad (4.41)
\end{aligned}
$$

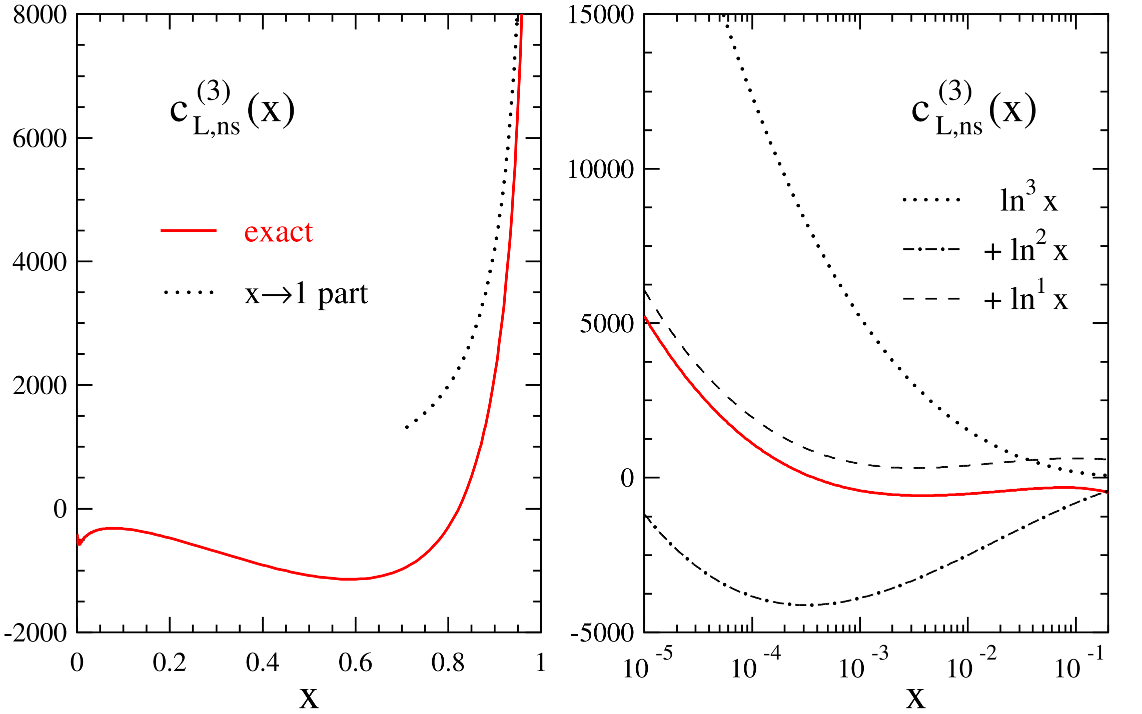

Figure 9: The three-loop non-singlet coefficient function $c^{(3)}_{L,\mathrm{ns}}(x)$ for four flavours. Also shown (left) are the large-x approximation by all terms (4.31) – (4.35) not vanishing for $x \to 1$, and (right) the small-x approximations obtained by successively including Eqs. (4.36) – (4.38).

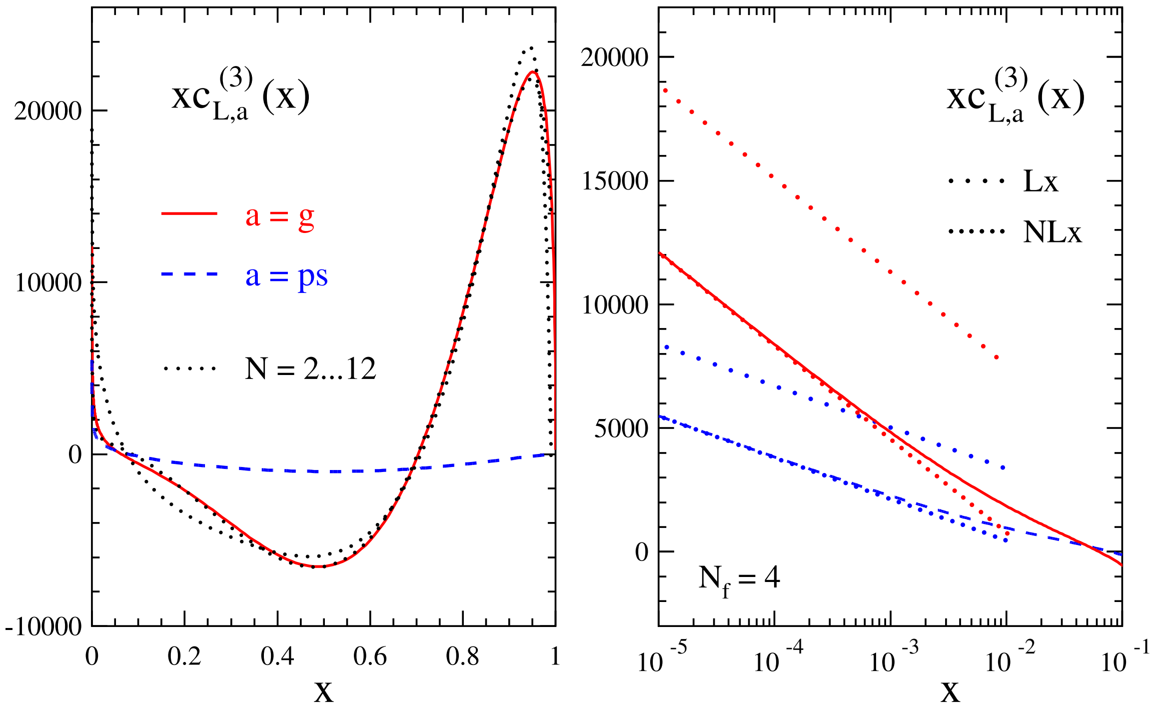

Figure 10: The three-loop pure-singlet and gluon coefficient functions $xc^{(3)}_{L,\mathrm{ps}}(x)$ and $xc^{(3)}_{L,\mathrm{g}}(x)$. Also shown (left) are the previous uncertainty band for the latter quantity [98, 99] inferred from the results of Refs. [41, 95], and (right) the leading (Lx) [95] and next-to-leading (NLx) small-x approximations as given by Eqs. (4.40) – (4.43) analogous to the right part of Fig. 8.

and

$$c^{(3)}_{L,\mathrm{g}}\Big|_{L_0/x} = C_A^2 n_f \left[-\frac{2176}{27}+\frac{64}{3}\zeta_2\right] = \frac{C_A}{C_F}\, c^{(3)}_{\mathrm{L,ps}}\Big|_{L_0/x}\,, \tag{4.42}$$

$$\begin{aligned} c^{(3)}_{L,\mathrm{g}}\Big|_{1/x} &= C_A^2 n_f \left[-\frac{44096}{81}+\frac{1040}{9}\zeta_2+\frac{320}{3}\zeta_3\right] + C_A n_f^2 \left[\frac{808}{27}-\frac{32}{9}\zeta_2\right] \\ &\quad + C_A C_F n_f \left[\frac{1792}{27}-\frac{32}{3}\zeta_2-\frac{128}{3}\zeta_3\right] + C_F n_f^2 \left[\frac{1936}{81}-\frac{64}{9}\zeta_2\right] . \end{aligned} \tag{4.43}$$

The exact C_F/C_A relation between the leading small-x terms [95] of $c^{(n)}_{a,\mathrm{ps}}$ and $c^{(n)}_{a,\mathrm{g}}$ does not hold for the subleading $1/x$-contributions at three loops. However, most coefficients (actually those for all colour-factor / ζ-function combinations not occurring in the leading terms) are still closely related. Besides the relations obvious from Eqs. (4.28) and (4.30) for $c_{2,\mathrm{g}}$ and Eqs. (4.41) and (4.43) for $c_{L,\mathrm{g}}$, we note that in both cases the sum of half the coefficient of $C_F n_f^2$ and the coefficient of $C_A n_f^2$ in the gluonic coefficient function equals that of $C_F n_f^2$ in the pure-singlet coefficient function. Numerically the C_F/C_A relation is violated by less than 5% for realistic values of n_f.

Eqs. (4.36) – (4.43) lead to the following numerical values for QCD,

$$\begin{aligned} c^{(3)}_{L,\mathrm{ns}}\big|_{L_0^3} &\cong -15.8025 \\ c^{(3)}_{L,\mathrm{ns}}\big|_{L_0^2} &\cong -276.148+21.3333\,n_f \\ c^{(3)}_{L,\mathrm{ns}}\big|_{L_0^1} &\cong -1356.17+200.691\,n_f-4.74074\,n_f^2 \\ c^{(3)}_{L,\mathrm{ns}}\big|_{L_0^0} &\cong -2226.25+408,058\,n_f+15.0123\,n_f^2 \end{aligned} \tag{4.44}$$

and

$$\begin{aligned} c^{(3)}_{L,\mathrm{ps}}\Big|_{L_0/x} &\cong -182.003\,n_f \\ c^{(3)}_{L,\mathrm{ps}}\Big|_{1/x} &\cong -885.534\,n_f+40.2390\,n_f^2\,, \end{aligned} \tag{4.45}$$

$$\begin{aligned} c^{(3)}_{L,\mathrm{g}}\Big|_{L_0/x} &\cong -409.506\,n_f \\ c^{(3)}_{L,\mathrm{g}}\Big|_{1/x} &\cong -2044.70\,n_f+88.5037\,n_f^2\,. \end{aligned} \tag{4.46}$$

The coefficients in both the non-singlet and singlet cases exhibit the pattern by now familiar from the three-loop splitting functions [10,11] and the coefficient functions for F_2 discussed above. The successive approximations of $c^{(3)}_{L,\mathrm{i}}$ by the leading small-x terms are compared in the right parts of Figs. 9 and 10 to the complete results (B.16) – (B.18). Also here the dominant $x \to 0$ contributions, $\ln^3 x$ for $\mathrm{i} = \mathrm{ns}$ and $x^{-1}\ln x$ for $\mathrm{i} = \mathrm{ps, g}$, alone do not provide useful approximations for practically relevant values of x. Such endpoint constraints are however phenomenologically important when combined with other partial results as, e.g., in Refs. [98,99] for the previously used approximations illustrated in the left part of Fig. 10 for $c^{(3)}_{L,\mathrm{g}}(x)$.

5 Numerical implications

In this section we finally discuss the size and convergence of the perturbative corrections to the structure functions F_2 and F_L in electromagnetic DIS. For brevity we confine ourselves to one physical scale $Q^2 = Q_0^2$ for almost all illustrations, and fix the renormalization and factorization scales by $\mu_r^2 = \mu_f^2 = Q^2$. The scale Q_0^2 is specified by an order-independent value of the strong coupling in the $\overline{\mathrm{MS}}$ scheme,

$$\alpha_s(Q_0^2) \,=\, 0.2 \quad \text{for} \quad n_f \,=\, 4 \,. \tag{5.1}$$

Depending on the precise value of α_s at the Z-boson mass, this choice corresponds (beyond the leading order) to a scale $Q_0^2 \approx 30\ldots50$ GeV^2, where especially F_2 has been measured over a wide range in x by fixed-target experiments and at the ep collider HERA [9].

We also assume, for a straightforward comparison of the effects of the various orders in Eqs. (2.15) (at $\varepsilon = 0$) and (4.1), that the operator matrix elements (2.5) and their all-N/all-x generalizations, the parton distributions (PDFs), do not depend on the perturbative order in α_s. We are aware that this is not the case in practical analyses in perturbative QCD, where these non-perturbative quantities are fitted to data. Our choice can be viewed as an idealization, representing a situation in which both $\alpha_s(Q_0^2)$ and the PDFs at this scale have been determined, independent of the order in α_s, by a non-perturbative solution of QCD. Specifically we choose

$$xq_{\rm ns}(x,Q_0^2) \,=\, x^{0.5}(1-x)^3 \tag{5.2}$$

for the flavour non-singlet combination and

$$\begin{aligned} xq_{\rm s}(x,Q_0^2) &= 0.6\,x^{-0.3}(1-x)^{3.5}\,(1+5.0\,x^{0.8})\,, \\ xg(x,Q_0^2) &= 1.6\,x^{-0.3}(1-x)^{4.5}\,(1-0.6\,x^{0.3}) \end{aligned} \tag{5.3}$$

for the singlet quark and gluon distributions. The same schematic, but sufficiently realistic input distributions have also been employed in Refs. [10, 11].

We start our illustrations of the perturbative expansion in Mellin-N space. As discussed above, the results for $N \neq 2, 4, 6, \ldots$ cannot be computed directly from the expressions in Appendix A, but are obtained by Mellin inverting (either analytically or numerically) the x-space expressions (4.3), (4.4) and (4.8) – (4.13) or (B.3) – (B.18). The expansions of $C_{a,\rm ns}(\alpha_s,N)$ and $C_{a,\rm g}(\alpha_s,N)$, $a = 2, L$, up to order α_s^3 are shown in Figs. 11 and 12 at our reference point (5.1). Here and below we use a linear scale up to $N = 15$, hence the main parts of these figures correspond to rather large values of x, recall Eq. (2.8) or Eq. (3.22). The small-x region will be addressed below.

The largest absolute corrections are found for $C_{2,\rm ns}$ at large N. Here the coefficient functions at order α_s^n behave as $a_s^n \ln^k N$, $k = 1, \ldots, 2n$, corresponding to the +-distributions in Eqs. (4.14) – (4.19). Hence the expansion in powers of α_s breaks down for $N \to \infty$ with $c_{2,\rm ns}^{(n+1)}/c_{2,\rm ns}^{(n)} \sim a_s \ln^2 N$. In the region of N shown in the figures, however, the three-loop effect is always smaller than half the two-loop contribution. $C_{2,\rm g}$ and $C_{L,\rm ns}$, on the other hand, vanish as $N^{-1} \ln^l N$ for $N \to \infty$,

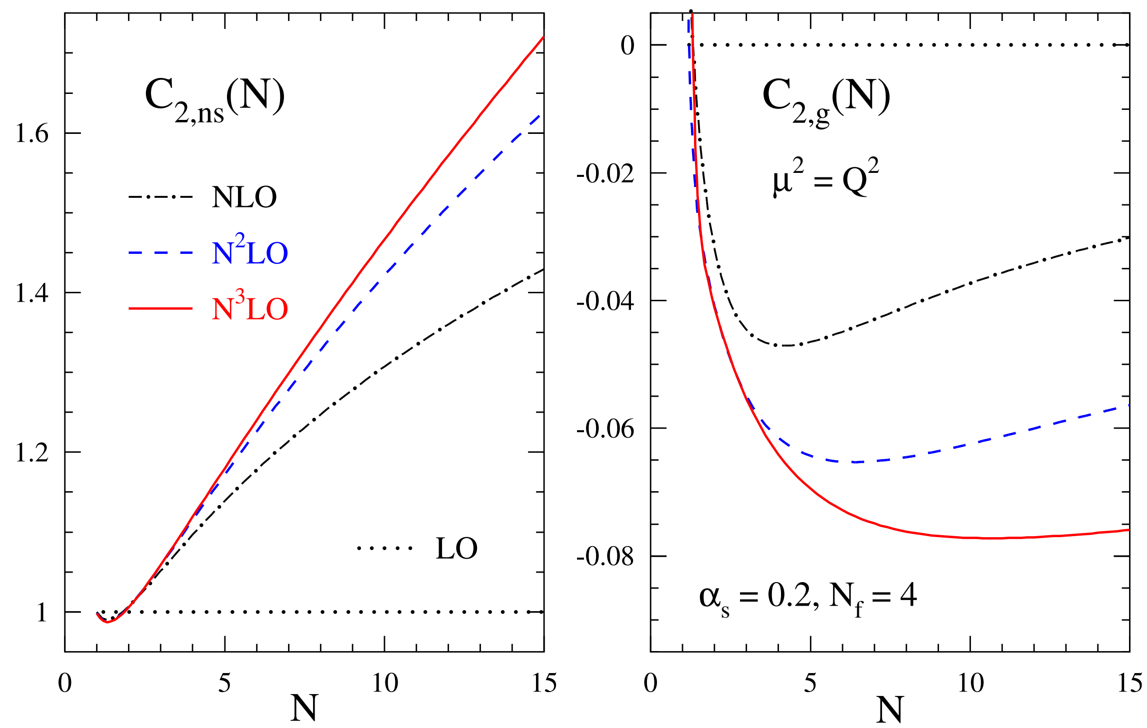

Figure 11: The perturbative expansion of the non-singlet (left) and gluon (right) N-space coefficient functions for $x^{-1}F_2$ at our reference point (5.1). The N^{n}LO curves include the $\varepsilon = 0$ terms up to order a_s^n in Eq. (2.15), obtained by Mellin inverting the results in Section 4 and Appendix B.

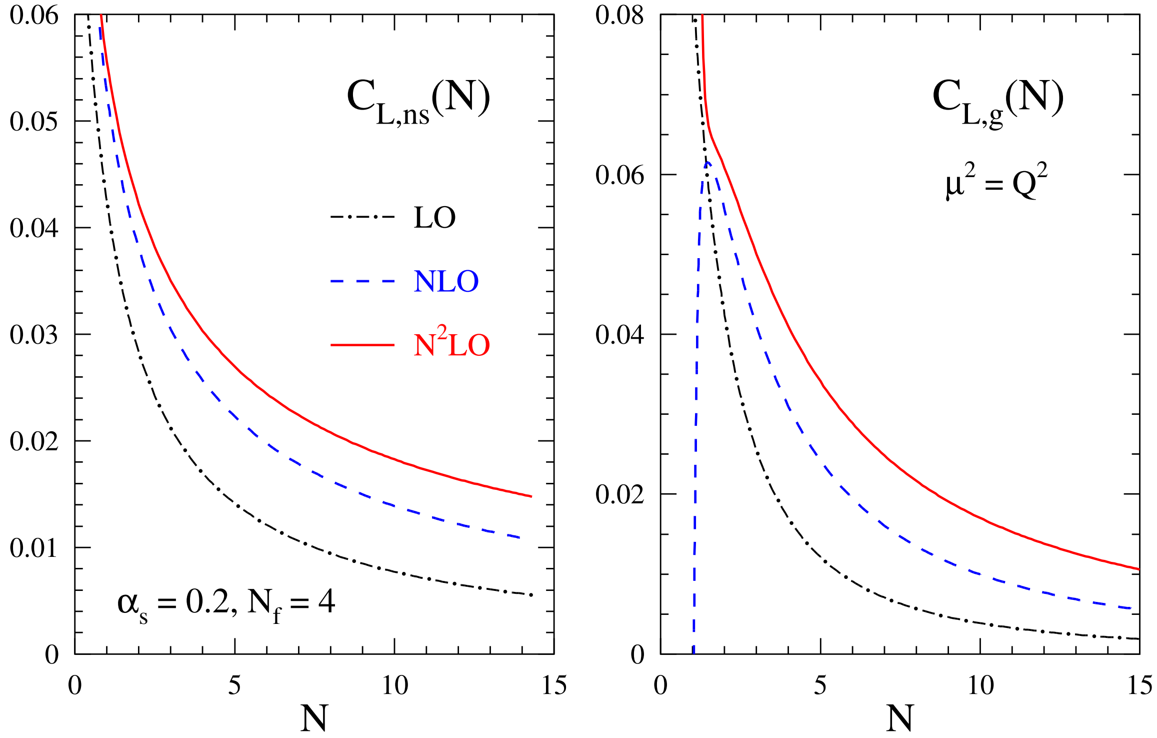

Figure 12: As Fig. 11, but for $x^{-1}F_L$ where the N^{n}LO results include the terms up to order a_s^{n+1}.

and $C_{L,\mathrm{g}}$ as $N^{-2}\ln^l N$, a behaviour that is not yet relevant, in particular for $C_{2,\mathrm{g}}$, at practically important values of N either. All these coefficient functions receive considerably larger relative α_{s}^3 corrections than $C_{2,\mathrm{ns}}$. In general the perturbative stability of F_L is worse than that of F_2.

Having calculated, for the first time, the complete third-order corrections to a one-scale process, inclusive DIS, we are in a unique situation to study the behaviour of the perturbation series. In order to illustrate the N-dependent convergence (or the lack thereof) of the corresponding coefficient functions, we introduce the quantity

$$\widehat{\alpha}_{a,i}^{(n)}(N) \;=\; 4\pi \frac{c_{a,i}^{(n-1)}(N)}{2\, c_{a,i}^{(n)}(N)} \; . \tag{5.4}$$

Recalling the normalization (2.12), $a_{\mathrm{s}} \equiv \alpha_{\mathrm{s}}/(4\pi)$, of our expansion parameter, $\widehat{\alpha}^{(n)}(N)$ represents the value of α_{s} for which the n-th order correction is half as large as that of the previous order. $\alpha_{\mathrm{s}} \lesssim \widehat{\alpha}_{a,i}^{(n)}(N)$ therefore defines, somewhat arbitrarily due to the choice of a factor of two, a region of good convergence of $C_{a,i}(\alpha_{\mathrm{s}},N)$. Obviously, the (absolute) size of the n-th and $(n-1)$-th order effects are equal for $\alpha_{\mathrm{s}} = 2\widehat{\alpha}^{(n)}(N)$. Thus the quantity (5.4) also indicates where the expansion appears not to be reliable any more for a given value of the Mellin variable, $\alpha_{\mathrm{s}} \gtrsim 2\widehat{\alpha}^{(n)}(N)$.

The function $\widehat{\alpha}^{(n)}(N)$ is shown in Fig. 13 for $C_{2,\mathrm{ns}}$ and $C_{2,\mathrm{g}}$ and in Fig. 14 for $C_{L,\mathrm{ns}}$ and $C_{L,\mathrm{g}}$ at $N \geq 2$. For the coefficient function $C_{2,\mathrm{ns}}$ dominating the corrections to F_2 in the large-N / large-x region, $\widehat{\alpha}^{(n)}(N)$ is always smaller than 0.2 at $N \leq 17$, and even smaller than 0.35 at $N \leq 6$. It is also important to note that the resulting safe region $\alpha_{\mathrm{s}} \leq \widehat{\alpha}_{2,\mathrm{ns}}^{(n)}(N)$ only marginally shrinks at three loops (N^{3}LO, $n = 3$ in Eq. (5.4)) with respect to the previous order. Thus we do not observe any sign of a breakdown of the perturbative expansion at phenomenologically relevant values of N. This also holds for the other cases shown in Figs. 13 and 14. In fact, while being considerably smaller than for $C_{2,\mathrm{ns}}$, the regions of fast convergence actually increase for the third-order (N^{2}LO for F_L) results, except for $C_{L,i}$ at small N where the stability is relatively best anyhow with, for instance, $\widehat{\alpha}_{L,i}^{(3)} = 0.20$ and 0.17 for $i = \mathrm{ns}$ and $i = \mathrm{g}$ at $N = 3$.

We end our N-space illustrations by estimating the size of the presently (and, presumably, in the near future) uncalculated fourth-order corrections to the non-singlet coefficient function at large N. For this purpose we make use of the Padé summation of the perturbation series, discussed in detail for QCD, e.g., in Refs. [100–102]. In this approach $C_{2,\mathrm{ns}}(N)$ in Eq. (2.15) (for $\varepsilon = 0$) is replaced by a rational function in a_{s},

$$\widetilde{C}_{2,\mathrm{ns}}^{[\mathcal{N}/\mathcal{D}]}(N) \;=\; \frac{1 + a_{\mathrm{s}} p_1(N) + \ldots + a_{\mathrm{s}}^{\mathcal{N}} p_{\mathcal{N}}(N)}{1 + a_{\mathrm{s}} q_1(N) + \ldots + a_{\mathrm{s}}^{\mathcal{D}} q_{\mathcal{D}}(N)} \; . \tag{5.5}$$

Here $\mathcal{D} \geq 1$ and $\mathcal{N} + \mathcal{D} = n$, where n stands for the maximal order in α_{s} at which the expansion coefficients $c_{2,\mathrm{ns}}^{(k)}(N)$ have been determined from an exact calculation. The functions $p_i(N)$ and $q_j(N)$ are determined from these known coefficients by expanding Eq. (5.5) in powers of α_{s}. This expansion then also provides the $[\mathcal{N}/\mathcal{D}]$ Padé approximant for the $(n{+}1)$-th order quantities $c_{2,\mathrm{ns}}^{(n+1)}$.

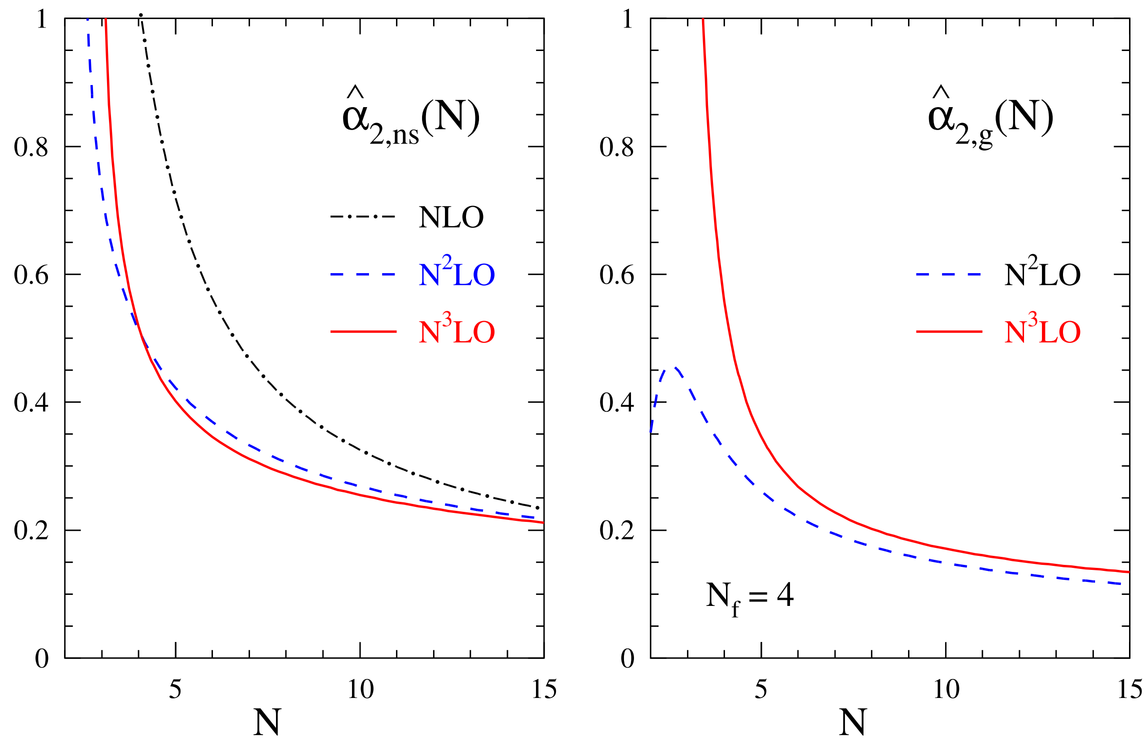

Figure 13: The N-dependent values (5.4) of α_s at which the effect of the n-th order (N^{n}LO) non-singlet and gluon coefficient functions for F_2 is half as large as that of the previous order. A NLO curve can only be shown for the non-singlet since only here the LO contribution does not vanish.

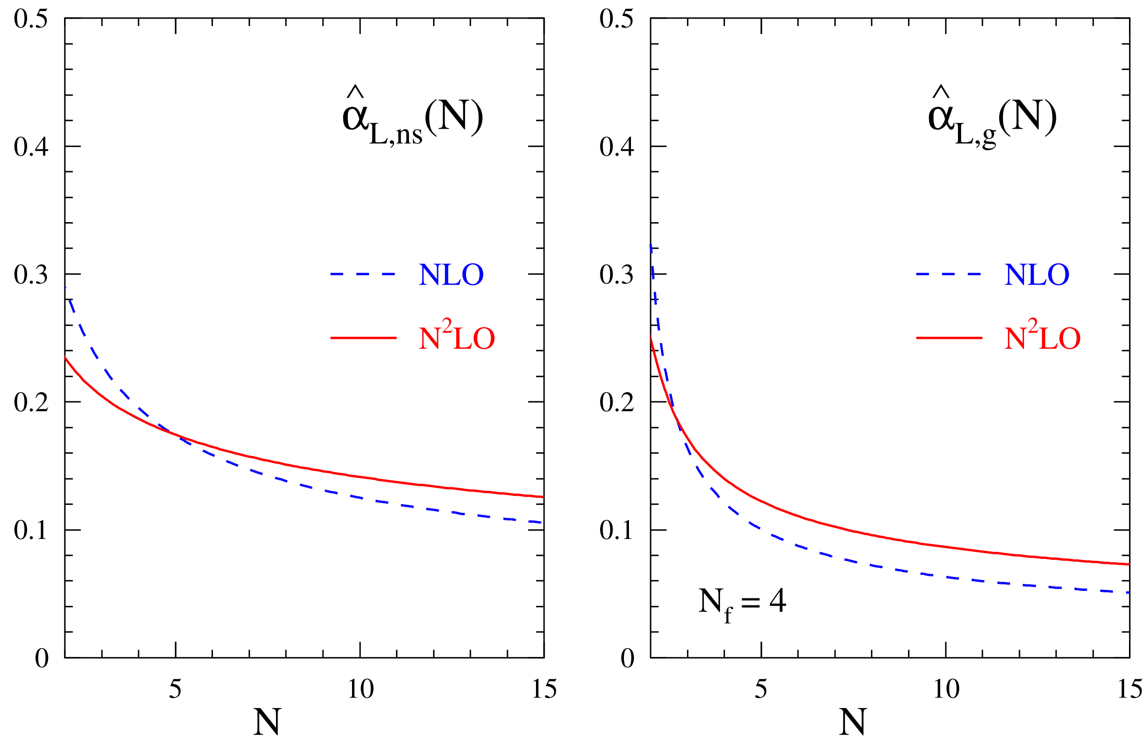

Figure 14: As Fig. 13, but for F_L where the terms up to order α_s^{n+1} form the N^{n}LO approximation.

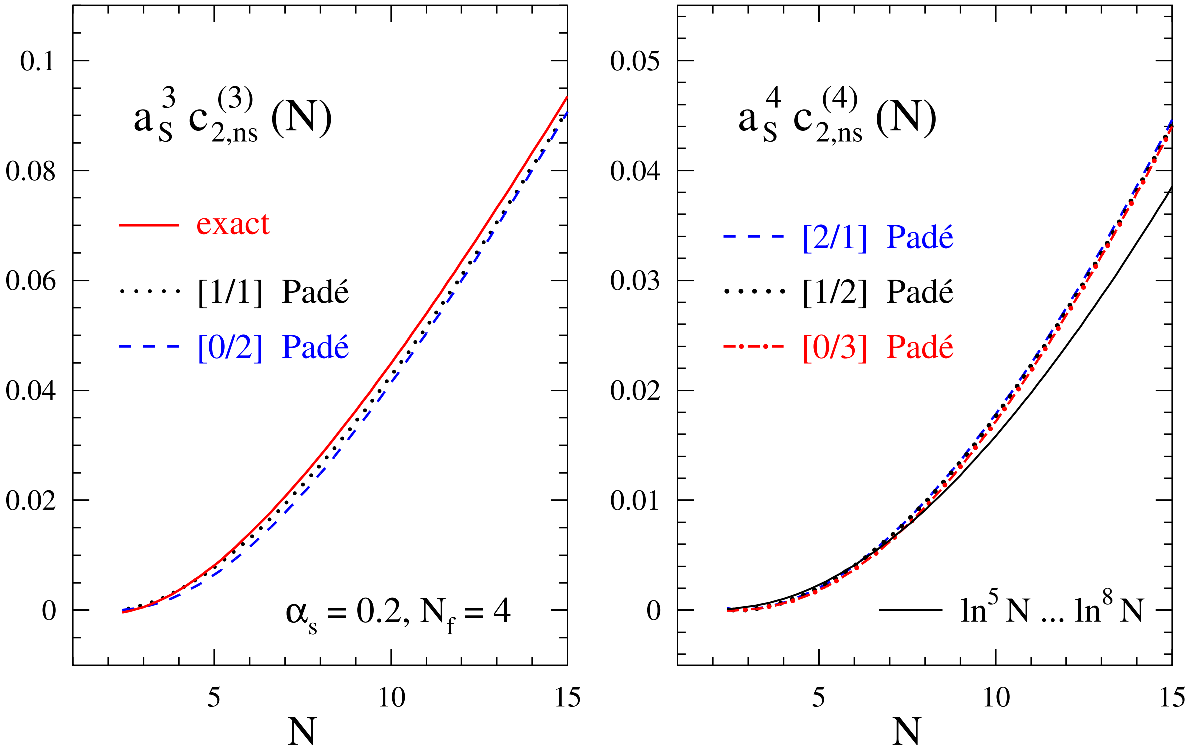

Figure 15: Padé estimates for the large-N behaviour of the three-loop (left) and four-loop (right) contributions to the non-singlet coefficient function $C_{2,\mathrm{ns}}(\alpha_s, N)$ at the reference point (5.1). The three-loop approximants are compared with our exact results. Also shown at four loops is the estimate by the sum of the four leading $\ln^k N$ terms fixed by the soft-gluon resummation [92].

In the left part of Fig. 15 the corresponding [1/1] and [0/2] Padé predictions for the three-loop coefficient function are compared to our new exact results. Obviously the Padé approximants provide a fair estimate of the true corrections. Hence it seems reasonable to expect that, at not too small values of N, the very similar [2/1], [1/2] and [0/3] fourth-order approximants shown in the right part of Fig. 15 correctly indicate at least the rough size of the four-loop corrections. This expectation is corroborated by a comparison (also shown in the figure) with the estimate by the four highest $\ln^k N$ contributions, $k = 5, \ldots, 8$ known from the next-to-leading logarithmic threshold resummation [92].

The x-space results for the non-singlet quantities $F_{2,\mathrm{ns}}$ and $F_{L,\mathrm{ns}}$ are shown in Figs. 16 and 17, respectively, for our reference input (5.1) and (5.2). In accordance with the left parts of Figs. 11 and 12, the relative large-x corrections are much larger for F_L than for F_2 (note the rather different scales of the right parts of Figs. 16 and 17). Nevertheless the third-order ($\mathrm{N^2LO}$) corrections to F_L amount to less than 10% for $x < 0.2$ and 3% at $x < 10^{-2}$, constituting a clear improvement over the NLO results. The three-loop corrections for $F_{2,\mathrm{ns}}$, on the other hand, even contribute less than 0.5% at $4 \cdot 10^{-5} \leq x \leq 0.65$, and exceed 3% only at very large x-values, $x \geq 0.78$, outside the measured region at scales $Q^2 > 30\ \mathrm{GeV}^2$, see Ref. [9].

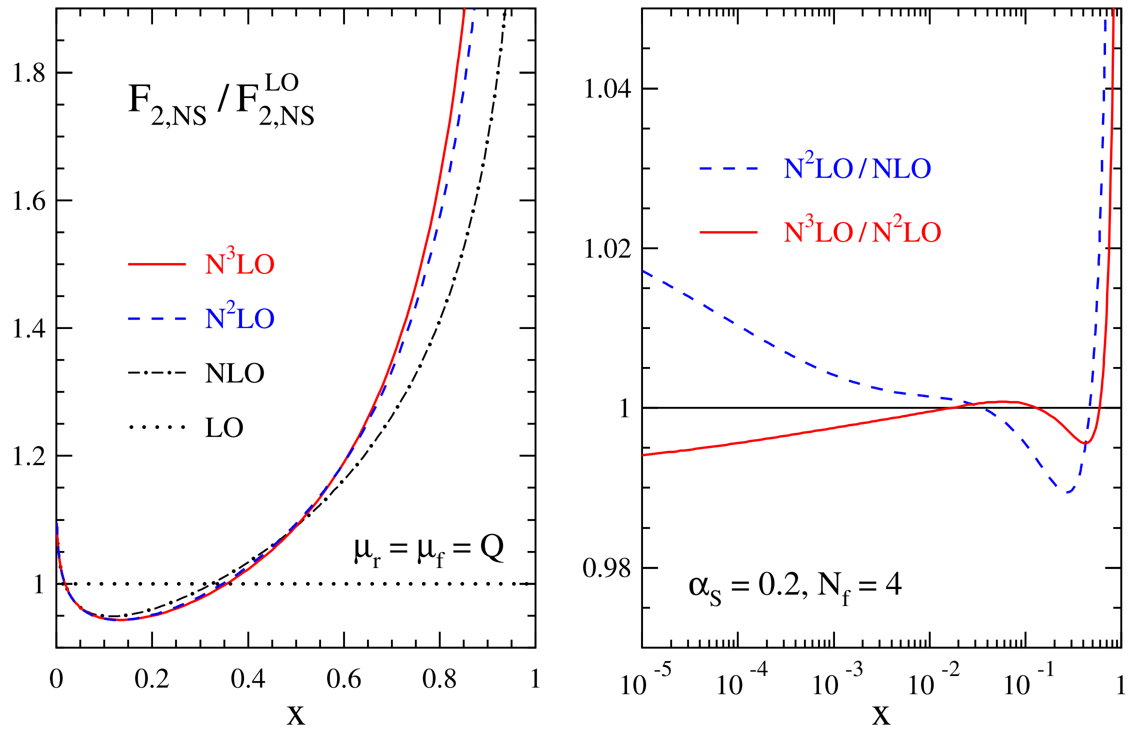

Figure 16: The perturbative expansion of the non-singlet structure function $F_{2,\rm ns}$ up to three loops (N^{3}LO). On the left all curves are normalized to the leading-order result $F^{\rm LO}_{2,\rm ns} = q_{\rm ns}$ given by Eq. (5.2), on the right we show the relative effects of the two-loop and three-loop corrections.

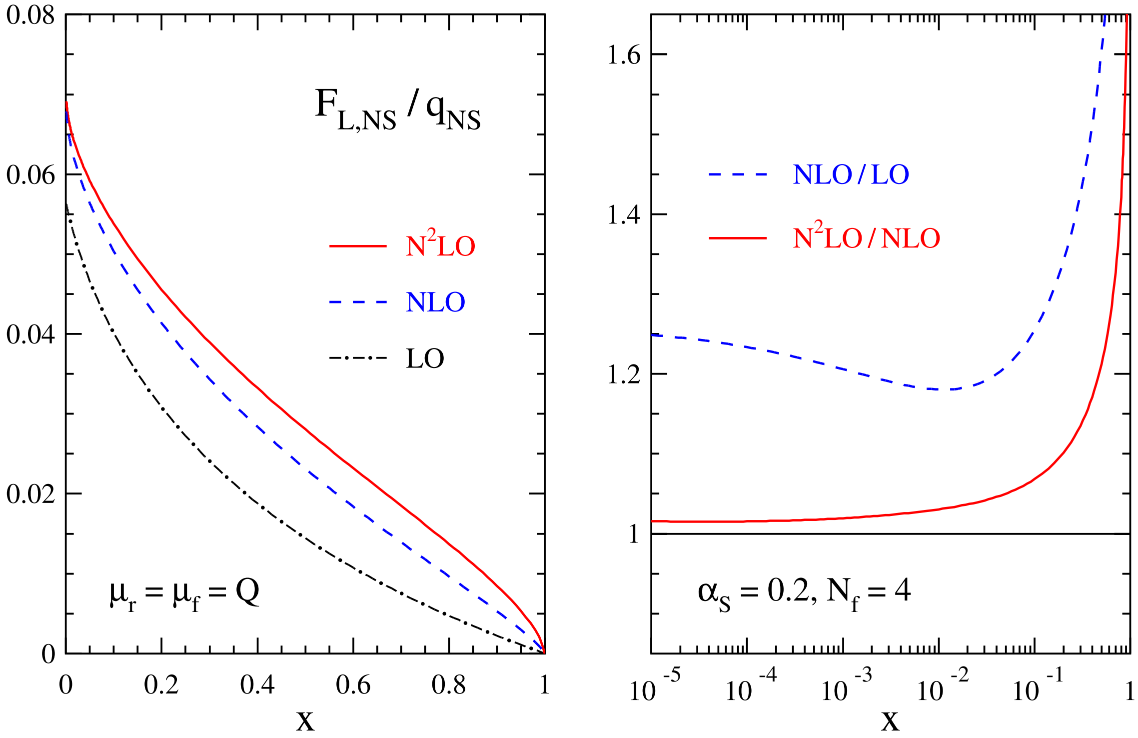

Figure 17: As Fig. 16, but for F_L where the terms up to order α_s^{n+1} form the N^{n}LO approximation. Also here the left plot is normalized to $q_{\rm ns}$, facilitating a direct comparison with $F_{2,\rm ns}$.

The corresponding contributions of the (typical) quark and gluon distributions (5.3) to the flavour-singlet part of the structure function F_2 are displayed in Fig. 18. The three-loop pure-singlet quark coefficient function $c^{(3)}_{2,\rm ps} \equiv c^{(3)}_{2,\rm q} - c^{(3)}_{2,\rm ns}$ contributes less than 0.1% at $x \geq 0.13$. Hence the large-x behaviour in the quark part (left graph) is completely analogous to that of $F_{2,\rm ns}$ just discussed. Likewise the effect of the third-order gluon coefficient function $c^{(3)}_{2,\rm g}$ (right graph) amounts to less than 0.2% of the lowest order result $q_{\rm s}$ at $x \geq 0.03$.

The situation is more interesting at small x, as at $x < 10^{-2}$ the two-loop corrections are larger, in both cases, than the one-loop contributions. Without our new three-loop results, this behaviour might be interpreted as indicative of an early breakdown of the expansion in $\alpha_{\rm s}$. Our results show, however, that this is not the case. In fact, at x-values relevant to collider experiments, the third-order contributions are always (considerably) smaller than their second-order counterparts, exceeding 1% only at $x < 4 \cdot 10^{-7}$ for $c_{2,\rm q} \otimes q_{\rm s}$ and at $x < 2 \cdot 10^{-5}$ for $c_{2,\rm g} \otimes g$. As illustrated already in Ref. [17], the perturbative stability of F_L is worse also in this region of x.

The above quark and gluon contributions are combined in the left part of Fig. 19. The total third-order correction is larger than 1% only outside the range $4 \cdot 10^{-5} \leq x \leq 0.65$. It rises towards $x \to 0$ and exceeds the size of the (opposite-sign) second-order contribution below $x \simeq 10^{-8}$. As all illustrations and numerical values presented in this section so far, these results refer to a point in the safely deep-inelastic region, $Q^2 = Q_0^2 \approx 30\ldots 50\ \mathrm{GeV}^2$, specified by Eqs. (5.1) – (5.3).

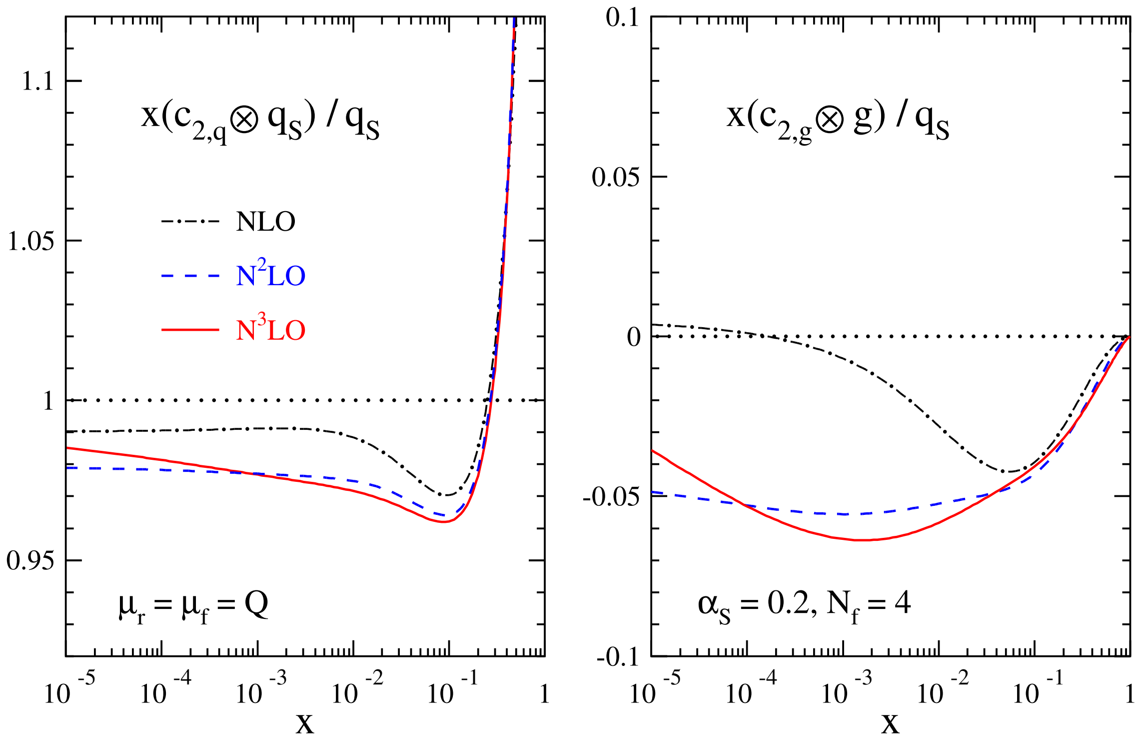

Figure 18: The perturbative expansion up to three loops (N^{3}LO) of the quark (left) and gluon (right) contributions to singlet structure function $F_{2,\rm s}$ at our reference point (5.1). All curves have been normalized to the leading-order result $F^{\rm LO}_{2,\rm s} = \langle e^2 \rangle\, q_{\rm s}$ given by Eq. (5.3).

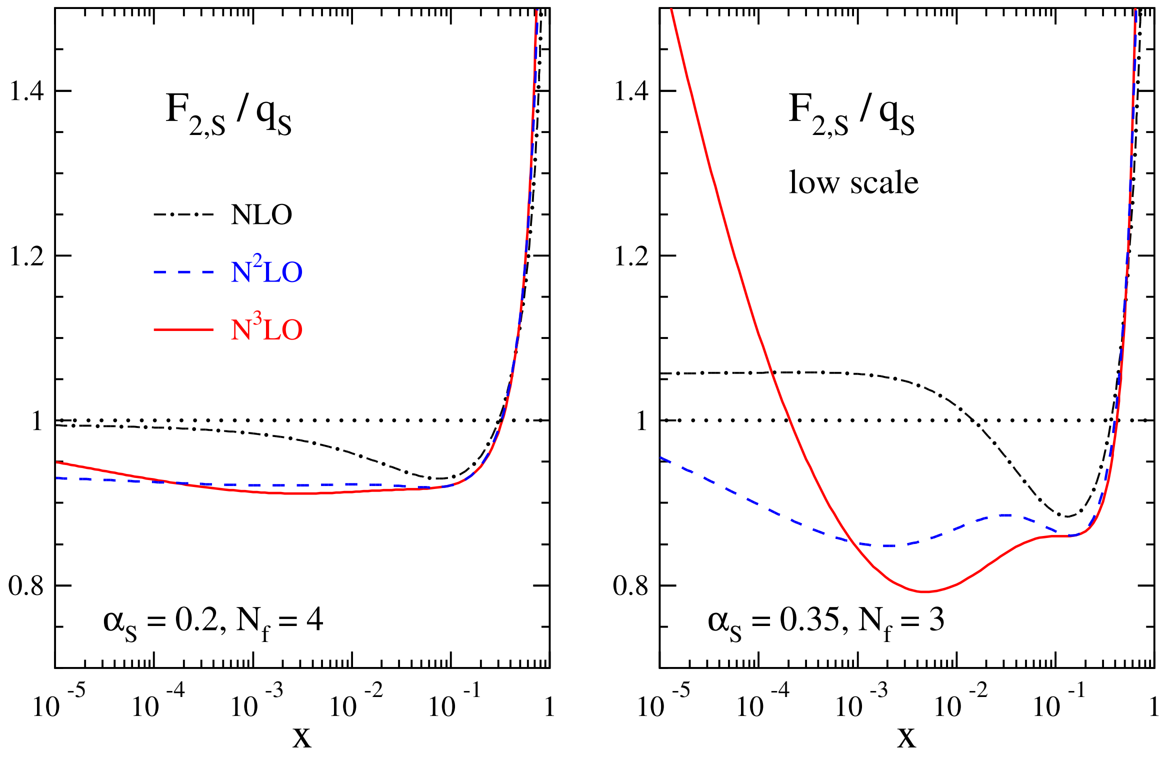

Figure 19: The flavour-singlet structure function $F_{2,s}(x,Q^2)$ at our standard reference point $Q_0^2 \approx$ 40 GeV^2 (left) and at the low scale $Q_1^2 \approx 2$ GeV^2 (right) up to the third order. All curves have been normalized to the respective leading-order results $F_{2,s}^{\rm LO} = \langle e^2 \rangle\, q_{\rm s}$ given by Eqs. (5.3) and (5.6).

The corresponding results for the singlet structure function $F_{2,s}$ at a low scale, $Q_1^2 \approx 2$ GeV^2 with $\alpha_s = 0.35$ and $n_f = 3$ active flavours, are shown in the right part of Fig. 19 for the (again order-independent, see above) quark and gluon distributions [11, 17]

$$
\begin{aligned}
xq_{\rm s}(x,Q_1^2) &= 0.6\,x^{-0.1}(1-x)^3\,(1+10\,x^{0.8})\ , \\
xg(x,Q_1^2) &= 1.2\,x^{-0.1}(1-x)^4\,(1+1.5\,x)\ .
\end{aligned} \tag{5.6}
$$

If all other parameters were kept equal, the N^{3}LO corrections (with respect to $F_{2,s}^{\rm LO} = \langle e^2 \rangle\, q_{\rm s}$ as shown in the figure) would be larger by a factor of about five here simply due to the increase in the coupling constant. The modified quark and gluon distributions, though, especially their much flatter small-x behaviour — $x^{-0.1}$ in Eq. (5.6) instead of $x^{-0.3}$ in Eq. (5.3), lead to a qualitatively different pattern at small x. While the three-loop corrections remain below 2% in the range $0.07 < x < 0.57$ and below 10% at $3 \cdot 10^{-4} < x < 0.73$, they rise sharply towards lower x at $x \lesssim 10^{-3}$. Consequently, the perturbative expansion of $F_{2,s}$ at low scales appears to be out of control at $x < 10^{-4}$. This rise for $x \to 0$ is very similar to that of $F_{L,s}$ in Ref. [17] where the relative third-order (N^{2}LO) corrections are however much larger over the full x-range.

Finally we need to address the relative importance of our new three-loop coefficient functions $c_{2,i}^{(3)}$ and the yet unknown four-loop splitting functions $P^{(3)}$. Together these two sets of quantities form the N^{3}LO approximation for F_2 once, as usual in order to resum large Q^2/μ_f^2 logarithms, the factorization scale μ_f is not kept fixed, but varied with the physical hard scale Q^2. The corresponding issue at N^{2}LO has been considered in Refs. [82, 86]. It was found that the effect of the three-loop splitting functions on the scaling violations of F_2 is small at $x > 0.01$ for both the non-singlet and singlet structure functions.

Here we confine ourselves to the non-singlet case, which is most important for the determination of α_s from the Q^2-dependence of the structure functions. Following Ref. [19] we express the scaling violation of $F_{2,\rm ns}$ in terms of the 'physical' N^{n}LO evolution kernel,

$$\frac{d}{d\ln Q^2}\, x^{-1}F_{2,\rm ns} \;=\; \Big\{ a_{\rm s}P^{(0)}_{\rm ns} + \sum_{l=1}^{n} a_{\rm s}^{l+1}\Big(P^{(l)}_{\rm ns} - \sum_{k=0}^{l-1}\beta_k\,\tilde{c}^{(l-k)}_{2,\rm ns}\Big)\Big\} \otimes \Big(x^{-1}F_{2,\rm ns}\Big) \tag{5.7}$$

with

$$\begin{aligned}
\tilde{c}^{(1)}_{2,\rm ns} &= c^{(1)}_{2,\rm ns}\,,\\
\tilde{c}^{(2)}_{2,\rm ns} &= 2\,c^{(2)}_{2,\rm ns} - c^{(1)}_{2,\rm ns}\otimes c^{(1)}_{2,\rm ns}\,,\\
\tilde{c}^{(3)}_{2,\rm ns} &= 3\,c^{(3)}_{2,\rm ns} - 3\,c^{(2)}_{2,\rm ns}\otimes c^{(1)}_{2,\rm ns} + c^{(1)}_{2,\rm ns}\otimes c^{(1)}_{2,\rm ns}\otimes c^{(1)}_{2,\rm ns}\,, \quad \ldots\quad .
\end{aligned} \tag{5.8}$$

Here $P^{(l)}$ are the l-loop splitting functions, recall Eq. (2.10), and β_k the coefficient of the β-function of QCD in Eq. (2.12). The coefficients (5.8) are given for $\mu_r = Q$, the explicit generalization to $\mu_r \neq Q$ up to N^{4}LO can be found in Ref. [19].

Given the small effect of the three-loop splitting functions $P^{(2)}$ at large x, we expect that a rough estimate of $P^{(3)}_{\rm ns}(x)$ is sufficient in Eq. (5.7). We choose the Mellin inverse of

$$P^{(3)}_{{\rm ns},\eta}(N) \;=\; \eta\,\Big[P^{(3)}_{\rm ns}(N)\Big]_{[1/1]\,\text{Padé}}\,, \quad \eta = 0, 2\,, \tag{5.9}$$

i.e., we assign a 100% error to the four-loop prediction of the [1/1] Padé summation.

The Q^2-derivative of $F_{2,\rm ns}$ is illustrated in Fig. 20, again assuming (now for the structure function) the non-singlet shape (5.2) at our reference point (5.1). Also for this quantity the N^{3}LO corrections are sizeable only at very large values of x. They rapidly decrease with decreasing x, for example from 6% at $x\!=\!0.85$ to 2% at $x\!=\!0.65$, and are smaller by a factor of two and three, respectively, than the N^{2}LO contributions at these points. As shown in the right part of the figure, the uncertainty due to the unknown four-loop splitting function is indeed very small over the whole x-range considered here. Therefore QCD analyses of the scaling violations can be extended to the N^{3}LO outside the small-x region. An idealized fit to $d\ln F_{2,\rm ns}/d\ln Q^2$ at $Q_0^2 \approx 40$ GeV^2, as described in more detail in Ref. [19], yields the following order-dependence of the central values:

$$\begin{aligned}
\alpha_s(Q_0^2)_{\rm NLO} &= 0.208\,, \quad \alpha_s(Q_0^2)_{\rm N^2LO} = 0.201\,,\\
\alpha_s(Q_0^2)_{\rm N^3LO} &= 0.200\,, \quad \alpha_s(Q_0^2)_{\rm N^4LO} = 0.200\,,
\end{aligned} \tag{5.10}$$

where the N^{4}LO kernel has been estimated by the Padé summation. Thus, even if the idealized fit underestimates the shifts by a factor of two, an $\alpha_{\rm s}$-uncertainty of 1% or less from the truncation of the perturbation series has been reached by the calculation of the N^{3}LO coefficient functions.

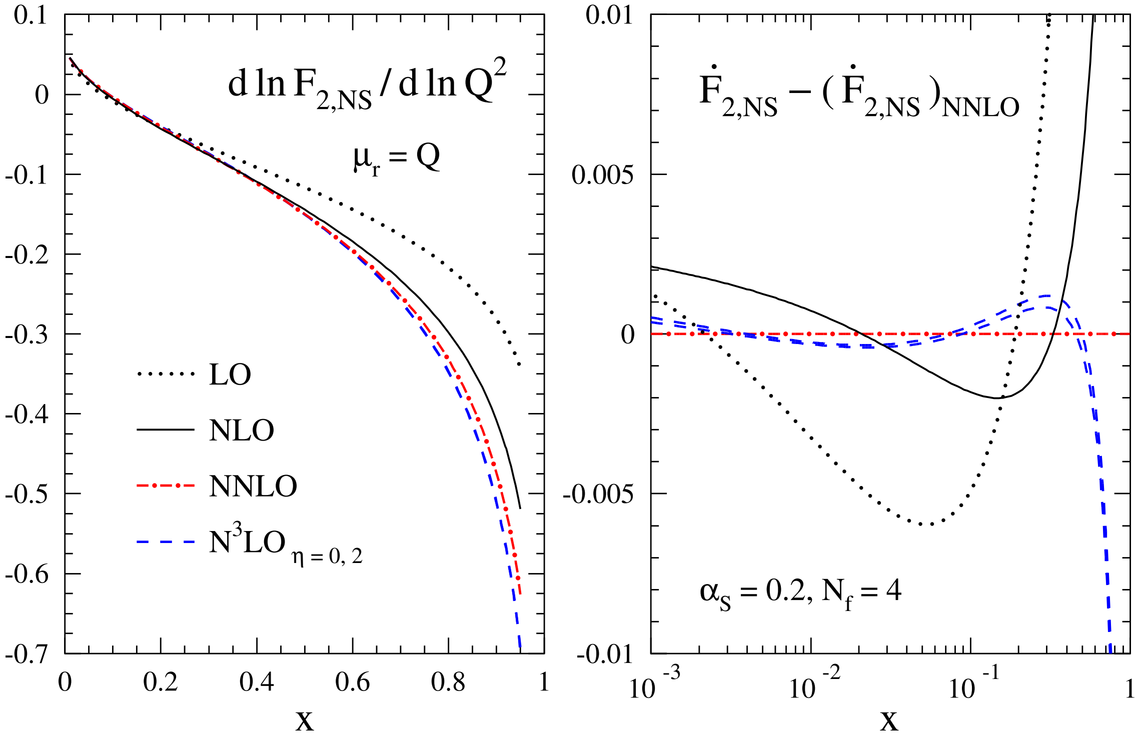

Figure 20: The perturbative expansion (5.7) of the scale derivative $\dot{F}_{2,\rm ns} \equiv d\ln F_{2,\rm ns}/d\ln Q^2$ for the initial condition $F_{2,\rm ns} = x^{0.5}(1-x)^3$ at the reference point (5.1). The two N^{3}LO curves indicate the uncertainty due to the four-loop splitting functions as estimated in Eq. (5.9).

6 Summary

We have calculated the complete third-order coefficient functions for the electromagnetic structure functions F_2 and F_L in massless perturbative QCD. Our calculation has been performed in Mellin-N space, as previous fixed-N computations of deep-inelastic scattering [39–42] using the optical theorem and a dispersion relation in the Bjorken variable x. However, generalizing the two-loop calculation of Ref. [16] and our previous computation of the fermionic non-singlet corrections at three loops [32], we have now obtained the complete third-order coefficient functions for all even values of N by deriving the analytic N-dependence of all required integrals through an elaborate iterative system of reduction equations. The full dependence of the coefficient functions on x and N has then been reconstructed from the even-N results by analytic continuation, making use of the relation between the harmonic sums $S_{\vec{n}}(N)$ [67] and the harmonic polylogarithms $H_{\vec{m}}(x)$ [85] in which the respective results can be expressed.

Our coefficient functions agree with all partial results available in the literature. The coefficients of the leading small-x terms $x^{-1}\ln x$ of the singlet quark and gluon coefficient functions were derived already in Ref. [95] in the framework of the small-x resummation. No corresponding result is known for the non-singlet case, in contrast to the splitting functions [103]. The first four large-x terms, $\ln^k N$ with $k = 3, \ldots 6$ in Mellin space, were predicted by the soft-gluon threshold resummation [92]. Most importantly, the even moments $N = 2,\ldots,12$ for the singlet case and $N = 2,\ldots,14$ for the non-singlet coefficient function were computed before [39–41] using the FORM [63, 64] version of the MINCER program [61, 62]. In fact, we have made extensive use of this program for checks at intermediate stages of our calculations. Finally our results also agree with the recent computation of the $N = 16$ non-singlet moments of F_2 and F_L [104], which was specifically performed as an independent simultaneous check of our calculations.

We have investigated the convergence of the perturbative expansion of the coefficient functions $C_{a,i}(N,\alpha_s)$ by determining, at $2 \le N \le 20$, the N-dependent range of α_s for which the n-th order corrections are at most half as large as the $(n-1)$-th order contributions. For $C_{2,\mathrm{ns}}$ this α_s-region shrinks significantly from the first to the second order, but only marginally from the second to the third. The coefficient functions $C_{2,\mathrm{g}}$ and $C_{L,i}$ exhibit larger corrections than $C_{2,\mathrm{ns}}$ — at $N = 6$, for example, the above α_s-region is $\alpha_s < 0.35$ for $C_{2,\mathrm{ns}}$, but $\alpha_s < 0.17$ for $C_{L,\mathrm{ns}}$ — however this smaller region actually increases from the second to the third order for most values of N. Thus, up to the third order, we find no sign of the supposed asymptotic character of the perturbative expansion.

Besides the phenomenologically less relevant limit $x \to 1$, the above region of N also excludes the small-x region opened up experimentally by HERA. The expansion of the coefficient functions is unstable for $x \to 0$ as $c^{(n)}/c^{(n-1)} \sim \alpha_s \ln^{\xi} x$ with $\xi = 2$ ($\xi = 1$) for the non-singlet (singlet) cases. This behaviour does not spoil the convergence of the α_s-expansion for x-values relevant to collider measurements in the safely deep-inelastic regime $Q^2 \gg 1$ GeV^2, however, due to an apparently systematic suppression of the coefficients of leading terms (see also Refs. [10, 11]) and the Mellin convolution with the parton distributions. At $Q^2 \approx 30$ GeV^2, for instance, the total third-order correction to F_2 is larger than 1% only outside the wide range $4 \cdot 10^{-5} \le x \le 0.65$, and exceeds 5% only at $x \lesssim 10^{-7}$ and $x > 0.8$. At low scales $Q^2 \approx 2$ GeV^2, on the other hand, the perturbative expansion appears to be out of control at $x < 10^{-4}$.

Our three-loop results for the splitting functions [10, 11] and F_L (briefly discussed already in Ref. [17]) facilitate NNLO analyses of deep-inelastic scattering over the full x-range covered by data. The present additional results for F_2 can be employed to effectively extend the main part of DIS analyses to the N^{3}LO at $x > 10^{-2}$ where the effect of the unknown fourth-order splitting functions is expected to be very small, for example leading to determinations of $\alpha_s(M_Z)$ with an error of less than 1% from the truncation of the perturbation series. For use in such analyses we have provided compact and accurate parametrizations of our very lengthy exact results. FORM files of these results, and FORTRAN subroutines of the exact and approximate coefficient functions can be obtained from the preprint server `HTTP://arXiv.org` by downloading the source of this article. Furthermore they are available from the authors upon request.

Finally our three-loop results for a one-scale process also are of theoretical interest, as they open up a new order in the study of perturbative QCD. As first further steps they facilitate the extension of the Sudakov resummations of threshold logarithms in DIS and of the quark form factor beyond the orders obtained so far [27–30, 32]. We have performed the required additional calculations for both cases and will report the results in a forthcoming publication [31].

Acknowledgments

We would like to thank S.A. Larin, F. J. Yndurain, E. Remiddi, E. Laenen, W.L. van Neerven, P. Uwer, S. Weinzierl and J. Blümlein for stimulating discussions. M. Zhou has contributed some FORM routines in an early stage of this project. We are grateful to T. Gehrmann for providing a weight-five extension of the FORTRAN package [87] for the harmonic polylogarithms. The Feynman diagrams in this article have been drawn using the packages AXODRAW [105] and JAXODRAW [106]. The work of S.M. has been supported in part by the Deutsche Forschungsgemeinschaft in Sonderforschungsbereich/Transregio 9. The work of J.V. has been part of the research program of the Dutch Foundation for Fundamental Research of Matter (FOM).

Appendix A: The exact Mellin-space results

Here we provide the exact even-N expressions for the coefficient functions $C_{2,i}$ and $C_{L,i}$ up to the third order in $a_s = \alpha_s/(4\pi)$. These results are expressed in terms of harmonic sums [65–68], following Ref. [67] recursively defined by

$$S_{\pm m_1,m_2,\ldots,m_k}(N) \;=\; \sum_{i=1}^{N} \frac{(\pm 1)^i}{i^{m_1}}\, S_{m_2,\ldots,m_k}(i) \;, \quad S(N) \;=\; 1 \;. \tag{A.1}$$

The sum of the absolute values of the indices m_k defines the weight of the harmonic sum. Sums with weight up to $2n$ occur in the n-loop coefficient functions for both F_2 and F_L. As in Section 3 we employ the notation (3.10),

$$\mathbf{N_\pm}\, S_{\vec{m}} \;=\; S_{\vec{m}}(N \pm 1) \;, \qquad \mathbf{N_{\pm i}}\, S_{\vec{m}} \;=\; S_{\vec{m}}(N \pm i) \;,$$

together with the abbreviations

$$\begin{aligned} g_{\rm qq} &= \mathbf{N_+} + \mathbf{N_-} \;, \\ g_{\rm qg} &= 2\mathbf{N_{+2}} - 4\mathbf{N_+} - \mathbf{N_-} + 3 \;. \end{aligned} \tag{A.2}$$

The N-independent zeroth-order quark coefficient function for F_2 is set to unity, recall Eq. (4.2). In the above notation the well-known first-order results for F_2 read

$$c^{(1)}_{2,\rm q}(N) \;=\; C_F\big(9(S_1 - 1) + 2g_{\rm qq}(S_{1,1} + 2S_1 - S_2) - 7(\mathbf{N_-} + 1)S_1\big) \;, \tag{A.3}$$

$$c^{(1)}_{2,\rm g}(N) \;=\; n_f\big(-2g_{\rm qg}(S_{1,1} + 4S_1 - S_2) - 6(\mathbf{N_-} - 1)S_1\big) \;. \tag{A.4}$$

The corresponding expressions for the two-loop coefficient functions [12, 13, 16] are given by

$$\begin{aligned} c^{(2)}_{2,\rm ns}(N) \;=\; & \delta(N-2)\Big\{C_F n_f(-4) + {C_F}^2\Big(-\frac{4189}{810} + \frac{96}{5}\zeta_3\Big) + C_A C_F\Big(\frac{3677}{135} - \frac{128}{5}\zeta_3\Big)\Big\} \\ & + \theta(N-4)\Big\{C_F\Big(C_F - \frac{C_A}{2}\Big)\Big(16S_{-3,1} + 48S_{-2,-2} + 144S_{1,-2} - \frac{16}{5}(\mathbf{N_{-3}} - \mathbf{N_{-2}})S_{1,-2} \end{aligned}$$

Appendix B: The exact x-space results

In this final appendix we write down the full x-space coefficient functions up to the third order. These functions can be expressed in terms of harmonic polylogarithms [83–85], for which we adopt the notation $H_{m_1,\ldots,m_w}(x)$, $m_j = 0, \pm 1$ of Ref. [85]. The n-loop coefficient functions for F_2 and F_L involve harmonic polylogarithms up to weight $w = 2n-1$. Below we use the short-hand notation

$$H_{\underbrace{0,\ldots,0}_{m},\pm 1,\underbrace{0,\ldots,0}_{n},\pm 1,\ldots}(x) \;=\; H_{\pm(m+1),\pm(n+1),\ldots}(x) \tag{B.1}$$

and suppress the argument x for brevity. Furthermore we employ the abbreviations

$$\begin{aligned}
p_{\rm qq}(x) &= 2(1-x)^{-1} - 1 - x\,,\\
p_{\rm qg}(x) &= 1 - 2x + 2x^2\,,\\
p_{\rm gq}(x) &= 2x^{-1} - 2 + x\,,\\
p_{\rm gg}(x) &= (1-x)^{-1} + x^{-1} - 2 + x - x^2\,.
\end{aligned} \tag{B.2}$$

All divergences for $x \to 1$ in Eq. (B.2) and below are to be read as the +-distributions $\mathcal{D}_k$ of Eqs. (4.5) and (4.6).

In this notation the one-loop coefficient functions for F_2 are given by

$$c^{(1)}_{2,\rm q}(x) \;=\; C_F\left(\frac{1}{2}(9+5x) - \frac{1}{2}p_{\rm qq}(x)(3+4{\rm H}_0+4{\rm H}_1) - \delta(1-x)(9+4\zeta_2)\right)\,, \tag{B.3}$$

$$c^{(1)}_{2,\rm g}(x) \;=\; n_f\left(6 - 2p_{\rm qg}(x)(4+{\rm H}_0+{\rm H}_1)\right)\,. \tag{B.4}$$

The exact two-loop results corresponding to the approximations (4.8) – (4.10) read

$$\begin{aligned}
c^{(2)}_{2,\rm ns}(x) \;=\; & C_F\left(C_F - \frac{C_A}{2}\right)\left(\frac{8}{5}(9p_{\rm qg}(-x)(1-x) + p_{\rm gq}(-x)(1-x^{-1}) + (37+17x)){\rm H}_{-1,0}\right.\\
&+ 4p_{\rm qq}(-x)(7\zeta_3 + 6{\rm H}_{-2,0} + 4{\rm H}_{-1,2} - 8{\rm H}_{-1,-1,0} + 10{\rm H}_{-1,0,0} - 3{\rm H}_{0,0,0} - 8{\rm H}_{-1}\zeta_2 - 2{\rm H}_0\\
&+ 2{\rm H}_0\zeta_2 - 2{\rm H}_3) - \frac{72}{5}p_{\rm qg}(x)((1+x)(\zeta_2 - {\rm H}_{0,0}) - 1 - {\rm H}_0) + \frac{8}{5}p_{\rm gq}(x)(1-{\rm H}_0)\\
&\left.+ 8(1-5x)({\rm H}_{1,0,0} - {\rm H}_1\zeta_2) - 8(1+5x)(2{\rm H}_{-1,-1,0} - {\rm H}_{-1,0,0} + {\rm H}_{-1}\zeta_2)\right)\\
&+ C_F n_f\left(\frac{1}{54}p_{\rm qq}(x)(247 - 144\zeta_2 + 180{\rm H}_{0,0} + 72{\rm H}_{1,0} + 72{\rm H}_{1,1} + 342{\rm H}_0 + 174{\rm H}_1 + 144{\rm H}_2)\right.\\
&\left.- \frac{1}{3}(7+19x){\rm H}_0 - \frac{1}{3}(1+13x){\rm H}_1 - \frac{1}{18}(23+243x) + \delta(1-x)\left(\frac{457}{36} + \frac{4}{3}\zeta_3 + \frac{38}{3}\zeta_2\right)\right)\\
&+ {C_F}^2\left(16{\rm H}_{-2,0} + \frac{1}{5}(33+37x){\rm H}_{0,0} + \frac{1}{4}p_{\rm qq}(x)(51 + 128\zeta_3 + 48\zeta_2 + 96{\rm H}_{-2,0} - 12{\rm H}_{0,0}\right.\\
&- 72{\rm H}_{1,0} - 72{\rm H}_{1,1} - 96{\rm H}_{1,2} - 96{\rm H}_{2,0} - 112{\rm H}_{2,1} - 32{\rm H}_{0,0,0} - 48{\rm H}_{1,0,0} - 128{\rm H}_{1,1,0} - 96{\rm H}_{1,1,1}\\
&+ 122{\rm H}_0 + 96{\rm H}_0\zeta_2 + 54{\rm H}_1 + 32{\rm H}_1\zeta_2 - 48{\rm H}_2 - 96{\rm H}_3) - \frac{1}{2}(43+63x){\rm H}_0 + \frac{1}{2}(59-109x){\rm H}_1\\
&- 4(1-19x)\zeta_3 + 2(1+x)(7{\rm H}_{1,0} + 2{\rm H}_{2,0} + 2{\rm H}_{2,1} + 5{\rm H}_{0,0,0} - 4{\rm H}_0\zeta_2 + 4{\rm H}_3) + 2(5+9x)({\rm H}_{1,1}
\end{aligned}$$

$$
\begin{aligned}
& - 36(1-4x^{-1})(\mathrm{H}_{1,0}\zeta_2 - \mathrm{H}_{1,3} + \mathrm{H}_{1,1,0,0} - \mathrm{H}_1\zeta_3) - 4459 + 1044\zeta_3 + 993\zeta_2 + 48\mathrm{H}_{0,0} \\
& - 1185\mathrm{H}_{1,0} - 1095\mathrm{H}_{1,1} - 450\mathrm{H}_{1,2} - 360\mathrm{H}_{2,0} - 450\mathrm{H}_{2,1} - 684\mathrm{H}_{1,0,0} - 450\mathrm{H}_{1,1,0} \\
& - 450\mathrm{H}_{1,1,1} - 716\mathrm{H}_0 + 36\mathrm{H}_0\zeta_2 + 511\mathrm{H}_1 - 216\mathrm{H}_2 + 144\mathrm{H}_3) + \frac{8}{15}(116-69x)\mathrm{H}_{-1}\zeta_2 \\
& - \frac{32}{15}(4+231x)\mathrm{H}_0\zeta_3 + \frac{16}{9}(39-31x)\mathrm{H}_0\zeta_2 - \frac{8}{135}(14097-33650x)\mathrm{H}_0 \\
& - \frac{8}{45}(1144-699x)\zeta_2\mathrm{H}_1 - \frac{8}{45}(2929-1069x)\mathrm{H}_1 + \frac{8}{45}(2393-4652x)\mathrm{H}_2 \\
& - \frac{16}{45}(147+383x)\mathrm{H}_3 - \frac{16}{15}(8-403x)\mathrm{H}_4 + 80(2-x)(\mathrm{H}_{1,2} + \mathrm{H}_{1,1,0} + \mathrm{H}_{1,1,1}) \\
& - \frac{8}{75}(64+641x){\zeta_2}^2 - \frac{16}{45}(1329-824x)\zeta_3 - \frac{8}{45}(1881-3125x)\zeta_2 + \frac{8}{135}(13933+1617x) \\
& + \frac{32}{3}x(7\mathrm{H}_{-3,0} + 10\mathrm{H}_{-2,2} + 15\mathrm{H}_{2,2} + 30\mathrm{H}_{3,0} + 33\mathrm{H}_{3,1} + 8\mathrm{H}_{-2,-1,0} + 19\mathrm{H}_{-2,0,0} + 15\mathrm{H}_{2,1,0} \\
& + 15\mathrm{H}_{2,1,1} + 38\mathrm{H}_{0,0,0,0} - 6\mathrm{H}_{-2}\zeta_2 - 19\mathrm{H}_2\zeta_2)\Big) \; . \qquad \text{(B.18)}
\end{aligned}
$$

Compact parametrizaztions of Eqs. (B.11) – (B.18) have been provided in Ref. [17].

References

[1] D.J. Gross and F. Wilczek, Phys. Rev. Lett. 30 (1973) 1343

[2] H.D. Politzer, Phys. Rev. Lett. 30 (1973) 1346

[3] D.J. Gross and F. Wilczek, Phys. Rev. D8 (1973) 3633

[4] H. Georgi and H.D. Politzer, Phys. Rev. D9 (1974) 416

[5] D.J. Gross and F. Wilczek, Phys. Rev. D9 (1974) 980

[6] D. H. Coward *et al.*, Phys. Rev. Lett. 20 (1968) 292

[7] E. D. Bloom *et al.*, Phys. Rev. Lett. 23 (1969) 930

[8] M. Breidenbach *et al.*, Phys. Rev. Lett. 23 (1969) 935

[9] Particle Data Group, S. Eidelman et al., Phys. Lett. B592 (2004) 1

[10] S. Moch, J.A.M. Vermaseren and A. Vogt, Nucl. Phys. B688 (2004) 101, hep-ph/0403192

[11] A. Vogt, S. Moch and J.A.M. Vermaseren, Nucl. Phys. B691 (2004) 129, hep-ph/0404111

[12] W.L. van Neerven and E.B. Zijlstra, Phys. Lett. B272 (1991) 127

[13] E.B. Zijlstra and W.L. van Neerven, Phys. Lett. B273 (1991) 476

[14] E.B. Zijlstra and W.L. van Neerven, Phys. Lett. B297 (1992) 377

[15] E.B. Zijlstra and W.L. van Neerven, Nucl. Phys. B383 (1992) 525

[16] S. Moch and J.A.M. Vermaseren, Nucl. Phys. B573 (2000) 853, hep-ph/9912355

[17] S. Moch, J.A.M. Vermaseren and A. Vogt, Phys. Lett. B606 (2005) 123, hep-ph/0411112

[18] J. Santiago and F.J. Yndurain, Nucl. Phys. B611 (2001) 447, hep-ph/0102247

[19] W.L. van Neerven and A. Vogt, Nucl. Phys. B603 (2001) 42, hep-ph/0103123

[20] A. L. Kataev, G. Parente and A. V. Sidorov, Phys. Part. Nucl. 34 (2003) 20, hep-ph/0106221

[21] S.I. Alekhin, JHEP 0302 (2003) 015, hep-ph/0211294

[22] J. Blümlein, H. Böttcher and A. Guffanti, Nucl. Phys. Proc. Suppl. 135 (2004) 152, hep-ph/0407089

[23] G. Sterman, Nucl. Phys. B281 (1987) 310

[24] S. Catani and L. Trentadue, Nucl. Phys. B327 (1989) 323

[25] L. Magnea, Nucl. Phys. B349 (1991) 703

[26] S. Catani and L. Trentadue, Nucl. Phys. B353 (1991) 183

[27] A. Vogt, Phys. Lett. B497 (2001) 228, hep-ph/0010146

[28] S. Catani, D. de Florian, M. Grazzini and P. Nason, JHEP 0307 (2003) 028, hep-ph/0306211

[29] L. Magnea and G. Sterman, Phys. Rev. D42 (1990) 4222

[30] L. Magnea, Nucl. Phys. B593, 269 (2001), hep-ph/0006255

[31] S. Moch, J.A.M. Vermaseren and A. Vogt, to appear

[32] S. Moch, J.A.M. Vermaseren and A. Vogt, Nucl. Phys. B646 (2002) 181, hep-ph/0209100

[33] J.A.M. Vermaseren, S. Moch and A. Vogt, Nucl. Phys. Proc. Suppl. 116 (2003) 100, hep-ph/0211296

[34] A. Vogt, S. Moch and J. Vermaseren, Proceedings of DIS 05, Strbske Pleso, April 2004, p. 231; hep-ph/0407321

[35] S. Moch, J.A.M. Vermaseren and A. Vogt, Nucl. Phys. Proc. Suppl. 135 (2004) 137, hep-ph/0408075

[36] S.A. Larin, F.V. Tkachev and J.A.M. Vermaseren, Phys. Rev. Lett. 66 (1991) 862

[37] S.A. Larin and J.A.M. Vermaseren, Phys. Lett. B259 (1991) 345

[38] S.A. Larin, F.V. Tkachov and J.A.M. Vermaseren, Phys. Lett. B272 (1991) 121

[39] S.A. Larin, T. van Ritbergen and J.A.M. Vermaseren, Nucl. Phys. B427 (1994) 41

[40] S.A. Larin, P. Nogueira, T. van Ritbergen and J. Vermaseren, Nucl. Phys. B492 (1997) 338, hep-ph/9605317

[41] A. Retey and J.A.M. Vermaseren, Nucl. Phys. B604 (2001) 281, hep-ph/0007294

[42] S. Moch, J.A.M. Vermaseren and A. Vogt, Nucl. Phys. B621 (2002) 413, hep-ph/0110331

[43] N. Christ, B. Hasslacher and A.H. Mueller, Phys. Rev. D6 (1972) 3543

[44] A.J. Buras, Rev. Mod. Phys. 52 (1980) 199

[45] E. Reya, Phys. Rept. 69 (1981) 195

[46] G. 't Hooft and M. Veltman, Nucl. Phys. B44 (1972) 189

[47] C.G. Bollini and J.J. Giambiagi, Nuovo Cim. 12B (1972) 20

[48] J.F. Ashmore, Lett. Nuovo Cim. 4 (1972) 289

[49] G.M. Cicuta and E. Montaldi, Nuovo Cim. Lett. 4 (1972) 329

[50] W. A. Bardeen, A. J. Buras, D. W. Duke, and T. Muta, Phys. Rev. D18 (1978) 3998

[51] G. 't Hooft, Nucl. Phys. B61 (1973) 455

[52] W.E. Caswell, Phys. Rev. Lett. 33 (1974) 244

[53] D.R.T. Jones, Nucl. Phys. B75 (1974) 531

[54] O.V. Tarasov, A.A. Vladimirov and A.Y. Zharkov, Phys. Lett. 93B (1980) 429

[55] S.A. Larin and J.A.M. Vermaseren, Phys. Lett. B303 (1993) 334, hep-ph/9302208

[56] T. van Ritbergen, J.A.M. Vermaseren and S.A. Larin, Phys. Lett. B400 (1997) 379, hep-ph/9701390

[57] M. Czakon, Nucl. Phys. B710 (2005) 485, hep-ph/0411261

[58] S.G. Gorishnii, S.A. Larin and F.V. Tkachev, Phys. Lett. 124B (1983) 217

[59] S.G. Gorishnii and S.A. Larin, Nucl. Phys. B283 (1987) 452

[60] P. Nogueira, J. Comput. Phys. 105 (1993) 279

[61] S.G. Gorishnii, S.A. Larin, L.R. Surguladze and F.V. Tkachov, Comput. Phys. Commun. 55 (1989) 381

[62] S.A. Larin, F.V. Tkachev and J.A.M. Vermaseren, NIKHEF-H-91-18

[63] J.A.M. Vermaseren, math-ph/0010025

[64] J.A.M. Vermaseren, Nucl. Phys. Proc. Suppl. 116 (2003) 343, hep-ph/0211297

[65] A. Gonzalez-Arroyo, C. Lopez and F.J. Yndurain, Nucl. Phys. B153 (1979) 161

[66] A. Gonzalez-Arroyo and C. Lopez, Nucl. Phys. B166 (1980) 429

[67] J.A.M. Vermaseren, Int. J. Mod. Phys. A14 (1999) 2037, hep-ph/9806280

[68] J. Blümlein and S. Kurth, Phys. Rev. D60 (1999) 014018, hep-ph/9810241

[69] S. Moch, P. Uwer and S. Weinzierl, J. Math. Phys. 43 (2002) 3363, hep-ph/0110083

[70] F.V. Tkachov, Phys. Lett. B100 (1981) 65

[71] K.G. Chetyrkin and F.V. Tkachev, Nucl. Phys. B192 (1981) 159

[72] F.V. Tkachov, Theor. Math. Phys. 56 (1983) 866

[73] G. Passarino and M. Veltman, Nucl. Phys. B160 (1979) 151

[74] T. van Ritbergen and R.G. Stuart, Nucl. Phys. B564 (2000) 343, hep-ph/9904240

[75] S. Laporta, Phys. Lett. B504 (2001) 188, hep-ph/0102032

[76] S. Laporta, Int. J. Mod. Phys. A15 (2000) 5087, hep-ph/0102033

[77] Y. Schröder, Nucl. Phys. Proc. Suppl. 116 (2003) 402, hep-ph/0211288

[78] C. Anastasiou and A. Lazopoulos, JHEP 07 (2004) 046, hep-ph/0404258

[79] M. Awramik et al., Nucl. Phys. Proc. Suppl. 135 (2004) 119, hep-ph/0408207

[80] D.I. Kazakov and A.V. Kotikov, Nucl. Phys. B307 (1988) 721

[81] K.G. Chetyrkin, A.L. Kataev and F.V. Tkachev, Nucl. Phys. B174 (1980) 345

[82] W.L. van Neerven and A. Vogt, Nucl. Phys. B588 (2000) 345, hep-ph/0006154

[83] A.B. Goncharov, Math. Res. Lett. 5 (1998) 497, (available at http://www.math.uiuc.edu/K-theory/0297)

[84] J.M. Borwein et al., Trans. Am. Math. Soc. 353 (2001) 907, math.CA/9910045

[85] E. Remiddi and J.A.M. Vermaseren, Int. J. Mod. Phys. A15 (2000) 725, hep-ph/9905237

[86] W.L. van Neerven and A. Vogt, Nucl. Phys. B568 (2000) 263, hep-ph/9907472

[87] T. Gehrmann and E. Remiddi, Comput. Phys. Commun. 141 (2001) 296, hep-ph/0107173

[88] S. Weinzierl, Comput. Phys. Commun. 148 (2002) 314, hep-ph/0203112

[89] A. Vogt, hep-ph/0408244; (to appear in Comput. Phys. Commun.)

[90] J. Blümlein, Comput. Phys. Commun. 133 (2000) 76, hep-ph/0003100

[91] J. Blümlein and S. Moch, hep-ph/0503188 (to appear in Phys. Lett. B)

[92] A. Vogt, Phys. Lett. B471 (1999) 97, hep-ph/9910545

[93] E. Gardi and R.G. Roberts, Nucl. Phys. B653, 227 (2003), hep-ph/0210429

[94] M. Krämer, E. Laenen and M. Spira, Nucl. Phys. B511 (1998) 523, hep-ph/9611272

[95] S. Catani and F. Hautmann, Nucl. Phys. B427 (1994) 475, hep-ph/9405388

[96] R. Akhoury, M.G. Sotiropoulos and G. Sterman, Phys. Rev. Lett. 81 (1998) 3819, hep-ph/9807330

[97] R. Akhoury and M.G. Sotiropoulos, hep-ph/0304131

[98] A.D. Martin, R.G. Roberts, W.J. Stirling and R.S. Thorne, Eur. Phys. J. C18 (2000) 117, hep-ph/0007099

[99] R.S. Thorne et al, Proceedings of DIS 05, Strbske Pleso, April 2004, p. 427; hep-ph/0407311

[100] M.A. Samuel, J. Ellis and M. Karliner, Phys. Rev. Lett. 74 (1995) 4380

[101] J. Ellis, E. Gardi, M. Karliner and M.A. Samuel, Phys. Lett. B366 (1996) 268

[102] J. Ellis, E. Gardi, M. Karliner and M.A. Samuel, Phys. Rev. D54 (1996) 6986

[103] J. Blümlein and A. Vogt, Phys. Lett. B370, 149 (1996), hep-ph/9510410

[104] J. Blümlein and J.A.M. Vermaseren, Phys. Lett. B605 (2005) 130, hep-ph/0411111

[105] J.A.M. Vermaseren, Comput. Phys. Commun. 83 (1994) 45

[106] D. Binosi and L. Theussl, Comput. Phys. Commun. **161** (2004) 76, hep-ph/0309015

[107] J.S. Guillen et al., Nucl. Phys. B353 (1991) 337